

Electronic Thesis and Dissertation Repository

8-24-2017 12:00 AM

Ultraprecise Single Point Inverted Cutting of Right Triangular Prismatic Retroreflectors: Process Enhancements and Cutting Mechanics

Nicolas Milliken, *The University of Western Ontario*

Supervisor: Ovidiu-Remus Tutunea-Fatan, *The University of Western Ontario*

Joint Supervisor: Evgueni V. Bordatchev, *The University of Western Ontario*

A thesis submitted in partial fulfillment of the requirements for the Master of Engineering Science degree in Mechanical and Materials Engineering

© Nicolas Milliken 2017

Follow this and additional works at: <https://ir.lib.uwo.ca/etd>



Part of the [Manufacturing Commons](#)

Recommended Citation

Milliken, Nicolas, "Ultraprecise Single Point Inverted Cutting of Right Triangular Prismatic Retroreflectors: Process Enhancements and Cutting Mechanics" (2017). *Electronic Thesis and Dissertation Repository*. 4810.

<https://ir.lib.uwo.ca/etd/4810>

This Dissertation/Thesis is brought to you for free and open access by Scholarship@Western. It has been accepted for inclusion in Electronic Thesis and Dissertation Repository by an authorized administrator of Scholarship@Western. For more information, please contact wlsadmin@uwo.ca.

Abstract

Automotive lighting industry relies on retroreflective components to increase driver awareness in low-light conditions since their primary functionality is to return incident light back to the source and/or observer with minimal scatter.

Presently, industry makes use of conventional pin-bundling techniques for the fabrication of the retroreflective components. This method is time consuming, labour intensive, and restrictive with respect to the design process. For these reasons, the ultraprecise single point inverted cutting (USPIC) technology was developed as an efficient alternative for manufacturing novel right triangular prismatic (RTP) retroreflective structures.

This thesis outlines a number of enhancements that improve both the quality and productivity of the USPIC technology. Furthermore, in-depth analyses of the USPIC cutting mechanics uncovered both certain process characteristics as well as possible future investigational avenues. Cumulatively, these contributions define USPIC as a viable, efficient and versatile process to be further exploited in the fabrication of dissimilar retroreflective structures.

Keywords

Retroreflector, Microfabrication, Automotive Lighting, Ultra-Precise Single Point Inverted Cutting, Cutting Kinematics, Cutting Mechanics, Surface Quality, Process Planning

Acknowledgments

As a proud member of our research group I would like to thank my advisors, Dr. Evgueni Bordatchev and Dr. Remus Tutunea-Fatan, for their limitless support and wealth of knowledge. I am grateful to have had the opportunity to pursue a master's degree among two exceptional people such as yourselves. Dr. Bordatchev, I appreciate your guidance and experience within technical research and microfabrication it has assisted me on multiple occasions. Your progressive thinking and innovative ideas are inspiring and provide great opportunities. Dr. Tutunea-Fatan, thank you for your perpetual mentorship and the confidence you have place in me time and time again. Your constant availability despite the nature of the inquiry is a testament to your prestigious character.

I extend my appreciation to my former colleagues Sama Hussein, and Benjamin Hamilton who contributed in pioneering this research and establishing a substantial foundation. I thank you both for providing an inviting environment for me to collaborate and further advance this research. It was a pleasure to work alongside both of you.

This research has been funded in part by an Queen Elizabeth II Graduate Scholarship in Science and Technology provided by the Province of Ontario and Ontario universities. I am honoured to have received this prestigious award and am grateful for the financial assistance it provided such that I could focus on my studies. The collaboration between Western University and the National Research Council of Canada (NRC) has made this research possible. Special thanks to NRC for allowing the use of their advanced facilities.

Finally, I would like to thank my family, friends, and loved ones for their support. You have provided me with the strength I needed to accomplish such an endeavour. Your generosity and encouragement are truly appreciated.

Table of Contents

Abstract	i
Acknowledgments.....	ii
Table of Contents	iii
List of Tables	vi
List of Figures	vii
List of Abbreviations	xii
Chapter 1: Introduction	1
1.1 Behaviour of Light	2
1.2 Retroreflection	4
1.3 Retroreflective Components	10
1.4 Manufacturing Methods	13
1.4.1 Pin-Bundling Technique	13
1.4.2 Diamond Micro Chiseling.....	19
1.4.3 Ultra-precise Single Point Inverted Cutting.....	23
1.5 Motivation.....	24
1.6 Objectives	25
1.7 Contribution	27
1.8 Overview.....	28
Chapter 2: Strategy Improvements and Process Planning	31
2.1 Manufacturing Setup.....	32
2.2 Material Removal Strategies.....	35
2.2.1 Unidirectional Strategy	35
2.2.2 Bidirectional Strategy	37
2.2.3 Two-Step Strategy	40

2.3 Structure Arrangement.....	41
2.4 Image Rasterization	43
2.5 Post-Processing	44
2.6 Validation of Fabrication Technique	49
2.7 Assessment of Machining Time.....	52
Chapter 3: Assessment of Surface Quality and Geometric Accuracy	56
3.1 Importance of Accuracy.....	57
3.2 Assessment of Pin-Bundling Technique.....	58
3.2.1 Surface Measurement Methodology	60
3.2.2 Surface Assessment of Pins	61
3.2.3 Surface Assessment of Electroform Die	63
3.2.4 Surface Assessment of Lens	65
3.3 Assessment of USPIC Technology.....	67
3.3.1 Qualitative Assessment of Facets	67
3.3.2 Observation of Cutting Tool	69
3.3.3 Optical Analysis.....	70
3.3.4 Quantitative Assessment of Facets	73
3.3.5 Single Facet Analysis.....	75
Chapter 4: Cutting Mechanics of the USPIC Strategies	78
4.1 Experimental Setup.....	79
4.1.1 Device Configuration.....	79
4.1.2 Coding and Data Processing	81
4.1.3 Physical Configuration of Experiments	82
4.2 Significant Kinematics	85
4.3 Cutting Mechanics	88

4.3.1	Cutting mechanics of the Unidirectional Strategy	89
4.3.2	Experiment 1: Isolated Config. Unidirectional Strategy vs DOC.....	95
4.3.3	Experiment 2: Unidirectional Strategy, Isolated vs Orthogonal	97
4.3.4	Cutting mechanics of the Bidirectional Strategy	99
4.3.5	Experiment 3: Isolated Configuration, Bidirectional Strategy.....	103
4.4	Significance of Cutting Mechanics	107
Chapter 5: Conclusion and Final Remarks		111
5.1	Summary and Conclusion	111
5.2	Future Work	113
5.3	Recommendations.....	114
References		117
Curriculum Vitae		121

List of Tables

Table 3.1 Geometric Assessment of phase 1 element in traditional pin-bundling technique, hexagonal pin. Surface roughness of retroreflective facets and edge radii between adjacent facets	63
Table 3.2 Geometric Assessment of phase 2 element in traditional pin-bundling technique, electroform die. Surface roughness of retroreflective facets	65
Table 3.3 Geometric Assessment of phase 3 element in traditional pin-bundling technique, retroreflective lens. Surface roughness of retroreflective facets	67
Table 3.4 Geometric assessment of RTP facets fabricated using USPIC technology	74

List of Figures

Figure 1.1 Behaviours of light: a) transmission, b) absorption, c) reflection, d) & e) refraction, f) refraction at critical angle, and g) total internal reflection (TIR)	4
Figure 1.2 The functionality of retroreflection and the operation of a retroreflector (RR) .	4
Figure 1.3 Geometric representation of the lens-and-mirror category of retroreflectors.....	6
Figure 1.4 Types of ICC retroreflectors and their geometric composition.....	8
Figure 1.5 ICC retroreflection, hollow retroreflector and prism retroreflector: hexagonal aperture ICC, triangular aperture ICC, and RTP	9
Figure 1.6 Relationship between aperture size and depth with respect to a hexagonal aperture ICC.....	14
Figure 1.7 Pin-bundling technology: a) Phase 1: hexagonal pins ground, lapped, and bundled, b) phase 2: electroforming structured surface of pin-bundle to form die, and c) phase 3: Injection moulding to produce retroreflective lens.....	16
Figure 1.8 Pin-bundling technique and the formation of pockets.....	17
Figure 1.9 Pin-bundling artifacts – concave grooves on pin-bundle and convex ridges on electroform die	19
Figure 1.10 V-shaped tool used in Diamond micro chiseling (DMC).....	21
Figure 1.11 Diamond micro chiseling cutting strategy.....	22

Figure 1.12 The process in which DMC uses triangular removal areas to fabricate hexagonal ICCs	23
Figure 2.1 Geometry of ultra-precise single point inverted cutting tool.....	32
Figure 2.2 Kugler Microgantry 5X CNC micromachining center	33
Figure 2.3 Single cycle of unidirectional USPIC strategy: a) cycle start, b) motion 1: plunge, c) motion 2: plunge continued, d) motion 3: plough, e) motion 4: retract, and f) motion 5: translate	36
Figure 2.4 Single cycle of bidirectional USPIC strategy: a) cycle start, b) motion 1: plunge, c) motion 2: plunge, d) motion 3: retract, e) rotation around C-axis, f) rotation complete, g) motion 4: translation to compensate rotation around C-axis, h) motion 1': plunge, i) motion 2': plunge, j) motion 3': retract, k) rotation around C-axis, and l) motion 4': translation to compensate rotation around C-axis.....	39
Figure 2.5 A representation of strategy specific material removal volumes for the two-step USPIC strategy (DOCs oversized to clarify concept).....	40
Figure 2.6 Geometric identification of RTP structure nomenclature.....	41
Figure 2.7 The offset and checker arrangements and the manipulation of the structures..	42
Figure 2.8 Image rasterization for defining RTP structure location during USPIC	44
Figure 2.9 Computer aided manufacturing (CAM) simulation of USPIC strategy using Vericut software	50

Figure 2.10 Retroreflective samples fabricated via USPIC technology in the offset arrangement.....	51
Figure 2.11 Visual appearance of structure arrangements and the 4 x 4 checker arrangement sample	52
Figure 2.12 Record of machining time of RTP structures fabricated in acrylic via USPIC	53
Figure 3.1 Recall of the 3 phases of the pin-bundling technique and photographic images of the specimens examined	60
Figure 3.2 Measurement methodology of phase 1 element in traditional pin-bundling technique, hexagonal pin	62
Figure 3.3 Geometric identification of phase 1 element in traditional pin-bundling technique, hexagonal pin	63
Figure 3.4 Measurement methodology of phase 2 element in traditional pin-bundling technique, electroform die.....	64
Figure 3.5 Geometric identification of phase 2 element in traditional pin-bundling technique, electroform die.....	65
Figure 3.6 Measurement methodology of phase 3 element in traditional pin-bundling technique, retroreflective lens	66
Figure 3.7 Geometric identification of phase 3 element in traditional pin-bundling technique, retroreflective lens	66

Figure 3.8 Optical microscopy of facets fabricated using USPIC technology	68
Figure 3.9 Observation of the USPIC tool and the correlation between cutting edge chip-fractures and linear scratches on fabricated facets.....	70
Figure 3.10 Samples assessed in optical performance testing: a) hexagonal ICC RRs via pin-bundling technique, and b) RTP RRs via USPIC technology	71
Figure 3.11 Fixture designed and fabricated for optical performance testing of retroreflective samples	72
Figure 3.12 Optical performance testing: a) hexagonal ICC RRs via pin-bundling technique, and b) RTP RRs via USPIC technology.....	73
Figure 3.13 Measurement methodology for surface quality of RTP facets fabricated using USPIC technology	74
Figure 3.14 Surface quality and characteristics of an RTP facet fabricated by USPIC: a) optical image, b) surface topographical image, c) surface profiles along feed direction (P1 – P3), and d) surface profiles across feed direction (P4 – P6).....	76
Figure 4.1 Experimental setup: a) block diagram flowchart, and b) photographic flowchart	80
Figure 4.2 LabVIEW data processing procedure.....	82
Figure 4.3 CAD representation of the CNC machining center, tool, dynamometer and workpiece	83

Figure 4.4 Experimental configuration: a) isolated cutting condition, and b) orthogonal cutting condition	85
Figure 4.5 Significant kinematics associated to cutting mechanics of the unidirectional strategy	86
Figure 4.6 Significant kinematics associated to cutting mechanics of the bidirectional strategy: a) fabrication of facet 1, and b) fabrication of facet 2.....	88
Figure 4.7 Detailed description of cutting force signatures during unidirectional USPIC strategy: a) complete cycle, and b) detail view of the final motions	91
Figure 4.8 Cutting mechanics of the unidirectional strategy in isolated configuration at 5 and 10 μm DOC, experiment 1	96
Figure 4.9 Comparative Cutting mechanics of the unidirectional strategy in isolated and orthogonal configurations	99
Figure 4.10 Detailed description of cutting force signatures during bidirectional USPIC strategy: a) single cut of facet 1, and b) detail view of retract motion.....	102
Figure 4.11 Comparative Cutting mechanics of the unidirectional strategy and bidirectional strategy in isolated configuration.....	105
Figure 4.12 Comparative Cutting mechanics of the symmetric cutting motions of the bidirectional strategy in isolated configuration.....	107

List of Abbreviations

CAD	Computer Aided Design
CAE	Computer Aided Engineering
CAM	Computer Aided Manufacturing
CC	Cube Corner
CNC	Computer Numeric Control
DAQ	Data Acquisition
DMC	Diamond Micro Chiseling
DOC	Depth of Cut
ICC	Inverted Cube Corner
MCD	Monocrystalline Diamond
MCS	Machine Coordinate System
NC	Numeric Control
RR	Retroreflector
RTP	Right Triangular Prism
TIR	Total Internal Reflection
USPIC	Ultraprecise Single Point Inverted Cutting
WCS	Workpiece Coordinate System

CHAPTER 1

Introduction

1 Introduction

1.1 Behaviour of Light

It is known that light behaves in manners which are characteristic of both particles and waves. In the 19th century Albert Einstein demonstrated that light had wave–particle duality and it was his light quantum theory that explained the various behaviours of light. Depending on the behaviour which is being observed light can be described as propagating wavefronts or light rays. Behaviours such as diffraction and interference are described using wavefronts while transmission, reflection, and refraction are described using rays. Since this study does not embody diffraction or interference the kinematics of light will be described via geometric optics (i.e. light rays). Light propagates linearly within homogenous media and its ray is defined as a vector perpendicular to the wavefronts. Geometric optics is an idealized model of light and its behaviours.

Transmission of light is described as an electromagnetic wave, such as visible light, passing through a material (Figure 1.1a). If during transmission of the light the object converts the energy of the photons into internal energy this is called absorption (Figure 1.1b). Reflection occurs when a light ray does not pass through or get absorbed by the material but rather gets redirected upon contact with the surface of the object. The law of reflection described this process geometrically, where the three vectors: the incident ray, reflected ray, and surface normal all lie in the same plane. Additionally, the angle of reflection is equal to the angle of incidence except that its orientation is mirrored with respect to the surface normal (Figure 1.1c). Interestingly, our mind’s perception of colour is actually the only colour within visible light that does not get absorbed by the object. The specific frequency of light associated to the colour we perceive is reflected off the object while all other frequencies

are absorbed. The reflected light frequency is then detected by our eyes and processed by the brain to determine the associative colour.

Refraction occurs when light passes between 2 materials with different refractive indices. If the incident light meets the boundary surface at any angle other than 0° , with respect to its normal, the direction of the light ray changes. This change is associated to the change in refractive indices of the material and can be determined via Snell's law, $n_1 \sin\theta_1 = n_2 \sin\theta_2$. When light passes from a lower to a higher index of refraction ($n_1 < n_2$) the angle relative to the normal decreases (Figure 1.1d). In contrast if the transition occurs in the opposite order ($n_1 > n_2$) the angle increases (Figure 1.1e). In this case where the index of refraction decreases, there is a unique incident angle which results in the refracted ray being parallel to the surface of separation between the media (Figure 1.1f). This angle is known as the critical angle and it represents the separation between refraction and total internal reflection (TIR).

When the incident angle is greater than the critical angle the transition surface between media acts as boundary for TIR (Figure 1.1g). This phenomenon is adequately named in that the boundary restricts any light from escaping the medium and therefore the light is entirely reflected off the boundary. Generally, when light comes in contact with a surface of an object multiple light behaviours are present. A percentage of the incident light may be absorbed while another amount may transmit through the medium at a refracted angle and the remaining percentage may be reflected. Since the light is entirely contained within the medium during TIR, applications such as optical prisms and fiber optics exploit this phenomenon.

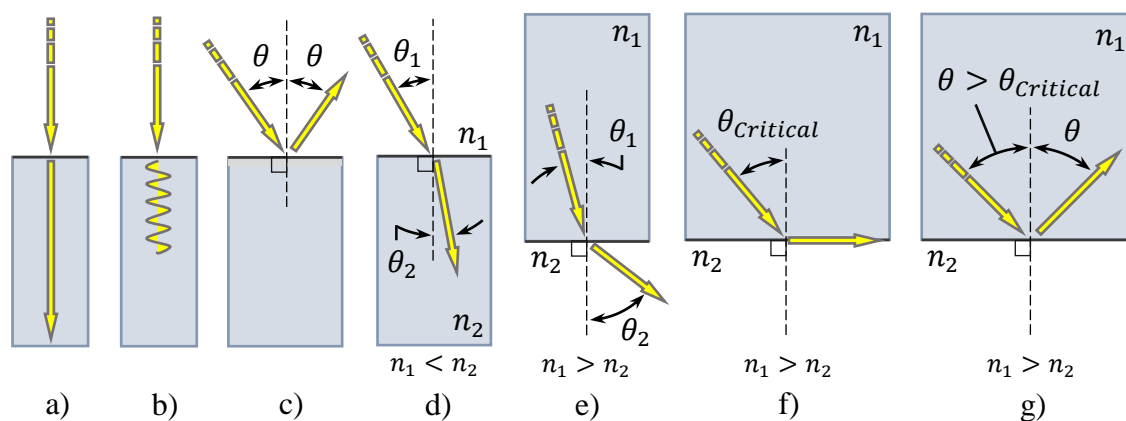


Figure 1.1 Behaviours of light: a) transmission, b) absorption, c) reflection, d) & e) refraction, f) refraction at critical angle, and g) total internal reflection (TIR)

1.2 Retroreflection

The final optical behaviour which is essential to this research is retroreflection. This effect is not necessarily an elementary behaviour of light but rather a result of specific geometry and behaviours or combinations of behaviours previously mentioned. The general definition of retroreflection is when light is redirected such that its resultant vector is parallel to the incident ray but opposite in direction (Figure 1.2) [1]. The practical use of such effect is to return incident light back to the source which emitted the wavefront. A device which would perform this optical function is described as a retroreflector (RR).

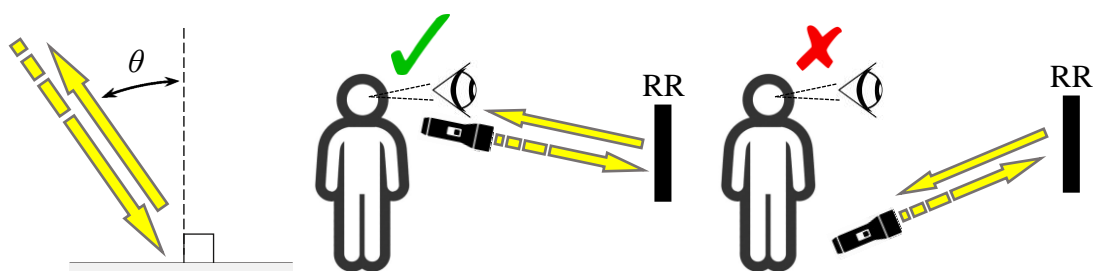


Figure 1.2 The functionality of retroreflection and the operation of a retroreflector (RR)

RRs are divided into two general categories, lens-and-mirror or inverted-corner-cube (ICC). This categorization is due to the difference in geometric configuration as well as the use of different behaviours of light. The lens-and-mirror RR, also known as “cat’s eye”, is geometrically described as a spherical lens with an reflective hemispherical surface. This type of RR is commonly used in high-visibility clothing, road signs and road surface markings. The paint used to mark the road consist of small glass spheres and functions as a lens-and-mirror RR [2, 3].

The incident light first contacts the non-reflective hemisphere of the lens, refraction occurs as the light passes through the boundary between the atmosphere and the lens. The light continues via transmission through the lens until reaching the opposing reflective hemisphere. The light ray is then reflected and transmits back through the lens. The light is refracted once more upon exiting the lens of the RR (Figure 1.3). It is essential to retroreflection that the returning ray is parallel and opposite to the incident ray therefore the refractive index of the lens needs to be carefully considered.

Using Snell’s law and the law of reflection the refractive index of the lens can be determined. Theoretically, for this configuration to function correctly the refractive index of the lens needs to be twice that of the external medium. The refractive index of the atmosphere (air) is similar to that of a vacuum, which is 1, therefore the refractive index of the lens needs to be 2. This configuration assures that the focal point, after the initial refraction, falls on the surface of the sphere. If the refractive index varies then the focal point will end up being internal or external to the surface of the lens. This results in the light not being theoretically retroreflected although many applications do use lenses which have a slightly different refractive index. A few reasons the refractive index may be altered

are to counteract the reflective surface being offset from the spherical lens or to introduce scatter [4].

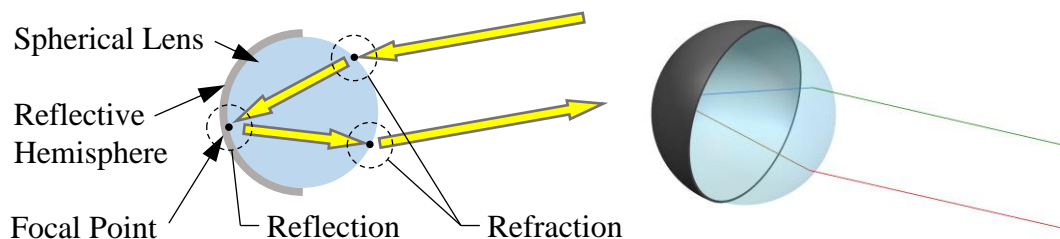


Figure 1.3 Geometric representation of the lens-and-mirror category of retroreflectors

ICC is the second general category of RRs and are dependent on the light reflecting off the geometric facets of a cube. Reflection can occur by the facets themselves being fully mirrored/reflective or making use of TIR. Therefore, ICCs can function as a configuration of polished plates or as an optical prism. The configuration of plates is known as a hollow RR. Unlike lens-and-mirror, ICCs do not require refraction to function correctly. Refraction is present in the prism RRs however it is not significant to its function. This category can be further broken down into three types of retroreflective elements, hexagonal aperture ICC, triangular aperture ICC, and the right-triangular-prism (RTP). The RTP geometry is generally not termed an ICC because it does not have significance to an individual corner/vertex of a cube. Rather, an RTP significance is more closely related to an edge of a cube. However, since an RTP relies on the same mutually orthogonal characteristics of a cube it is categorized as an ICC. The hexagonal and triangular aperture ICCs require 3 facets to accomplish retroreflection while the RTP relies on 2. The facets which encounter light are termed participating-facets.

Geometrically each of these elements can be described as first starting with a unit cube positioned in the positive XYZ spatial coordinates. An RTP would then require a 45° rotation about one edge (-Y rotation in Figure 1.4). After, the geometry would need to be trimmed about an X-Y plane at a height which is equal to or less than the height of the centroid of the cube. After the geometry is trimmed the critical facets are the internal faces of the hollow cube. The hexagonal and triangular geometries can be described as the unit cube rotated -45° about Y, and further rotated $+35.2644^\circ$ about X (Figure 1.4). From this orientation, the upper 3 surfaces are removed and the critical facets are again the internal/inverted faces of the hollow cube. At this point the geometry represents the hexagonal CC because when viewing from a +Z position (top view) the boundary of the facets form a hexagon. To produce a triangular aperture this element needs to be trimmed by a X-Y plane with a height equal to or less than the height of the lower 3 vertices of the cube (excluding the base vertex).

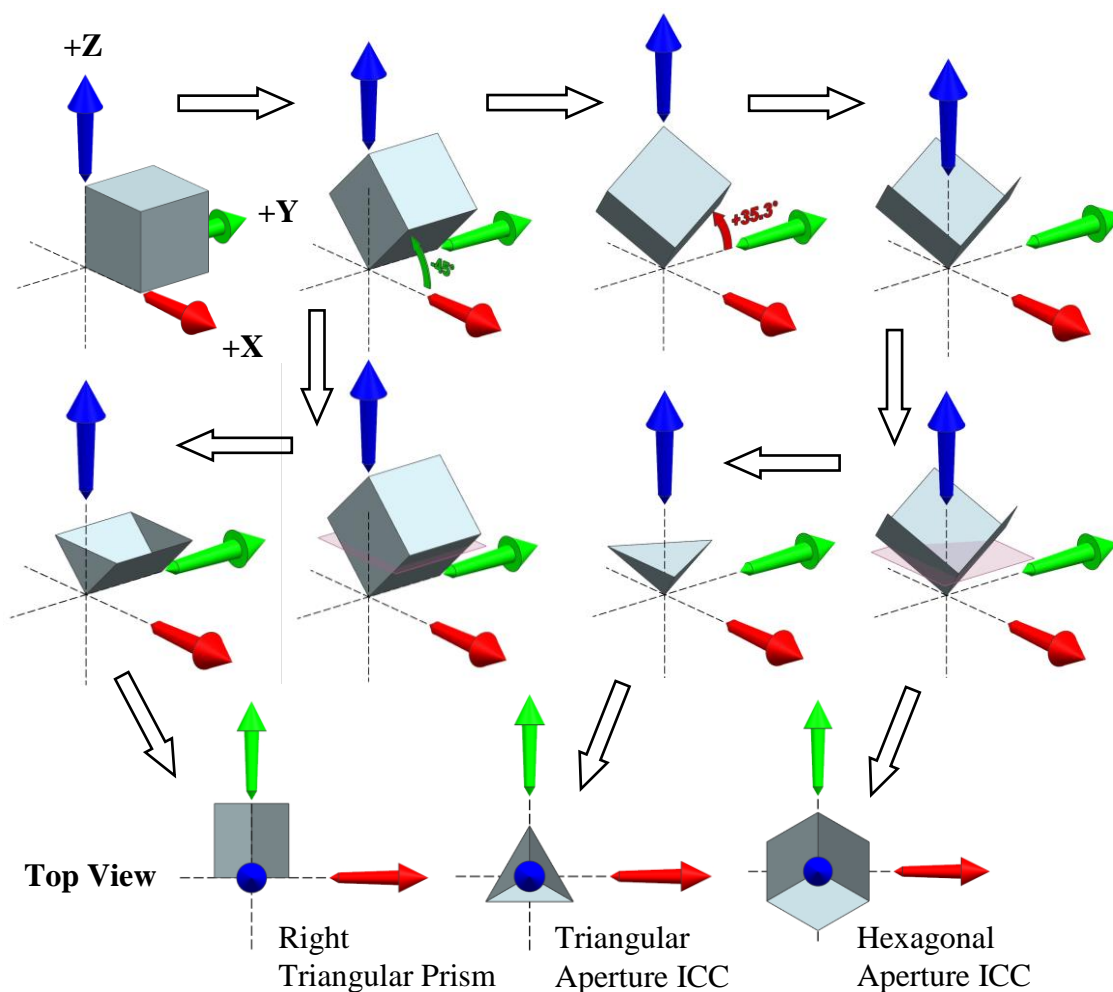


Figure 1.4 Types of ICC retroreflectors and their geometric composition

ICC retroreflection can be summarized as a specific sequence of reflections to produce a resultant ray that is parallel and opposite to the incident light. However, these reflections may occur via reflection or TIR depending on whether the element is a hollow or prism RR. Regardless of the technique used the functionality is identical. A hollow RR would result in the incident light directly contacting the facet while a prism RR would require the light to first enter the prism before contacting the internal surface of the facet. Depending on the type of ICC the light may undergo 2 or 3 reflections/TIRs. As long as the included angles are

90° between adjacent facets the resultant ray will be retroreflected. The mutually orthogonal arrangement of facets is critical and is a fundamental characteristic of a cube. For a prism structure the only difference is the refraction which takes place as the light enters the planar face of the structure. However, since the entrance surface is planar and the light is retroreflected within the element the exiting light is refracted such that it eliminates the effect of the initial refraction. The cancellation of the refractive behaviour make the two configurations function in the same manner. The prism RR has the advantage of light transmission when light encounters the element from the opposite side. This dual sided characteristic of the prism RR is commonly used in automotive tail light lenses for illumination. In contrast the hollow RR does not relying on TIR and eliminates the potential for light to exit the facet if the incident angle is less than the critical angle [1].

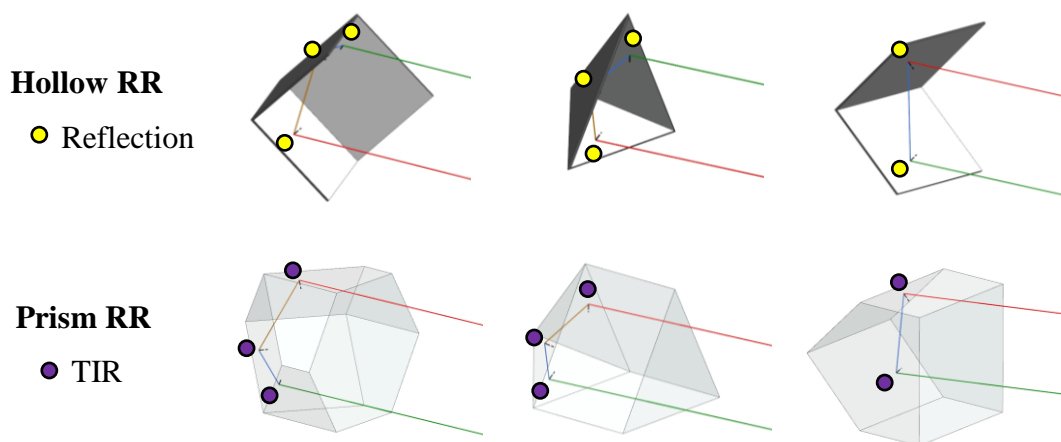


Figure 1.5 ICC retroreflection, hollow retroreflector and prism retroreflector: hexagonal aperture ICC, triangular aperture ICC, and RTP

The clear difference between the 3 types of ICCs is their geometry however they also show widely different retroreflective performance. The hexagonal and triangular aperture ICC function very similar apart from their effective aperture. The effective area is calculated as

the total area which can retroreflect light at a given incident angle. A hexagonal aperture ICC and a RTP theoretically have 100% effective area at 0° incident angle while a triangular aperture is restricted to $2/3^{\text{rds}}$ of its entire area. As the incident angle deviates from 0° the effective area declines for each RR. However, the triangular aperture ICC declines at a much less rapid rate and at an incident angle of approximately 20° the effective area of the triangular aperture ICC surpasses the hexagonal [1]. The RTP geometry does not decline rapidly until an incident angle greater than 4° therefore at minimal incident angles this geometry proves to be the most efficient. After 4° the efficiency of an RTP decreases quickly being surpassed by both hexagonal and triangular ICCs. To summarize, each of the 3 ICC geometries has an area of optimal effectiveness. The RTP works very well for minimal incident angles, the hexagonal aperture ICC is most effective for angles between 4° and 20° and above 20° the triangular aperture ICC is most efficient. Therefore, each RR may have a more appropriate application depending on the requirements such as observation distance, angle, light source, etc. This study is strictly focused on the RTP geometry because of its emerging design capabilities and its more ideal manufacturing potential.

1.3 Retroreflective Components

Photonic devices are characterized by their ability to create, manipulate or detect radiant energy (e.g. light). These components range across a vast area, from everyday life to the pinnacle of today's scientific achievements. The advancements and attention currently circulating the photonics industry is comparable to the effect of integrated circuits within the electronics industry. More relevant is the significance of precision diamond machining

to manufacture photonics components. Within this section a singular focus will be placed upon retroreflective components which are light manipulation photonic components.

Natural retroreflection was first observed by Benvenuto Cellini in 1562, where the light was manipulated by a droplet of water atop a blade of grass. This configuration is representative of the lens-and-mirror RR and was originally modeled by Lommel in 1874. It wasn't until 1887 that the ICC was first introduced by Doctor A. Beck of Germany. Initially the geometric configuration of the 3 plane mirrors was called the Beck "Zentralspiegel" (central reflector) a special form of a triple reflector. We now know this as the hollow RR. Nearly 20 years later, in 1906, Rudolf Straubel patented the prism type ICC [1].

Retroreflectors are now used across multiple industries including metrology, communications, atmospheric research, and transportation. Each making use of the optical performance of retroreflectors in different applications. Surveying equipment uses optical systems including retroreflectors to make accurate distance measurement. Inter-satellite communication is an interesting application of free space optical communication using retroreflectors. Absorption spectroscopy is a useful atmospheric research tool and commonly the measurement system includes retroreflective components [4-8].

Automotive retroreflective components are used for safety applications in low light conditions. Their function is to provide vehicle/object awareness while driving in low light conditions. They are extensively used to increase visibility of the road, vehicles, traffic signs and nearly any object. This is accomplished by redirecting external light, such as oncoming vehicle head lights, back to the originating source. Thanks to minimal scattering

the RR redirects some of the emitted light back towards the oncoming vehicle. This results in the RR being highly visible to the oncoming driver and in extension the driver is aware of the object/vehicle the RR is attached to. RRs are passive optical elements, which means they function by manipulating external light rather than emitting light of their own. Thus, retroreflective components provide a constant increase to automotive safety without the requirement of power or operation.

A side from RR's ability to increase road safety they are also a staple in vehicles styling and aesthetic appeal. The automotive industry is continuously in search of new styling, and more enhanced lighting components. Recently the field of automotive lighting has exploded thanks to the arrival of micro-optical structures and micromachining technologies [9, 10]. This has opened a completely new limitless option for automotive lighting components to attract and excite consumers. Automakers have already begun to incorporate discrete lighting accents to various vehicle components. These small but significant additions are revolutionary to the industry and would not be possible without the recent developments in micro-scale optics and advanced micromachining technologies [11].

Micro-scale optics or micro-optics are defined as optical systems which range in size from a few micrometres to a millimetre in size. Similarly, micromachining is subject to this scale as well [12]. Typical RRs used in the automotive industry exceed the micro-scale and furthermore they are not manufactured using any advanced machining technique. Instead automotive RRs are still being manufacturer via a manufacturing technique that was developed in the 1970's. This technique is known as the pin-bundling technique and relies heavily on the time-consuming process of electroforming. There are physical limitations

associated to this technique that eliminate the plausibility of fabricating micro-scale RRs. Therefore, it is universal for automotive ICC retroreflectors to be among the macro-optics classification.

1.4 Manufacturing Methods

1.4.1 Pin-Bundling Technique

Within the automotive industry, the hexagonal aperture ICC is the most common RR used. Typically, the aperture size ranges from 2 – 3 millimetres in diameter (i.e. circumscribed circle of hexagon). The retroreflective surface area required by automotive manufacturers can be greater than 100 cm² per individual are. Therefore, thousands of individual RRs are needed to span the associated surfaces. These RRs are arranged in an array such that their aperture edges are coincident with edges of adjacent RRs. This hexagonal pattern is more commonly known as a honeycomb pattern.

The industry does not deviate from the range of aperture size mentioned above. The reason for this can be attributable to 2 separate limitations. The reason retroreflective aperture size does not typically exceed 3 mm is related to the desired lens thickness. The thickness of the lens is dependent on the size of the retroreflective element. For example, a hexagonal RR of aperture diameter 2.5 mm requires a lens thickness greater than 1.8 mm while a 10.0 mm RR would require a thickness greater than 7.1 mm (Figure 1.6). Additional thickness is required for the illumination element of the lens. The illumination element serves 2 purposes; first to provide the true structure of the lens and bind the prism RRs together, and second to allow the tail light emitting component to illuminate the entire lens [13, 14]. Due to several criteria involving fit, form and function an automotive lighting lens is

generally in the range of 5 mm thick. This thickness must include both illumination element and retroreflective element.

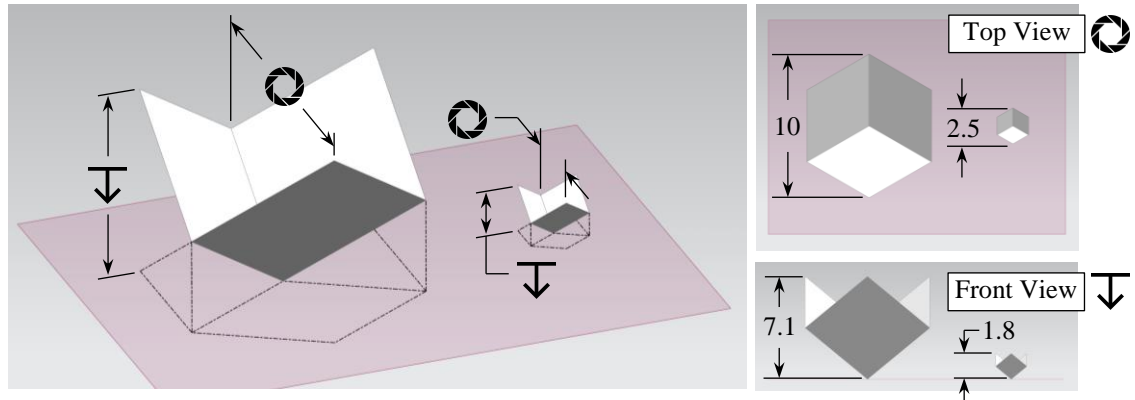
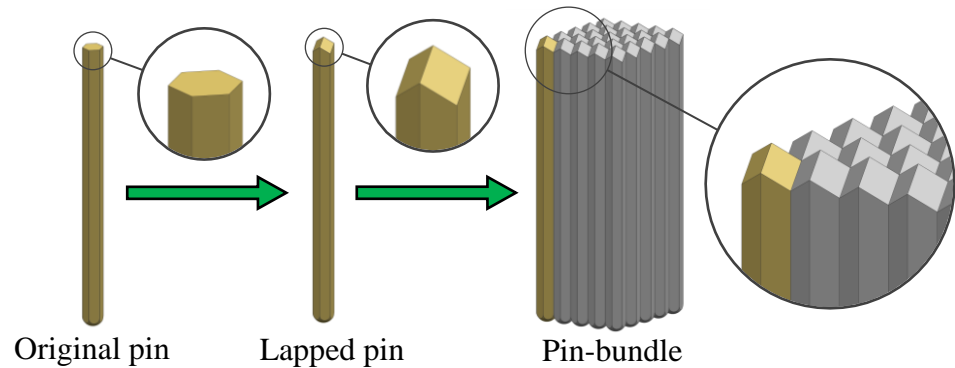


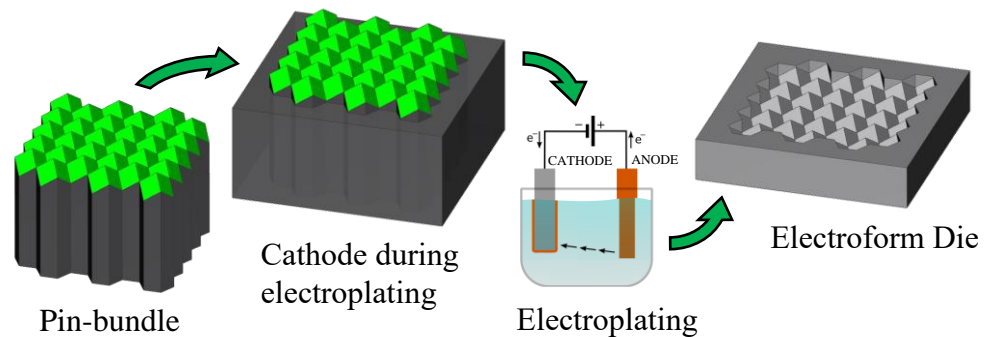
Figure 1.6 Relationship between aperture size and depth with respect to a hexagonal aperture ICC

The geometric characteristics of these hexagonal RR posed a difficult manufacturing problem which has resulted in a unique manufacturing process to be developed specifically for these features. This process has been described as the pin-bundling technique and was developed in the early 1970's [15]. The process consists of multiple steps encompassing expensive, time-consuming and labour intensive strategies. The initial phase is to grind and lap hexagonal pins to produce 3 facets mutually orthogonal. The facets also need to converge at a single vertex which is coincident with the longitudinal axis of the pin. This effectively generates a convex corner cube on a single end of the hexagonal pin. The newly lapped pins are then arranged so to match the desired surface contour and to align correctly with all adjacent pins (Figure 1.7a). The bundle is then held together, fixed tightly, and used as the cathode in a time-consuming electroforming process. During this process an electric current dissolves the anode and slowly deposits it onto the structured surface of the pin-bundle. This process continues until an approximate layer thickness of 10 mm is

achieved. At its completion, the anode deposit is separated from the pin-bundle and the pins are then recycled to be re-lapped and used for future arrangements. The anode deposit commonly known as the electroform is now retroreflective portion of the injection moulding die for the automotive lens. Prior to including the electroform in the complete die it must undergo further machining to be properly positioned relative to the rest of the die. Once properly assembled the completed die is then used in the favourable process of injection moulding. It is critical to note that the described process of manufacturing a complete die incorporating a retroreflective area takes approximately 12 – 14 weeks [14].



a)



b)

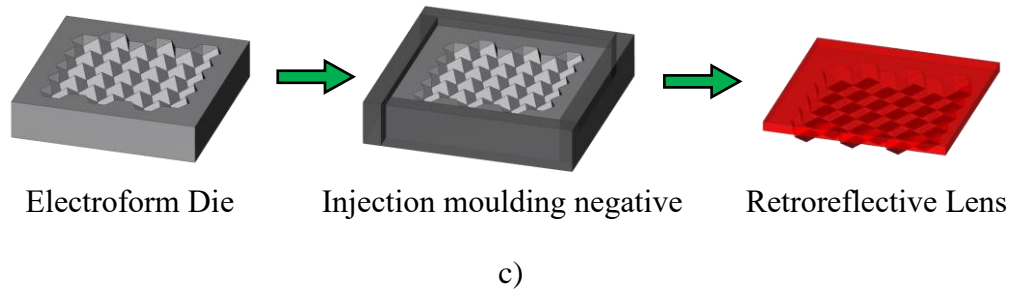


Figure 1.7 Pin-bundling technology: a) Phase 1: hexagonal pins ground, lapped, and bundled, b) phase 2: electroforming structured surface of pin-bundle to form die, and c) phase 3: Injection moulding to produce retroreflective lens

The pin-bundling technique for fabrication hexagonal ICCs significantly limits the ability to develop new more appealing styling and aesthetics. It is necessary to understand at this point that the pin bundle represents a solid body of the finished retroreflective optical part. Each pin represents a single ICC structure/RR on the automotive lens. In the case of a perpendicular flat surface, all pins are bundled at the same height forming an ideal array of RRs without any optical non-uniformities. Therefore, this technology works effectively on arrays represented in Figure 1.8a. However, when the pins are arranged to follow a surface that is not continuously perpendicular to the longitudinal axis of the pins artifacts, called pockets, begin to form.

Within a pin-bundle each pin is constrained by its contact with adjacent pins. This contact between the side surfaces of the pins leaves each pin with only 1 degree of freedom, neglecting friction. This linear degree of freedom is collinear to the individual pin's longitudinal axis. This linear position is eventually constrained such that the structured surface of the pin-bundle matches the desired surface. However, this is a difficult task because it requires an additional surface to be designed and fabricated that mimics the

desired final surface. This additional surface is then used as a fixture to contact each pin and position it correctly along its longitudinal axis.

The use of hexagonal pins introduces optical artifacts on inclined and curved surfaces as shown in Figures 1.8b and 1.8c. The solid body of each pin is used for alignment and orientation within the bundle, this effectively creates the hexagonal (honeycomb) pattern. All pins then share a common parallel constraint about their longitudinal axis. This prevents any pin from orientating separate from the entire bundle and therefore limits the bundle's ability to accommodate surface changes. In order to follow the desired surface curvature, pins are extended or retracted along their longitudinal axis.

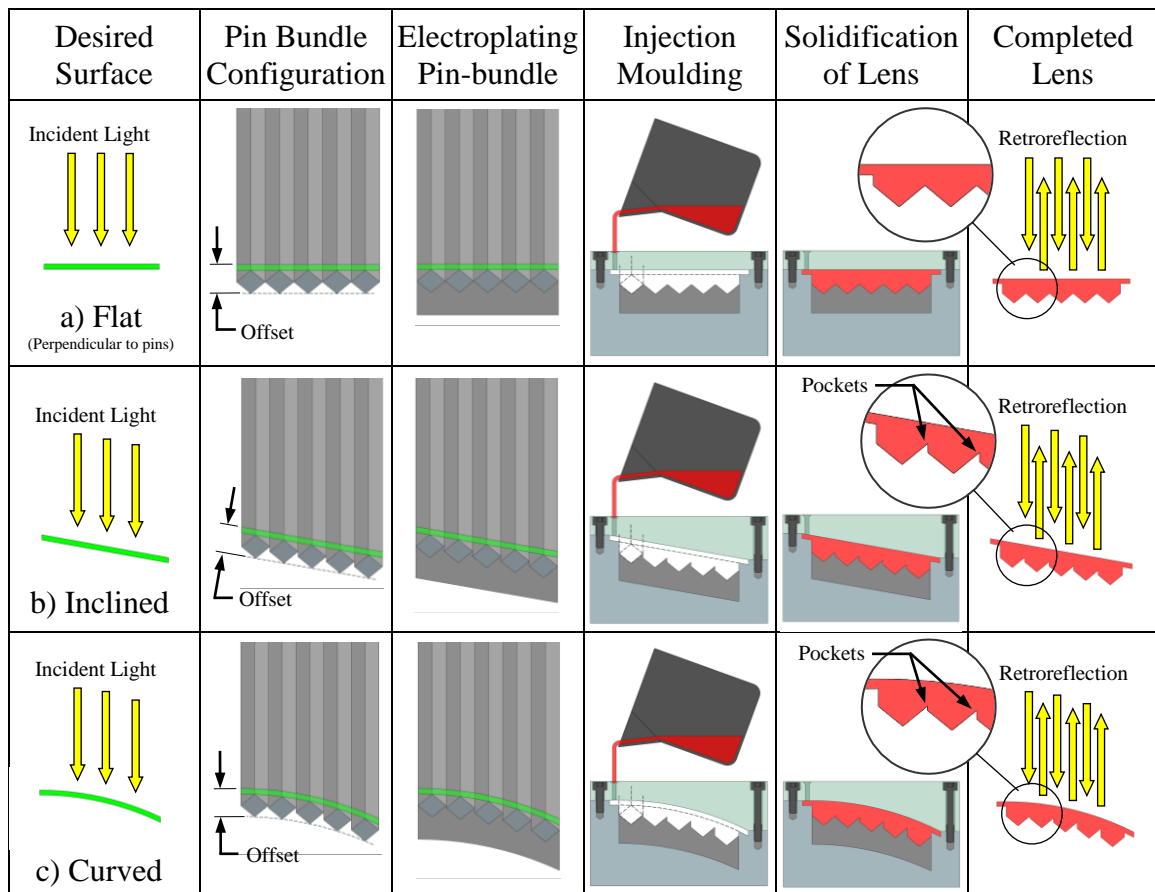


Figure 1.8 Pin-bundling technique and the formation of pockets

When adjacent pins are positioned at different heights artifacts are produced between individual ICCs. These artifacts are described as pockets within the 2-dimensional representation in Figure 1.8b and 1.8c. However, when examining their effect in 3-dimensions the artifacts more closely resemble grooves running along the full length of aperture edges. The impact of these artifacts on the optical performance of the RRs is rather unclear at this time and optical simulation studies are required to clarify their relationship with performance and function. The artifacts which originate during pin-bundling are replicated onto the electroform and therefore are present in the die during injection moulding. Since the pins do not and can not have draft angles complications arise during evacuation of injection moulded parts from the cavity of the die. The artifacts which are seen on the pin-bundle and lens are concave in nature (i.e. pockets, grooves) whereas the electroform is the negative geometric match having convex artifacts (i.e. protrusion, ridges). The scale and fragility of these convex artifacts make them prone to damage. Figure 1.9 shows a pin-bundle for hexagonal ICCs with 3 mm aperture size. The pins are configured such that there is an offset of 200 μm between adjacent rows. This is a measure of the projected distance along the common axis of the bundle from the tip of one pin to the tip of another in an adjacent row. This offset is not generally only between adjacent rows and does not typically stay constant when considering freeform surfaces. In this example, the arrangement is uniform and the offset is held constant. Even with such a minute offset the artifacts begin to form on two edges of every aperture. This pin arrangement represents an inclined surface of only 5 degrees with respect to the common normal of the bundle. The greater the incline or offset between adjacent pins, the greater the size of the associative artifacts.

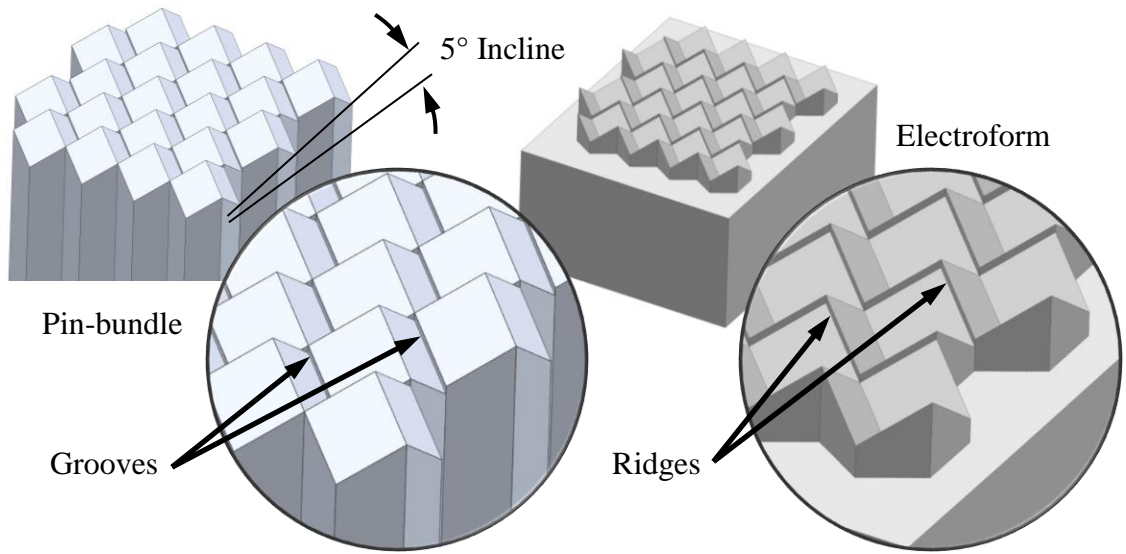


Figure 1.9 Pin-bundling artifacts – concave grooves on pin-bundle and convex ridges on electroform die

A more preliminary complication associated to pin-bundling occurs during the design methodology for automotive retroreflective lenses. It is standard practice for automakers to design retroreflective lighting components with the understanding that the pin-bundling technique will be used for manufacturing. Pin-bundling is the universal and only technology available to manufacture ICC RRs in the automotive industry. Automakers must design to suit this manufacturing technique and take pre-emptive measures against conflicts within this process. Therefore, from the moment a retroreflective design is conceived it is already being restricted by the limitation of this manufacturing method. This significantly limits innovations in styling and advanced visual appearance.

1.4.2 Diamond Micro Chiseling

The transitions from the pin-bundling to material removal (e.g. micromachining) technologies enables a greater flexibility in terms of RR geometry and - when accompanied by optimized cutting strategies – an increased productivity. Since injection moulding is an

ideal manufacturing method for mass production the material removal approach does not eliminate this process. Instead, material removal processes associated to ICC retroreflective geometry are strictly focusing on the fabrication of the injection moulding die. The ability to directly manufacture the die without the use of electroforming has many benefits. It is important to understand – for this technology and also for the novel technology presented in this thesis – that the material removal process is intended for the injection moulding die not the final lens product.

The nature of the retroreflective geometries prevents the use of classical tool path planning strategies associated with micromilling operations [16]. Among other material removal technologies, diamond micro-chiseling (DMC) [16-18] was identified as a viable alternative to pin-bundling-electroforming process. DMC has been utilized to fabricate aperture sizes as small as 150 μm . To date, DMC was solely presented in the context of hexagonal ICC RRs that were cut in a flat and horizontal base surface. This technology allows for a direct machining of the injection moulding die by means of a V-shaped diamond tool whose motions are controlled by an ultraprecise five-axis micromachining system. The diamond tool cuts each RR structure in multiple layers to improve the final surface finish and reduce tool wear.

To achieve the required geometric accuracy and optical functionality, ICC RRs have been produced by means of the ultraprecise five-axis CNC machining system and diamond tooling. The geometry of the diamond tool involved in DMC resembles that of a 50° V-shaped turning tool, yet is specific to the DMC process. For DMC purpose, the tool was aligned in the machine such that the conventional clearance and rake faces have been switched and therefore the cutting mechanics is different than that of turning, even if the

tool is almost the same. The tool features a 22° rake angle and the clearance face has an angle of $2-3^\circ$ [18].

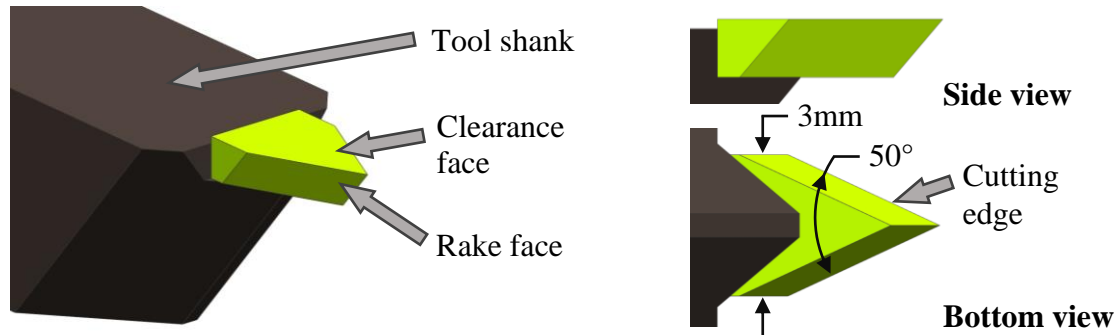


Figure 1.10 V-shaped tool used in Diamond micro chiseling (DMC)

The two rotary axes of the five-axis machining system are required for the alignment of the tool with the facets of the structure to be cut. The machine used in the DMC process had a five-axis head/table tilting or hybrid configuration such that the tool can be rotated around the B-axis, while the workpiece can be reoriented by rotating C-axis. In DMC, the cutting process follows a sequence of motions, removing material in layers to form a 3-sided cavity. The tool must be perfectly aligned with the plane of the RR facet to be cut. The use of an ultra-precise computer numerical control (CNC) micromachining center makes this task possible.

From this position, the tip of the tool is moved parallel to the edges of the facet in a two-step process: i) plunge along the first edge to the apex, followed by ii) retract along the second edge. This V-shaped motion completes only a single layer of one facet of the retroreflective structure. The remaining two facets of the structure are completed in the same manner but only after the workpiece has been rotated 120° about C-axis. This rotation allows for the clearance face of the tool to be parallel with the next RR facet. It is important

to note that after the indexing motion of the workpiece, the relative position between the tool and the structure has changed. The tool must again be perfectly aligned parallel and coincident to the next facet to be cut.

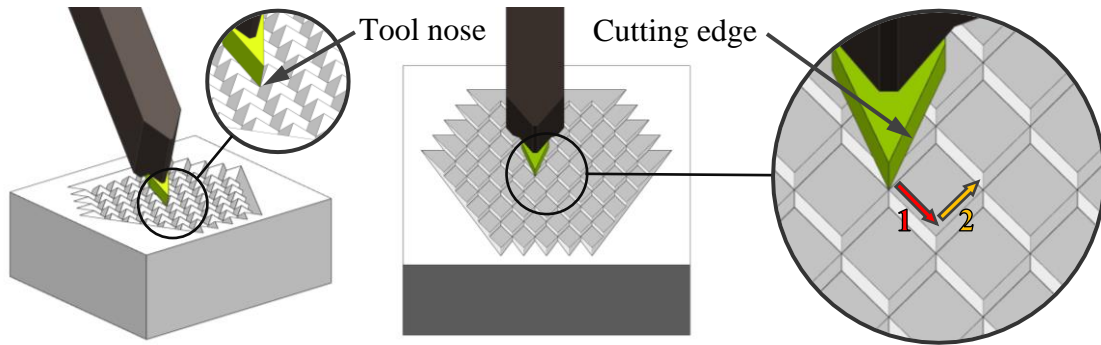


Figure 1.11 Diamond micro chiseling cutting strategy

For each chip or cutting layer the tool is repositioned once per facet prior to the V-shaped motion. The chip associate to the layer being cut is not detached from the workpiece until the 3rd cutting motion is complete. At this point the 3 cutting trajectories would be repeated at a larger depth, this entire sequential process will repeat until the desire structure size is achieved. Each structure in the array requires the same material removal process. The DMC process for a single structure creates a triangular aperture ICC however when multiple triangular ICCs are positioned in an overlapped configuration it is possible to produce hexagonal aperture ICCs (Figure 1.12).

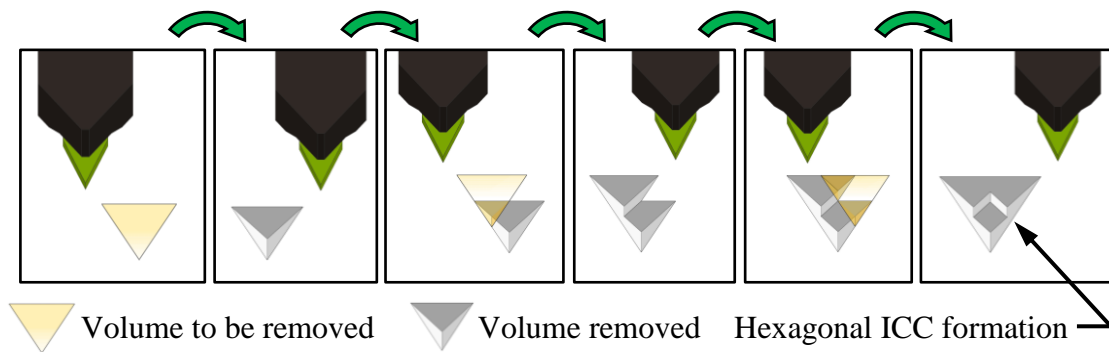


Figure 1.12 The process in which DMC uses triangular removal areas to fabricate hexagonal ICCs

This unique manufacturing method validated the concept of material removal for retroreflective dies. However, since this achievement, there has not been any published information regarding the optical performance of the machined die or any subsequent lens-inverse. Additionally, no direct surface quality assessment was performed on the fabricated sample. Without this representative data, it is impossible to compare the functionality between the traditional pin-bundling technique and DMC.

1.4.3 Ultra-precise Single Point Inverted Cutting

Alternative to DMC, ultra-precise single point inverted cutting (USPIC) was introduced as a viable option to generate RTP retroreflective geometries. This technology was first introduced in [19]. After the introduction of this technology, additional directions of research were identified and then developed into the work presented in this thesis. Machine kinematics and preliminary fabrication techniques were presented in [19-22] and the geometric development of the RTP and its optical functionality were introduced in [13, 14, 19]. By contrast, the present study takes the previous work one step further by focusing on

the development of more efficient cutting strategies, surface assessment and cutting mechanics. The USPIC technology will be thoroughly explain in the following chapter.

1.5 Motivation

Retroreflective geometries pose a high level of difficulty for manufacturing. Many of the associated complications are attributable to the structures keen concave edges. Traditional machining and material removal techniques are not applicable, and therefore unique manufacturing methods have been developed. The automotive industry standard for such components involves poor design practices and labour/time intensive processes. In effort to remedy these issues, innovative material removal techniques have been developed. The USPIC technology aims to revolutionize our ability to manufacture retroreflective structures. Its motivation is to provide a more efficient and less restrictive manufacturing process. In extension, the work presented in this thesis is equally motivated with an emphasis on enabling the technological ability to do so.

It is idealized that this technology will provide industry with many advantages while maintaining production demands. The increase in manufacturing efficiency will stem from the elimination of the pin-bundling and electroforming process. Thus, there will be a large decrease in labour requirements and time consumption. The lead time associated with injection moulding dies, containing retroreflective structures, will be reduced. The reduced lead time will impact design deadlines allowing for more refined products to be developed. More effort spent in the design stage generally reduces the amount of effort spent on design changes and rework. The cost of which is significantly higher than that of the design stage.

Additional advantages are related to the novel material removal technique. This manufacturing approach allows for more creative and diverse design implementation of RRs. The limitations regarding retroreflective structure orientation, size and arrangement that are associated with pin-bundling can be surpassed. Seemingly endless possibilities for retroreflective components can then be explored by designers. The versatile design and manufacturing process will invoke new styling and aesthetics soon to be desired by consumers. The demand which develops provides additional motivation for this new technology.

Innovative lighting components have always been a dominant characteristic within the automotive industry and they play an important role in consumers' purchasing decisions. Just-Auto published a review and forecast on the global market of automotive lighting and stated: "Automotive lighting technology is evolving at an unprecedented and accelerating pace" [23]. This statement embodies all vehicle lighting functions and although light emission components (e.g. head lights) are significant, consumers have shown strong emphasis towards safety performance and crash avoidance. Retroreflection provides the automotive industry with an pivotal tool to increase road safety and therefore makes the manufacturing of RRs essential.

1.6 Objectives

This research has been in collaboration of and in continuation of the preliminary development of the USPIC technology. The objectives have been separated into the following categories: 1. manufacturing strategy improvements and process planning, 2. assessment of geometrical accuracy and surface quality, and 3. preliminary investigation of cutting mechanics. The manufacturing strategy has a large impact on process efficiency

and its capability. Geometrical accuracy and surface quality directly impact optical performance and a benchmark of conventional RRs has yet to be established. Cutting mechanics provide insight into the tool-workpiece interaction and help to identify complications within the process.

The efficiency of the manufacturing method relies upon several factors. This study focuses on reducing machining time and increasing the versatility of the process. Machining time is to be reduced through sub-routine coding and the reduction of auxiliary motions. Versatility is being improved with regards to structure positioning and alternative structure patterns. Process planning allows for optimization of cutting parameters and logical machining order of structures. Similar studies have been done on separate microcutting processes [24, 25].

The accuracy of the fabricated structures is important to their functionality and therefore a consistent observation and assessment procedure is required. Documentation of initial achievements and advancements would be helpful for the progression of this research. Additionally, information regarding surface quality of the traditional pin-bundling technique has not been reported. The lack of historical data makes it difficult to benchmark this novel manufacturing method and therefore an assessment of the entire pin-bundling process is required. Preliminary analysis of USPIC fabricated structures is to be completed. It is common for micromachining technologies to evaluate fabricated surface roughness [26, 27].

Cutting mechanics of the novel manufacturing process are to be recorded and described in detail. The reason this is necessary is to initiate a greater understanding of the unique

cutting kinematics and overall fabrication method. Although the process has similarities to turning the short and interrupted cuts make the processes distinct. Cutting force characteristics and their relationship to the tool cutting position need to be clearly identified. Relationship between cutting mechanics and chip thickness (i.e. depth of cut) will also be observed. The understanding of a process's cutting mechanics provides significant benefit when trying to improve upon accuracy, increase tool life and avoid excess undesirable cutting forces. Cutting mechanics of micromachining processes is a relatively new research area [28].

1.7 Contribution

The overall contribution of this thesis is the continued development and improvement of the novel USPIC manufacturing method. However, under closure inspection the contribution is several progressive steps towards advancing this technology – an accumulation of multiple smaller contributions. These can be summarized in relation to the three previously outlined objectives. Manufacturing strategy improvements and process planning, assessment and improvement of surface quality and geometrical accuracy, and preliminary investigations of cutting mechanics.

Improvements of the manufacturing strategy include the development of the integrated strategy and a detailed description of the primary strategies kinematics. Also, sub-routine style post-processing was introduced to benefit process efficiency. Process planning has been improved through the implementation of image pixelization and a new “checkerboard” structure arrangement.

An optical analysis fixture was built for a more concise and replicable observation process of retroreflective samples. Advanced surface assessment data collected on multiple phases on the pin-bundling technique. Effectively benchmarking the universal manufacturing process for the automotive industry. Equal surface assessment conducted on USPIC samples.

Initial cutting mechanics of the primary strategies documented and analyzed. Detailed association between cutting kinematics and mechanics. Preliminary understanding of cutting mechanics developed through strategic experiment configurations. Critical recommendations regarding kinematics.

1.8 Overview

In conclusion of this chapter a brief synopsis of the following content will be described. The organization of this thesis is relevant to its three objectives and the chapter configuration will follow an identical structure. In contrast, the path in which this research followed was much more fluid and continually adapted to changing motives – as does most research.

Chapter 2 can be summarized as cutting kinematics and manufacturing strategies. Within this chapter a detailed description of the two primary modes of material removal will be detailed. Critical positions within these strategies will be defined and used throughout the thesis. Each of these strategies is in accordance to a single retroreflective structure, more specifically an RTP structure. These strategies are repeated for each structure within the desired fabrication and therefore an additional aspect, structure arrangement, is added to this chapter. Structure arrangement is the position or location of a structure in relation to

adjacent structures. Once an arrangement is determined the next step is to determine the true coordinates of each structure with respect to the workpiece. In order for this to be done the desire area needs to be identified, whether it be a geometric shape or complex image. Finally, once the strategies are defined and the process is understood the chapter will conclude with some experimental validation.

Chapter 3 will logically follow by taking these USPIC fabricated samples and assessing the fabricated structures. Since TIR and reflection are dependent on surface quality, surface analysis of the participating retroreflective facets is practical. Increased surface roughness correlates to increased scatter and therefore poor surface quality reduces retroreflective efficiency. Characteristics relating to surface imperfections will be identified. It is common to assess surface quality during microcutting [29].

Without any historical data on the quality of the retroreflective optics being made it is difficult to assess the state and progress of this technology. Therefore, the next logical step is to complete a comprehensive analysis of the pin-bundling technique, including its three phases. This information, to our understanding, has not been previously disclosed and the current industry testing does not involve surface/geometric assessment. Rather, the industry is conducting pass-fail testing of final product parts using an application based apparatus. Information regarding the geometric accuracy and internal steps of the process is either being withheld or not assessed. The information documented in this study has been recorded from limited or singular sample of each phase of the pin-bundling technique. Therefore, the data is only a single example of industry quality. However, it is a significant improvement over the current absences of data. Once complete, this chapter establishes a precedence for automotive retroreflective lenses

and gives this technology an ability to benchmark itself and identify progression with respect to structure quality.

The fourth chapter of this thesis is crucial once surface quality improvements are desired. The observations made in the Chapter 3 show significant complications in regards to surface quality. It is suspected that the problems are associated to tool wear and cutting mechanics. Under this assumption, the next logical step was to establish a experimental setup for measuring cutting forces during the USPIC process. The concept being that this data would provide incite into the cutting mechanics and identify critical areas within the defined strategy kinematics. Within this chapter the experimental setup will be described as well as the physical configuration of the experiments. The primary strategies will be analyzed separately and across slightly different configurations. Force profile characteristics will be clearly identified with respect to critical positions and motions establish in the second chapter. The acquired data presented in this chapter will contribute as a preliminary investigation of the USPIC cutting mechanics and will help progress this research in the future.

Chapter 5 is the conclusion of the work presented in this thesis and includes a summary of the critical aspects and advancements made to the USPIC technology. The observations made throughout the previous chapters are significant for future recommendations. The progression of this work does not conclude here as collaboration and extension of this work has already begun. Within this chapter specific recommendations will be made in regards to observations related to cutting kinematic, process planning, surface quality and cutting mechanics. Also, a brief outline will be included of the future of this work and the efforts being made in separate newly established branches.

CHAPTER 2

Strategy Improvements and Process Planning

2 Strategy Improvements and Process Planning

2.1 Manufacturing Setup

Similar to DMC, USPIC makes use of a monocrystalline diamond (MCD) cutting tool as mandatory prerequisite for adequate retroreflective efficiency (and hence the term “ultraprecise”). However, the geometry of the tool used in USPIC operations has been tailored to RTP fabrication and therefore it is significantly different than that used in the fabrication of CC geometries. While having a custom-design, the geometry of the USPIC cutting tool is comparable to that of a grooving tool that typically used in turning operations (Figure 2.1). The wedge angle was chosen to be 50° to prevent the adherence of the chips to the adjacent RTP facet, especially since this could potentially damage its surface finish as the tool reaches the root of each cut. This angle does contribute to a large positive rake angle that is far from being ideal for machining purposes [30], and therefore could be regarded as more of an RTP-fabrication compromise. The width of the tool determines the smallest possible structure size, but larger structures are possible by effectively cutting multiple structures next to one another. Currently the tools which are used in this research range from 0.1 – 2.0 mm in width.

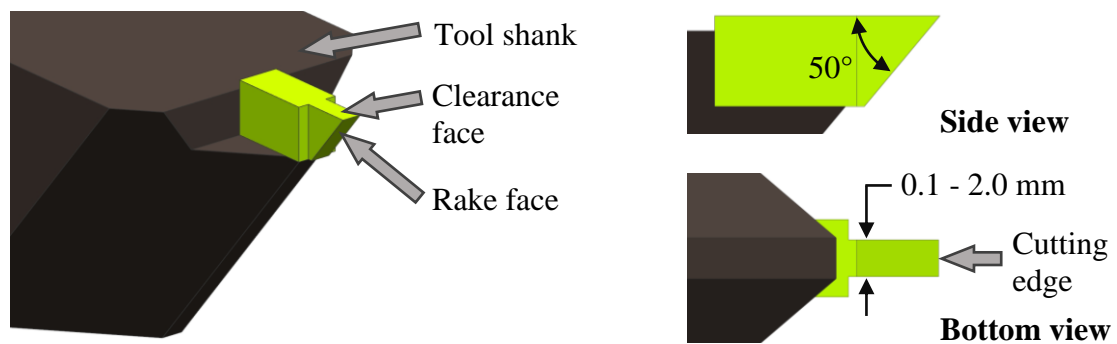


Figure 2.1 Geometry of ultra-precise single point inverted cutting tool

This tool is mounted in a Kugler Microgantry 5X micromachining center. This is a vertical CNC machining center with trunnion-style rotary axes and aerostatic bearings specifically designed for micromachining and microstructuring. The configuration of this machine is such that the base supports the X and Y axis motions independently. The X axis supports the Z axis and tool holder while the Y axis supports the A and C rotary axes. Finally, the workpiece is mounted atop the C rotary platform. The machine and its configuration can be seen within Figure 2.2 below.

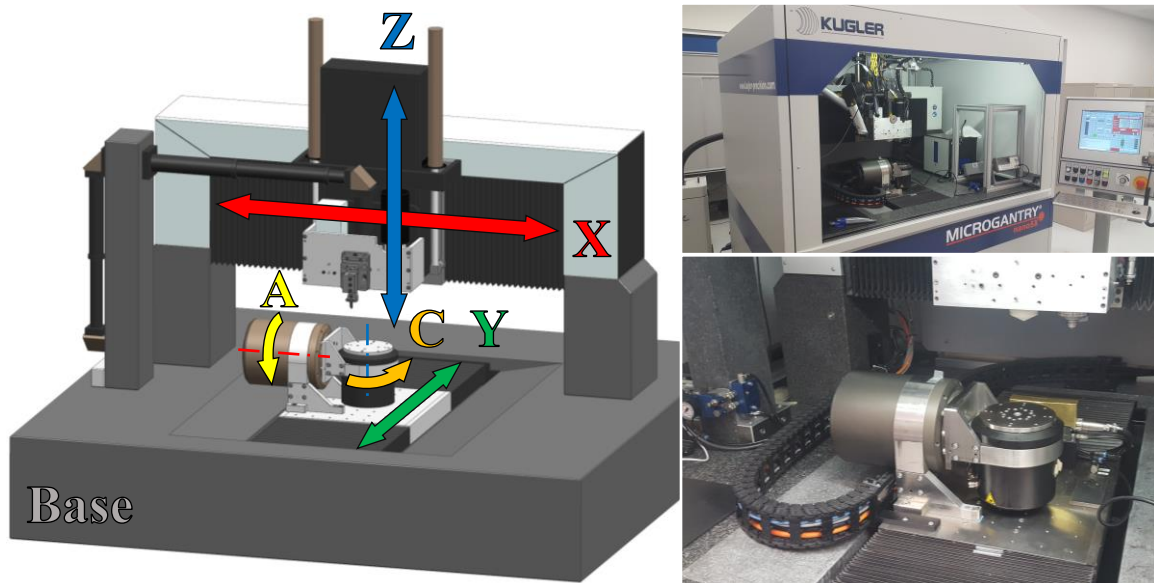


Figure 2.2 Kugler Microgantry 5X CNC micromachining center

The premise of this research is to directly machine retroreflective structures into the injection moulding die. However, for this study the workpiece material was primary acrylic. The reason acrylic was chosen is because during machining and preliminary code verification acrylic is more forgiving and allows for a prolonged tool life. Additionally, using acrylic allows for direct optical testing in contrast with automotive lenses. The common acrylic sample used in this study has dimensions 30 x 30 x 0.5 mm and is

transparent. These samples were fixtured using a vacuum stage mounted on the C-axis of the CNC machining center. Aluminum alloy 6061 was also used as the workpiece material for a single fabricated sample. This sample was fixtured using adhesive which was removed post fabrication. The aluminum sample was fabricated such that a hot embossing press may replicate the retroreflective structures on to a transparent plastic. However, the completion of this task has been left for future efforts. Within this study the aluminum sample provides the notion that this technology is versatile among its design, fabrication and the material selection.

Micromachining involves the removal of material and chip evacuation is still important, despite the miniature scale at which this microcutting take place. The Kugler system uses a spray mist coolant system which is orientated by the operator. The spray mist is a combination of compressed air and isoparaffinic fluid. The fluid acts as a lubricant on the rake face of the tool and provides additional lubricant between the forming chip and remaining workpiece (self-contact). The force associated with the compressed air helps to evacuate chips once they are separated from the workpiece. If chip evacuation is not sufficient, extreme complications arise. Upon completion of fabrication, chips which are not removed are generally stuck within the retroreflective structure. Additional spray mist and flooding of the surface may be successful in removing the remaining chips but it is not a guarantee. Prior to this complication there is a more significant problem which may arise during the machining process. If during the fabrication, the chips begin to stick and accumulate and increased amount of force is placed on the tool. If the chip build up becomes excessive the tool can and will fracture. In addition to the spray mist coolant/lubricant, chip removal techniques must be designed into the fabrication strategies.

2.2 Material Removal Strategies

Typically, when manufacturing a retroreflective component several identical structures are fabricated adjacent to one another. This allows the designer to increase the retroreflective surface area without increasing the components thickness. Currently USPIC also uses several identical structures in an array to cover a specified surface however this technology is not limited in doing so and can have diversity with respect to the structures dimensions if that is desired. Regardless of the changes to the RTP dimensions the cutting strategy for each structure follows the same logic. The material removal strategy is relevant to an individual structure and is repeated for each consecutive structure. There are two primary material removal strategies used in USPIC – these are termed unidirectional and bidirectional which is in relation to the singular and dual cutting directions the strategies have respectively.

2.2.1 Unidirectional Strategy

The kinematics of this strategy requires completely different cutting mechanics for each of the two facets of the RTP structure. As depicted in Figure 2.3, the cutting tool engages the vertical facet in a way that is conducive for the achievement of a higher quality surface finish, while the horizontal facet is engaged in a manner that typically results in a lower surface finish. The vertical and horizontal cutting motions have been termed plunging and ploughing. The unidirectional USPIC strategy is implemented through cycles where each cycle is defined by a cutting depth with respect to the RTP height. Each cycle starts with positioning the cutting tool at a clearance height above the root of the current plunging motion. This is described as position A_i in the represented cycle below (Figure 2.3). The vertical plunging motion then commences and the tool tip travels

from point A_i to B_i (motion 1). This position, B_i , is synonymous with the initial contact of the tool with the surface of the workpiece. As the tool continues from position B_i to C_i (motion 2) the chip is formed through the single point inverted cutting process. The next horizontal ploughing motion from position C_i to D_i (motion 3) is required to release the chip by shearing its lower edge from the adjacent surface. At this point the chip is removed by a stream of compressed air and cutting lubricant. To complete the unidirectional cycle, the tool retracts vertically to position E_i (motion 4), avoiding any collisions, and translates to the next cycle start position A_{i+1} (motion 5).

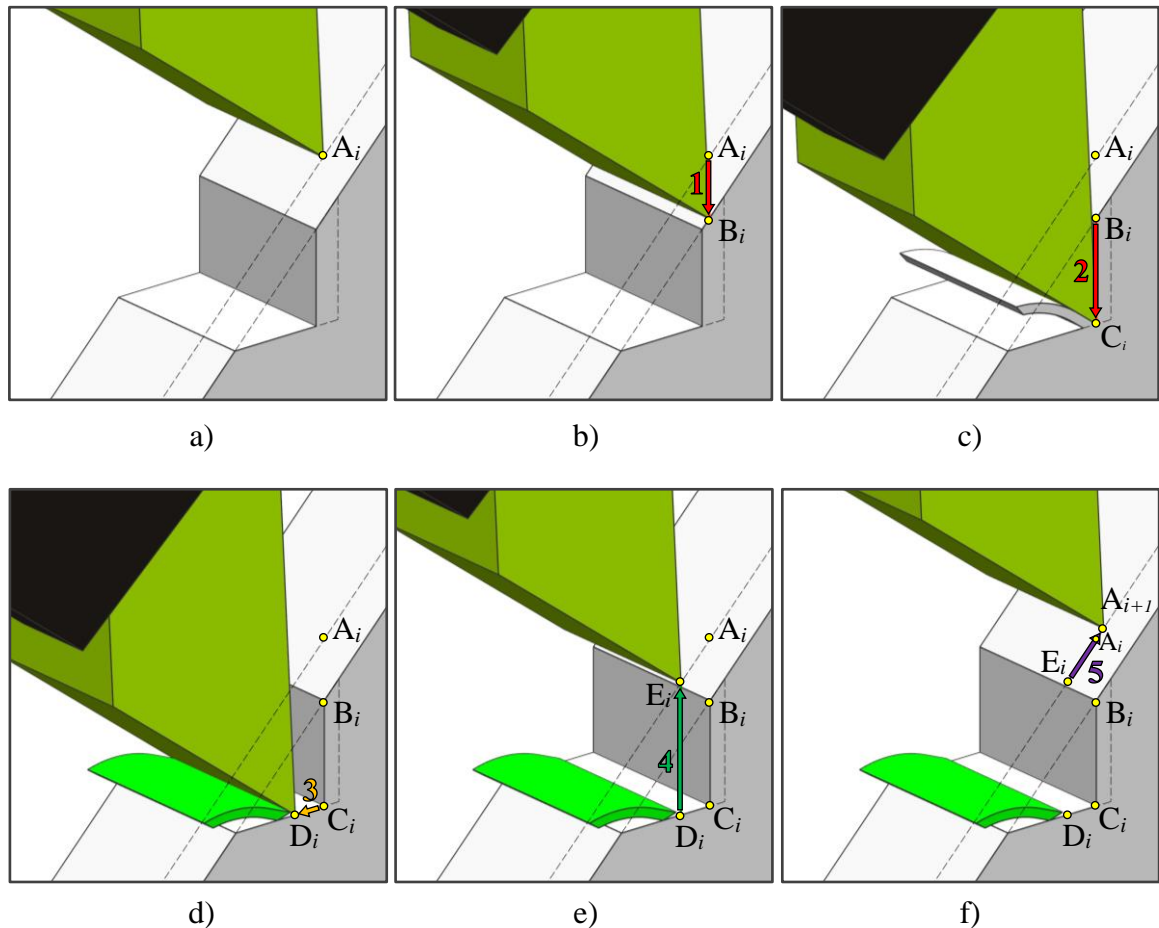


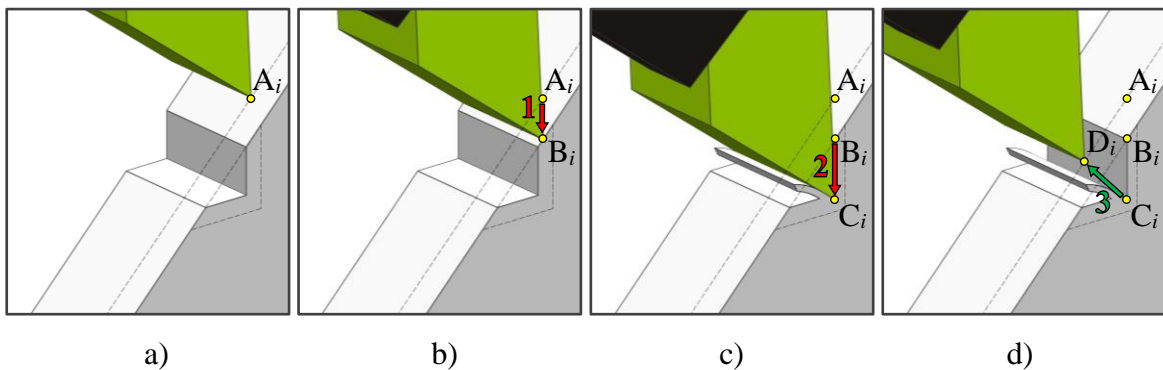
Figure 2.3 Single cycle of unidirectional USPIC strategy: a) cycle start, b) motion 1: plunge, c) motion 2: plunge continued, d) motion 3: plough, e) motion 4: retract, and f) motion 5: translate

In this regard, plough cutting is associated with a clearance angle of at least 90° . This configuration results in a negative rake angle equal to or greater than the wedge angle. By contrast, plunge cutting is associated with a cutting mechanics characterized by a small clearance angle and positive rake angle. Since the surfaces cut through plunge or plough cutting contribute directly to the optical functionality of the RTP, this unidirectional strategy tends to be insufficient/inappropriate to generate the required surface finish. However, its high material removal rate makes this strategy a good candidate for roughing procedures in which surface finish is not the main concern.

2.2.2 Bidirectional Strategy

By contrast with unidirectional USPIC approach, the kinematics of bidirectional strategies results in superior cutting conditions for both RTP facets as it shown in Figure 2.4. However, while three-axis motions are sufficient for unidirectional instances, bidirectional cutting scenarios typically require the full functionality of a five-axis machining system. The bidirectional USPIC strategy is also implemented through cycles where each cycle is defined by a cutting depth with respect to the RTP height. Similar to the uni-directional strategy each cycle starts with positioning the cutting tool at a clearance height above the root of the current plunging motion. Once again, this is described as position A_i in the represented cycle below (Figure 2.4). The vertical plunging motion then commences and the tool tip travels from point A_i to B_i (motion 1). The tool continues from position B_i to C_i (motion 2) and half the chip is formed. Position C_i in this strategy is different from the previous strategy as the tool tip engages slightly into the adjacent facet equal to the depth of cut. At this point in the cycle the tool retracts along the bisector of the RTP from position C_i to D_i (motion 3) finishing at the

clearance height. Following this step the workpiece is rotated about the C-axis (orange arrow, Figure 2.4e to 2.4f), typically the C-axis is not located in a desirable location with respect to the RTP structure being cut. Therefore, after the rotation is complete the tool is required to be repositioned at the beginning of the adjacent side plunging motion (motion 4). This new initial position for the adjacent facet is represented as position A_i' . The remainder of the cycle is symmetrical to the initial 4 motions apart from the facet in which it produces. At position C_i' the chip is fully separated from the workpiece and the pressurized stream of lubricant can evacuate the chip. In Figure 2.4 the bi-directional strategy has been simplified by located the C-axis (orange arrow) along the midplane of the width of the RTP. This was done to clearly represent the cycle in a pictorial manner however in common practice this is not the case. Thus, motion 4 and 4' are continually changing and are not bound to a specific vector. The translational motion is always parallel to the clearance plane that is offset from the top surface of the workpiece but its direction and magnitude is directly dependent on the location of the RTP structure with respect to the C-axis.



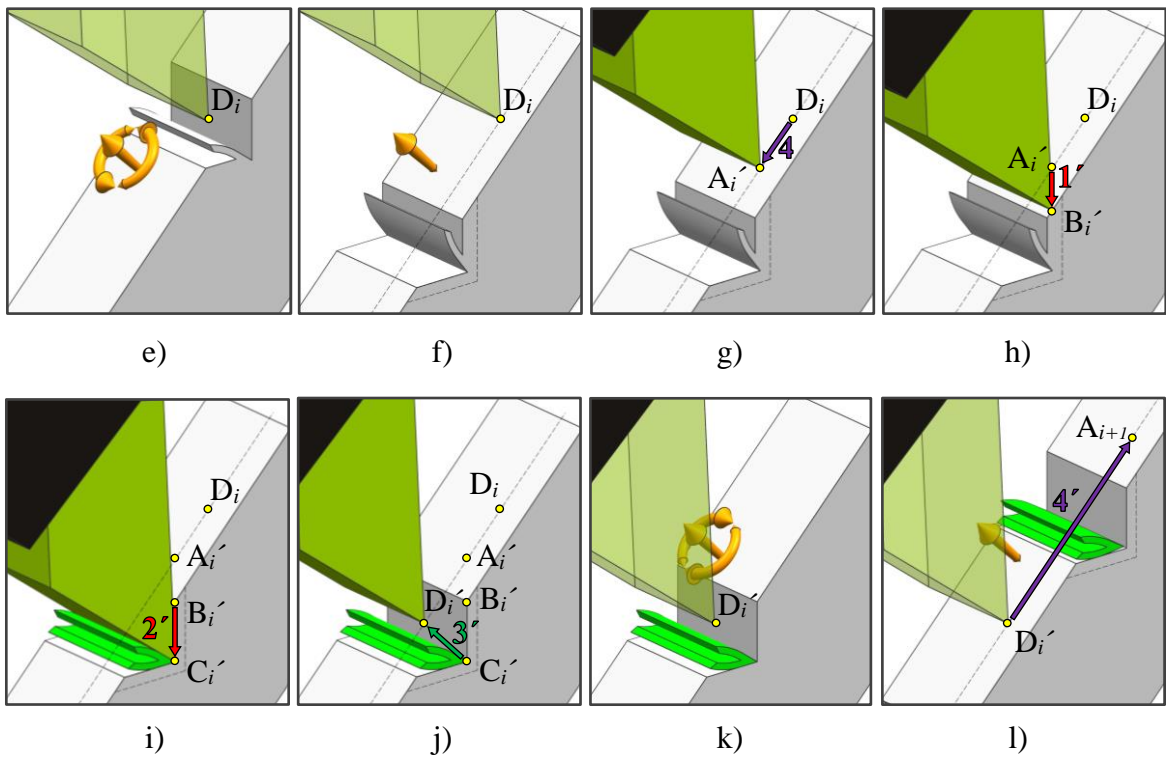


Figure 2.4 Single cycle of bidirectional USPIC strategy: a) cycle start, b) motion 1: plunge, c) motion 2: plunge, d) motion 3: retract, e) rotation around C-axis, f) rotation complete, g) motion 4: translation to compensate rotation around C-axis, h) motion 1': plunge, i) motion 2': plunge, j) motion 3': retract, k) rotation around C-axis, and l) motion 4': translation to compensate rotation around C-axis

The primary role of the two rotary axes of the five-axis machine is to adequately align the cutting tool with the RTP facets to be cut. This type of machining is also known as $3\frac{1}{2}/2$ -axis machining, because the rotary axes are held stationary as the tool removes material [31]. In this bidirectional approach, the two active facets of the RTP are being cut alternatively (always from their “aperture-proximal end”). Because of this strategy, “ploughing” becomes unnecessary since the entire RTP can be generated by means of “plunging” motions. However, since the relatively low feed rate of the rotary axes increases the overall machining time, bidirectional approach will primarily remain an appropriate option for RTP finishing operations.

2.2.3 Two-Step Strategy

Following the discussion above, it becomes apparent that an enhanced RTP-cutting strategy would include separate roughing and finishing procedures. Along these lines, the unidirectional USPIC strategy has been used to rough-cut the structure and resulted in a near-complete geometry, while the bidirectional USPIC strategy has been used as a finishing procedure.

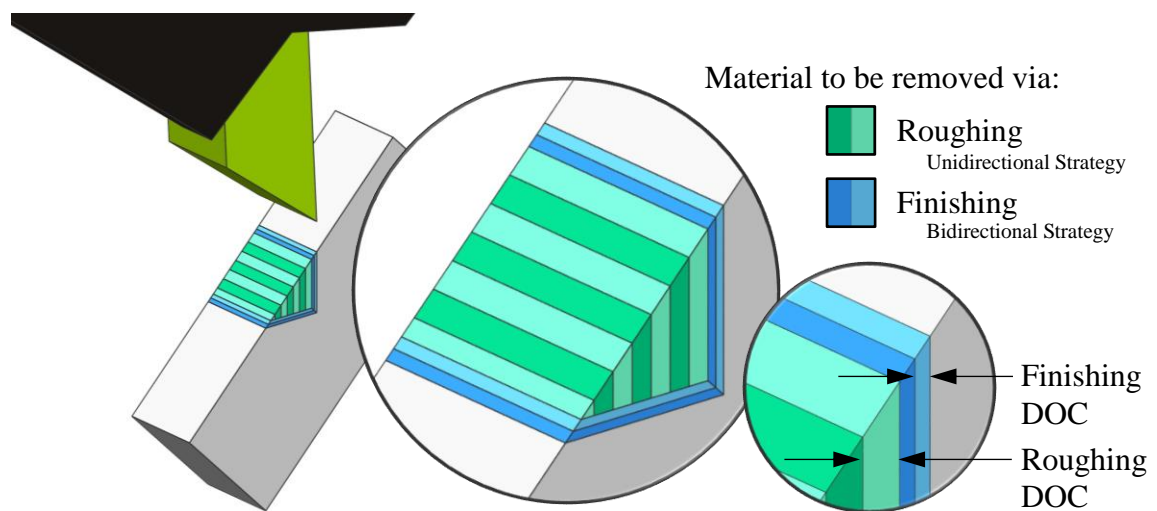


Figure 2.5 A representation of strategy specific material removal volumes for the two-step USPIC strategy (DOCs oversized to clarify concept)

This strategy represents a further iteration of the original $3\frac{1}{2}/\frac{1}{2}$ -axis cutting that was introduced in the past [22]. While most of the process settings and parameters were kept unchanged, a special calibration protocol was devised and used to ensure the post-indexing parallelism between the RTP facet and the rake face of the diamond tool. In this context, it is important to note that the calibration procedure requires that the tool alignment be within $\pm 1 \mu\text{m}$ in order for the chips to be properly released from the workpiece throughout cutting.

2.3 Structure Arrangement

Once the material removal strategy is determined the next task is to locate each of the individual structures. An RTP has a rectangular aperture and if the base of the structure is set equal to its width the aperture becomes square. The geometric description of an RTP can be seen in Figure 2.6. Although there are many patterns which can totally consume a surface using rectangles these arrangements are not present in this study and are currently in development. For simplicity, an RTP with a square aperture was chosen for producing larger surface arrays.

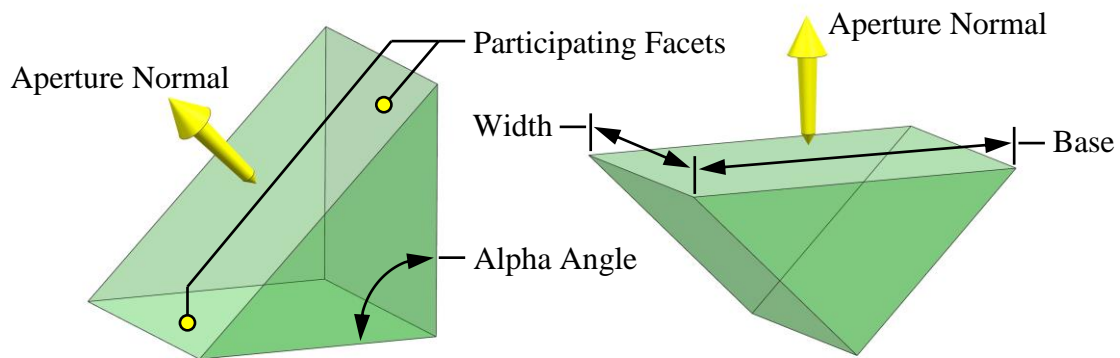


Figure 2.6 Geometric identification of RTP structure nomenclature

The initial arrangement includes rows of RTPs running along the structures base dimension. Each row is offset to the adjacent row by half the length of the base dimension (Figure 2.7). If the offset is not present, the structures' facets are coincident and the structures aligned to create V-shaped grooves. When the offset is implemented on every other row the area becomes skewed. For example, if a 4 x 4 array of RTPs is desired then the 2nd and 4th row would be offset and by offsetting these rows the height of the array increases by half the length of the structure's base (Figure 2.7). This small change in height

is typically insignificant however within micromachining, or machining in general, it is best not to exceed you predefined profile. A simple logic has been added to remove this effect, each even numbered row is shifting in the positive direction by 50% of the base dimension and the first structure in each of these rows is removed. This eliminates the elongation of the array but it reduces the amount of RTPs within the array by half the quantity of rows. Therefore, instead of 16 RTPs within a 4 x 4 array there would be 14.

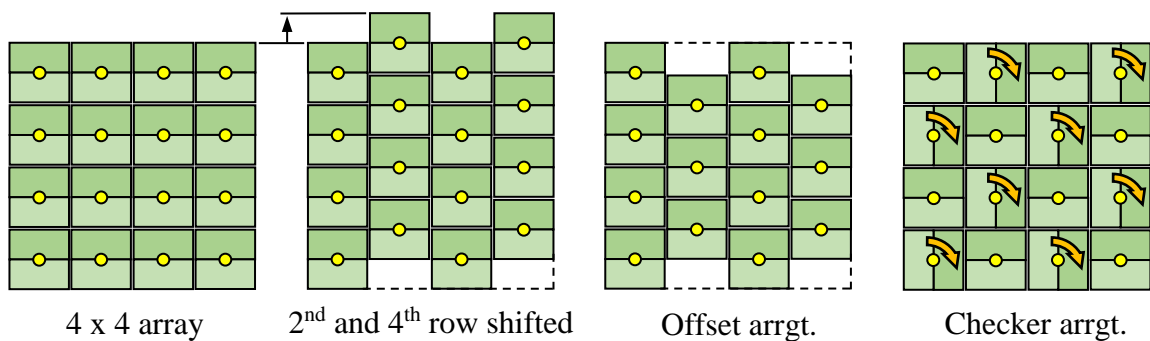


Figure 2.7 The offset and checker arrangements and the manipulation of the structures

The next arrangement is achieved by rotating the orientation of the structures 90° from adjacent structures. When the structures are configured in this manner the it resembles that of the traditional checker pattern. There are several benefits to this arrangement however it requires more effort in regards to process planning and machining. One advantage to this arrangement is that the predefined profile does not get skewed because the aperture is square and fills the same amount of area when rotated 90°. A greater advantage is seen in its optical performance because the rotation of half the structures allows this the RR to operate sufficiently under two separate rotational axes.

2.4 Image Rasterization

After the structure arrangement is defined the next step is to determine what area is desired to be cut. Typically, an entire surface would be filled with RRs however for other purposes, such as automotive lighting aesthetics, a designer may want to add a company logo or perhaps warning/alert symbols to a lighting component. In this circumstance the area becomes intricate and the effort needed for locating the structures becomes vast. Therefore, an image rasterization code was implemented to quickly define cutting coordinates for each RTP and improve the capability of this technology.

The desired image is first acquired from an external source and edited using a standard graphics program. Editing is necessary because the code associates each pixel to an individual RTP structure. Therefore, if you want to fabricate a surface with dimensions 20 x 30 mm, using a 0.5 mm tool width then the image needs to be modified such that its pixel dimensions are 40 x 60.

$$\frac{\text{Surface Size}}{\text{Structure Size}} = \text{Image Size}$$

$$e.g. \quad \frac{20 \times 30 \text{ mm}}{0.5 \times 0.5 \text{ mm}} = 40 \times 60 \text{ pixels}$$

Then using MATLAB software, the image is brought in and convert to grayscale. Each pixel is then given an intensity from 0 – 255, white being represented as 255 and black as 0. The operator defines a cut-off threshold for pixel intensity such that each pixel is either 1 or 0, these values represent cut or do not cut respectively. This produces a binary image and the threshold can be adjusted to better suit different images. The images presented in

Figure 2.8 below were created using a 70% cut-off, therefore only pixels with an intensity less than 179 are set to be cut.

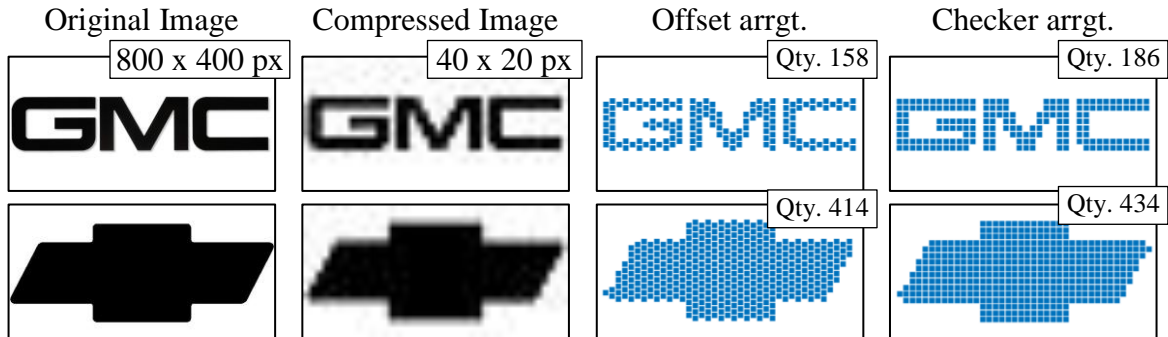


Figure 2.8 Image rasterization for defining RTP structure location during USPIC

As seen in Figure 2.8 the image quality is dependent on the compression and the structure arrangement. The checker pattern does not require pixels/structures to be shifted and as a result the image quality is generally better. However, these images were presented with a low quantity of structures to better observe the difference in arrangements. If these images were fabricated using a 0.5 mm tool they would only cover 20 x 10 mm therefore it is likely that the emblem or logo would be larger. If the number of structures increased (i.e. increased image size, increase surface area) the quality of the image, specifically the visual appearance of its edges, would increase significantly and the effect of the offset arrangement would be less noticeable.

2.5 Post-Processing

The image rasterization code also contributes to the post-processing by retrieving the tool width specified by the operator and it calculates the structure coordinates relevant to each pixel. The code positions the structures symmetrically about a predefined point. Each

coordinate is representative of the centroid of the aperture. This is helpful when using the checker arrangement because the 90° rotation does not affect the structures position. All of the coordinates are associated to the workpiece coordinate system (WCS) with both rotational axes of the machine set to 0° . The movement of these points is complicated and dependent of 5 axis machine kinematics. During USPIC fabrication the A-axis is positioned at 45° with some deviation depending on desired clearance angle. Additionally, the C-axis is rotated 180° multiple times during bidirectional cutting and therefore it is essential to have an accurate transformation matrix that is representative of the machine in use. The comprehensive transformation matrix being used in USPIC technology includes axial misalignment of the A and C axes and was first presented here [22]. This transformation matrix allows each structure to be located regardless of the position of A and C.

Currently each structure within the array is identical and therefore can be fabricated using the same series of tool motions. Once a structure is located via the transformation matrix the tool translates to a routine start position. The start position vector is dependent on the active sub-routine and the A-axis position. This vector is the difference between the centroid of the aperture and the start position. After the transformation locates the structure this vector is used to offset the coordinates so that the tool moves to an appropriate position at a clearance height and in-line with the sequential cut. From this position the active line within numerical control (NC) programming code is directed to the beginning of the sub-routine. Separate sub-routines are used for the different processes of roughing and finishing. The reason the routines are separated is because of the 180° C-axis rotation that is required for the bidirectional strategy. If the routines were combine that would result in the machining process to undergo two C-axis rotations for each RTP structure. Since the

rotation consumes a significant amount of time and the quantity of structures can be upwards of thousands this is not ideal. Instead the routines are separated and therefore the code can execute roughing and finishing of one side for each structure prior to the first C-axis rotation then the code executes the first finishing pass of the 2nd facet and the second rotation is performed. If the routines were combined the program would execute roughing of a single structure and then finishing of that same structure and then move on to the next structure after complete. For example: to fabricate 25 structures with 2 finishing cuts on each facet – a combined routine would perform 100 rotations (4 rotations for each structure) however when separate only 4 rotations would be required. When the routines are separate the number of rotation is solely dependent on the desired number of finishing cuts. Sub-routines allow for a more versatile and effective process planning and the significant reduction in C-axis rotation greatly reduces the machining time.

Sub-routines were also implemented in incremental coordinates therefore the cutting motions are not effected by the transformation matrix. The reason this is a beneficial is because the tool is aligned with respect to the Z-axis and the cutting motions are relevant to the tool orientation. The strategies outlined above make use of Z and Y axes motions and both strategies require a constant X-position. If the cutting coordinates are sent through the transformation matrix the axial misalignment contributes to slight movements in the X-direction. Any X-axis motion during cutting is not desired because the tool geometry does not support cutting in this direction.

In addition to these improvements an additional variable was added to the post-processing code. The original assumption and theorized value for the alpha angle of an RTP is 90°, this angle contributes to the light being redirected parallel but opposite to the incident light.

Slight decrease in the angle causes convergence and divergence occurs upon an increase [14]. These both cause light to scatter and therefore contradict the definition of retroreflection. However, the ability to manipulate this attribute allows the manufacturer to tailor the structure to the specific optical function. Many applications of RRs do require light to scatter slightly, for example if light did not scatter off tail light RRs of vehicles the RRs would only be visible inline with the head lights of the oncoming vehicle. Since the driver's line of sight is elevated from the location of the head lights the RRs need to scatter the light slightly for the driver to see them.

The post-processor also uses the specific NC programming language to display progress data. The final code which is written for the Kugler keeps track of current structure being cut and this information can be retrieved while the fabrication is occurring. The NC code displays progress reports on the Kugler controller when the roughing process is 25, 50, 75 and 100% complete. The finishing progress is separated with regards to the users defined number of finishing cuts. The program will display which cut is currently being performed and on which facet (e.g. Finishing cut 1 of 3 C-axis at 180°). The structure tracking variable is also reset and used to count again during the finishing procedure. These improvements to the post-processing code allow for a much greater process monitoring ability.

The consolidated MATLAB code incorporates each of these aspects of post-processing to produce an NC code compatible with the Kugler Microgantry. Prior to running the code a dramatic alignment procedure must be performed. The alignment procedure is used to determine the vector displacement between the Renishaw probe and the center of the cutting edge of the tool. The accuracy of this vector is of the utmost importance and deficient establishment of this vector will cause improper cutting kinematics. It is critical

to obtain an accuracy of $\pm 1 \mu\text{m}$ during the alignment procedure. In addition to establishing this vector the post-processing code requires a few more details before the code can run correctly. The transformation matrix requires an accurate representation of the rotational axes on the machine and therefore each axis needs to be defined by a point (i.e. rotational center) and a vector (i.e. rotational axis). Thankfully, these details are defined by an included operation within the Kugler's internal functions. As mentioned previously the transformation matrix is comprehensive and includes axial misalignments, an example of this will follow. The A-axis is described as a rotary axis about the X-axis and therefore its rotational vector is theorized as (1,0,0). However, this is never truly the case and during the mounting and fixturing of the axis a misalignment arises. For example, the internal calibration of the Kugler shows that the A-axis rotational vector is precisely (0.9999999681, 0.0001291168, 0.0002169075). The misalignment is of a very small scale however it is not negligible because of the micro-scale features which are being fabricated. The final information which is required before running the post-processor is the WCS. After the vector between the Renishaw and the tool is established the location of the WCS can be found using the Renishaw probe. Now the post-processor is calibrated for the machine and current setup, which includes the 5-axis machine kinematics, workpiece fixturing, and tool orientation.

To run the post-processor the user must define the manufacturing parameters, these include structure size and geometry, tool width, clearance angle and height, chip thickness for both roughing and finishing, and respective feedrates. After the code commences the user is prompted for the NC code title and depending on the desired fabrication, the user may be prompted with the image rasterization code. The code then requests an image to be

processed and converted into structure coordinates. The post-processing completes and displays several figures, these include vector representation of tool path for the roughing and finishing strategies separately. If the image rasterization code is used the code will also display a representation of the structure arrangement. The important outcome of the post-processor is that it produces a separate file, the NC code, which is directly used for fabrication with the Kugler micromachining center.

2.6 Validation of Fabrication Technique

Once the NC code is written, the next step is to validate the code and the fabrication process. This is an important step because improper process coordinates may and typically will cause damage to the tool, workpiece, or worst case the micromachining center. Since the NC code is being written through a novel post-processing program it is generally difficult to simulate this code. Most computer aided manufacturing (CAM) programs do not supply this reverse feature and only simulate machining code which was defined through features within the relative program. Within this study a software called Vericut was used to validate the post-processing code. This software has the ability to take low level NC code and simulate tool path and material removal. Before this could take place the Kugler CNC machining center needed to be represented as a 3-dimensional model. A accurate computer aided design (CAD) model was created in Siemens PLM Software NX. The model then needed to be imported and configured within Vericut using this software's tools for defining the machine kinematics. The geometrical representation of the machine, its kinematics, and tool path helps to identify code errors, potential collisions, and limits within the fabrication process. Figure 2.9 below shows a visual representation of the successful Vericut code validation.

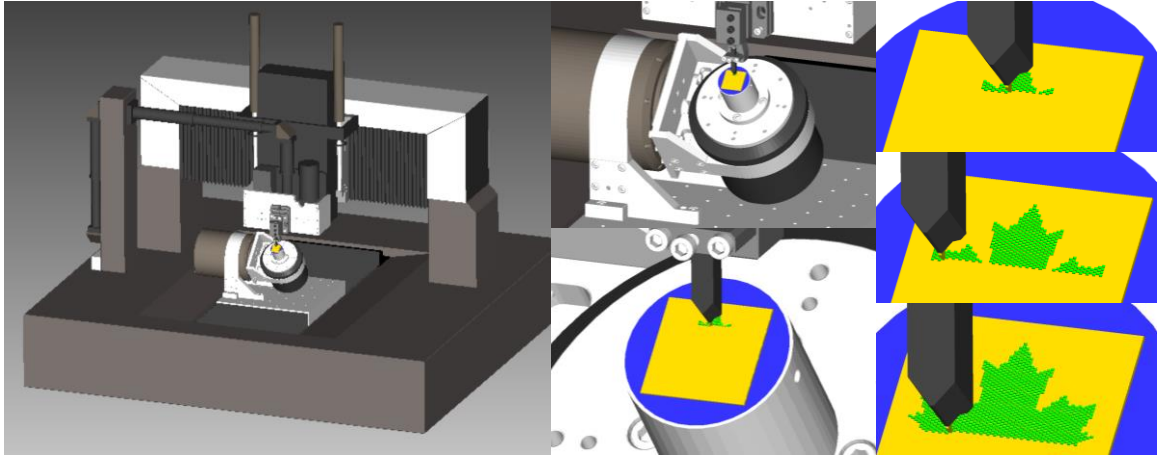


Figure 2.9 Computer aided manufacturing (CAM) simulation of USPIC strategy using Vericut software

After validation, the post-processing via Vericut, it could then be used safely with the micromachining center. Multiple samples were cut within the 0.5 mm thick acrylic and a single sample cut in aluminum. All with the offset structure arrangement and of aperture size $451 \times 451 \mu\text{m}$. These samples include a square array (25×25), a maple leaf, a National Research Council (NRC) and University of Western Ontario (UWO) abbreviation, and Chevrolet logo (bow tie emblem). The quantity of structures within each of these sample is respectively 613, 1244, 1150, and 919. The ability to fabricate these samples provides validation to the post-processing program and material removal strategies while demonstrating the feasibility of this technology. These samples can be seen within Figure 2.10 and the optical function of these samples can be qualitatively assessed using these photographs. The acrylic samples in the photographs are orientated such that the cut structures are upon the opposite face. This allows TIR to occur and retroreflection to take place. The area machined on to these samples stands out from the stock workpiece seen in the lower left of the figure therefore signifying a functional retroreflective area.

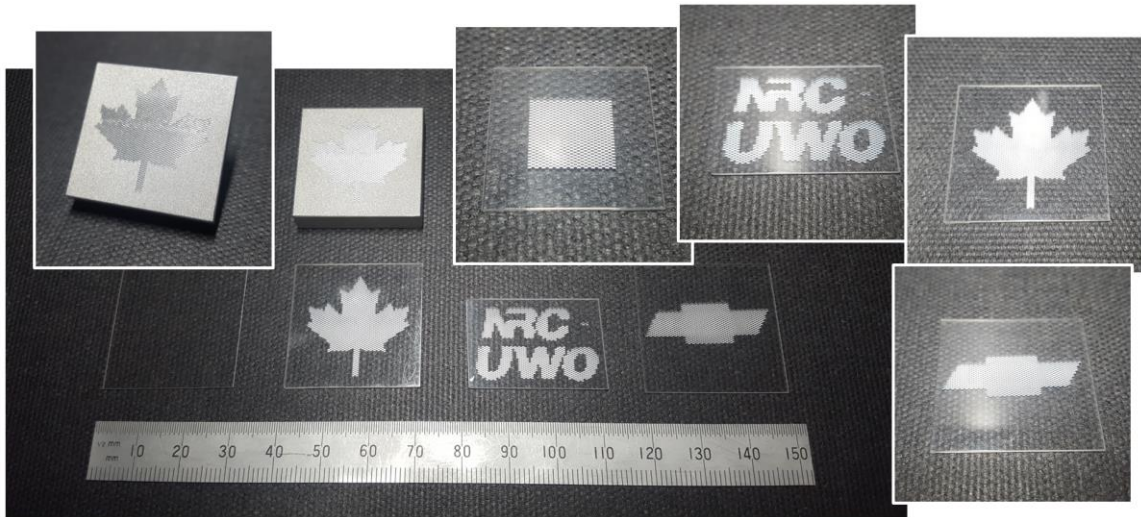


Figure 2.10 Retroreflective samples fabricated via USPIC technology in the offset arrangement

The checker structure arrangement was developed at a later date in the progression of this research and therefore only one sample has been fabricated. The area which was fabricated is a 4 x 4 array with RTP aperture size of 947 x 947 μm . The workpiece is transparent acrylic similar to previous samples however the stock workpiece was thicker, approximately 6 mm. This sample as well as the contrast between the structure arrangements is presented in Figure 2.11. This figure displays a direct comparison between structure size and arrangement. It demonstrates RTPs with different aperture sizes, the checker arrangement consists of structure approximately twice the size of the offset arrangement.

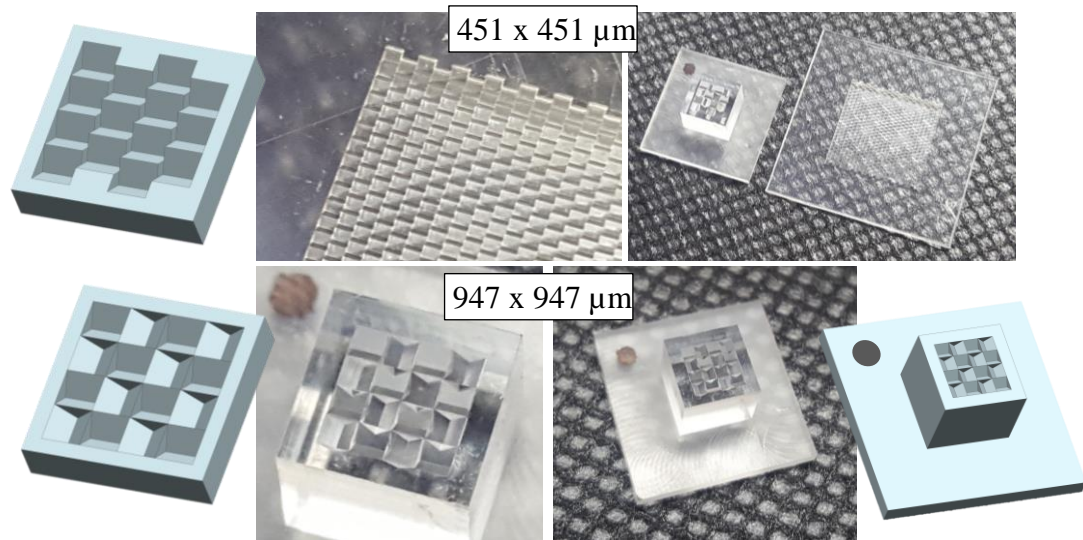


Figure 2.11 Visual appearance of structure arrangements and the 4 x 4 checker arrangement sample

2.7 Assessment of Machining Time

During the fabrication of the samples that have the offset arrangement the machining time was recorded. The machining time is heavily dependent on the manufacturing parameters and therefore this data is only a single representation of the fabrication time. The above samples which were fabricated in the 0.5 mm thick acrylic were all fabricated with the same manufacturing parameter. These parameters are as follows: structure width and base 451 μm , clearance height 200 μm , roughing DOC 15 μm , finishing DOC 5 μm , 2 finishing cuts of both facets, length of ploughing motion 100 μm , roughing feedrate 50 mm/min, and finishing feedrate 20 mm/min. In addition to the samples mentioned previously, other samples were completed with a lower quantity of structures to analyze a wider spectrum of fabrication time. Additional samples include a single structure and square arrays of dimensions 3, 5, and 7 (i.e. 1, 8, 23, and 46 total structures). The overall machining time

was recorded for each of these fabrication processes and the information is present in Figure 2.12.

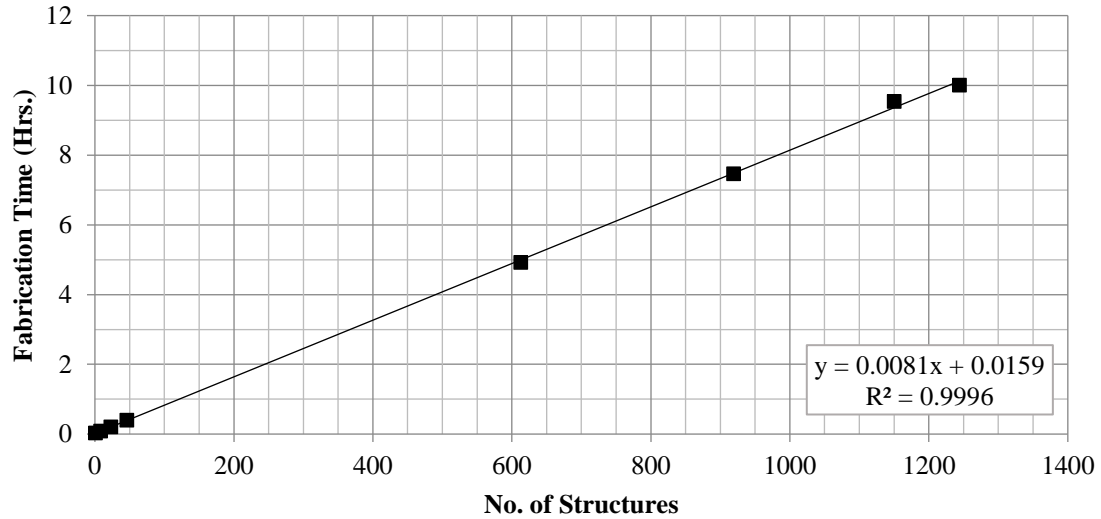


Figure 2.12 Record of machining time of RTP structures fabricated in acrylic via USPIC

This preliminary data is shown with respect to the quantity of structures, the approximate relationship being 30 seconds per RTP. Using these manufacturing parameters each structure corresponds to a surface area of $451 \times 451 \mu\text{m}$. Using this information, the manufacturing time per unit of surface area can be calculated.

$$\frac{1 \text{ structure}}{0.0081 \text{ hr}} \times \frac{(0.451 \times 0.451) \text{ mm}^2}{1 \text{ structure}} = 25.1 \frac{\text{mm}^2}{\text{hr}}$$

If a typical automotive lens requires a retroreflective surface area of 100 cm^2 ($10,000 \text{ mm}^2$) then the machining time would be 398 hrs using this preliminary estimate. If the CNC machining center was running continuously this would require less than 17 days. However, this estimate is based on machining acrylic and the manufacturing parameters for such soft material are typically of a faster pace. This suggests that the machining time will increase

for a workpiece material that is more suited for an injection moulding die. Despite this potential increase this estimate is still promising in contrast to 10 – 12 weeks that is currently needed for the production of a injection moulding die, with included retroreflective area. Furthermore, this technology is still at its infancy and process optimization has yet to be a priority. Optimization of machining process will be a definite priority in the future of this research and therefore the optimization will counteract the change in workpiece material.

The estimate shown above is relative to a single manufacturing setup and is strongly dependent on the selected tool width. The machining time can be simplified as a calculation of tool path and relative feedrate therefore regardless of the size of the tool within the tool holder the same NC code would elapsd the same amount of time. Of course, the NC code is developed with the tool width in mind but this idea helps to identify the strong relationship between tool width, surface area, and machining time. If a larger tool was used in the experiments above, for example an RTP aperture defined as $902 \times 451 \mu\text{m}$ (i.e. width \times base) the machining time would be identical while neglecting the small change associated to the new location of the structures. The machining strategy is dependent on the cross-sectional area of the RTP and the width is dependent on the tool width. Within this example the cross-sectional area is equal to the samples fabricated above and therefore the fabrication strategy and designated tool path per structure is also equal. Since the width of the tool is doubled in the example, the fabricated surface area would also be double while maintaining the same machining time. Similarly, the opposite occurs when the tool width is reduced. This correlation can be used in favour of the USPIC technology because typical automotive RRs are in the range of 2 – 3 mm, approximately 4 – 6 times larger than the

machining configuration documented above. If a larger tool was used during USPIC the fabricated surface area per hour would increase reducing the required time needed to fabricate an average retroreflective area. The correlation between fabrication time and tool width is not as straightforward as it has been presented, mainly because if the tool width increases so too may the base dimension, an increase to the base of the structure increases the cross-sectional area. A larger cross-sectional area results in an increase fabrication time per structure. This along with many other parameters effect machining time and for this reason it is difficult to estimate machining time for different manufacturing setups. Even so, the future of this technology looks promising with respect to the fabrication time of retroreflective surface area.

CHAPTER 3

Assessment of Surface Quality and Geometric Accuracy

3 Assessment of Surface Quality and Geometric Accuracy

3.1 Importance of Accuracy

Geometric accuracy and surface quality play an important role in retroreflection. This is because retroreflection is made up of a combination of reflections/TIRs and these behaviours are dependent on the incident angle with respect to the surface. If the geometry is not accurate then the light will not be redirected in the desired way. As previously mentioned, changes to internal angles cause the return light to converge or diverge, this occurs even at minimal deviations of half a degree [14]. If the manufacturing process is not accurate the structure being created will not function effectively as a RR. Quality control is essential in all areas of manufacturing.

In order for reflection/TIR to occur without scattering, a surface quality of less than 10 nm must be achieved. This quality of surface is generally referred to as an optical quality surface [32-34]. The society of the Plastics Industry (SPI) maintains a surface finish standard, the optimal surface finish is classified as A-1 and this corresponds to a R_a of 0.5 – 1.0 micro-inch (12.5 – 25 nm). SPI A-1 is a loose tolerance for optical surfaces and generally a good optical surface roughness is < 12 nm. A prism RR requires TIR to occur at an incident angle greater than the critical angle. When surface quality becomes poor the microscopic profile of the surface fluctuates increasingly and allows for some light to contact the areas of the surface at an angle greater than the critical angle. This light then transmits through the surface exiting the prism RR in the wrong direction. Therefore, the increased surface roughness again reduces the retroreflective efficiency of the structure.

Finally, geometric accuracy and surface quality are measurable and can be used to determine product quality prior to manufacturing the desired component. This is an additional quality control aspect which could be introduced in the manufacturing process that may prevent insufficient parts being made. The documentation of these attributes also provides a novel benchmark and assists greatly in progress assessment for past, present, and future work. Within the beginning of this chapter the surface quality and a few geometric characteristics of the pin-bundling technique will be examined. Subsequently, the USPIC technology will be thoroughly examined through observation of the tool and fabricated workpiece.

3.2 Assessment of Pin-Bundling Technique

The automotive industry commonly uses hexagonal ICC RRs within tail light lens. Since prism RRs rely on TIR it is desired that the facets of these ICCs are of optical quality (i.e. $S_a < 10$ nm). Essentially, this is the requirement for all participating facets, whether or not this is being achieved is unclear because this information has yet to be documented by manufacturers. It is known that automotive lenses which have included retroreflective areas are tested to ensure functionality. The entire pin-bundling process is completed and the resulting lens must comply with the surface vehicle standard SAE J594 – reflex reflectors [35]. This testing ensures overall functionality of the final product however it does not provide any information on the consecutive steps within the process.

To better understand the entire process, each stage of the manufacturing process must be analyzed separately. Therefore, geometric analysis has been performed at critical stages within the manufacturing process. The geometric accuracy is critical to the functionality of each RR; this includes the surface quality of each facet as well as the accuracy of the

included angles and unavoidable edge radii between adjacent facets. It is known that theoretically retroreflectors consist of many keen edges, both convex and concave, each posing a high degree of manufacturing difficulty. Theoretically the included angle between adjacent facet is exactly 90° however it is known that manufacturers alter this dimension to increase application based performance. To avoid revealing industry secrets the included angles between facets will not be present, rather this study will mainly focus on surface quality of individual facets. The data provided is the first analytical representation of the elements associated with the pin-bundling technique.

For the purposes of analyzing the entire manufacturing process, the pin-bundling technique will be broken down into 3 phases: the bundling of hexagonal pins, the electroforming process, and finally the automotive lens. These will be further described as the pin (phase 1), the die (phase 2), and the lens (phase 3) for simplicity. The samples examined in this study are not from the same process and do not have direct correlation between one another. Therefore, the findings are representative of a single element or elements from the associative phase of the manufacturing process. It would be ideal to analyze the consecutive steps within a single process however this study did not have the ability to acquire such specimens.

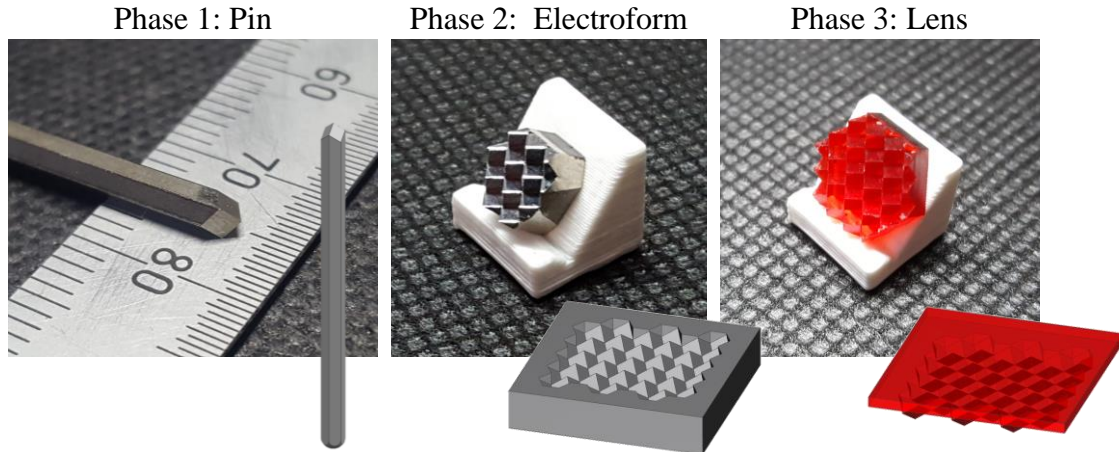


Figure 3.1 Recall of the 3 phases of the pin-bundling technique and photographic images of the specimens examined

3.2.1 Surface Measurement Methodology

The following surface topographical analysis for each phase of the process has been performed in an identical way. The process used to analyze the retroreflective facets was white light interferometry. The objective used was a Nikon CF Plan 10X/0.30 DI $\infty/0$ EPI with a FOV of 1754.40 x 1320.96 μm . The entire area is captured at 1360 x 1024 px, representing a 1.29 μm special resolution. At this point a sub-region of 1 x 1 mm is further analyzed, which aids in the consistency of the analysis. The sub-region is selected within the retroreflective facet so to avoid the effect of the edges. The following step after the extraction of the sub-region is to remove a planar form from the entire area. This removes any tilt in the recorded data which originates when the normal of the facet being assessed is not coincident with the direction of the objective. Once the form is removed from the data the initial surface roughness is used to determine the appropriate sampling size and respective cut-off frequency to segregate the roughness (S_a) from the waviness (W_a). Typically, at this stage in the measurement process the surface roughness was

approximately 100 nm, as per ISO 4288 this falls within the range of 0.1-2 μm S_a . Therefore, the first selection of cut-off frequency is 0.8 mm. In our study, the application of this cut-off frequency consistently dropped the S_a value into the next range. Per ISO 4288 the next range is defined as an S_a over 0.02 μm and up to 0.1 μm with a cut-off frequency and sampling length of 0.25 mm. Once applied the S_a again drops to the next range, this range consists of S_a up to 0.02 μm (20 nm). This is the final range and the associated cut-off frequency is 80 μm which is the spatial frequency that segregates the surface roughness from its waviness. The ISO standard also provides the sampling length of 80 μm , and the evaluation length of 40 μm . Throughout this study all assessed surfaces were consistently within this range of roughness and therefore all results have been processed with an 80 μm cut-off spatial frequency. The sub-region selected was larger than the recommended evaluation length and therefore averaging across the full 1x1 mm area has been completed. The ISO standard 16610-61 was used on the 1 x 1 mm area with an 80 μm cut-off to evaluate the surface roughness and waviness for all assessed surfaces. To reiterate, the described process is the same for all facets throughout the 3 phases below.

3.2.2 Surface Assessment of Pins

The hexagonal pins were examined in 2 states. The first, a freshly ground and lapped pin (new) and second, a pin after it has been used to produce an electroform mould (used). Pin 1, within table 3.1, represents a newly lapped pin and the remaining pins (pin 2 - 4) represent used pins. Figure 3.2 represents the measurement methodology for a single facet of pin 1, this process has been repeated for all pin facets. The average surface roughness amongst all 4 pins is an impressive 2.7 nm and the average surface waviness is 13.2 nm. The best surface roughness observed was 1.6 nm and the worst was 4.9 nm. In addition to

surface quality, edge radii between adjacent facets were also measured. The new pin averaged $3.86 \mu\text{m}$ edge radius while the used pins averaged $30.15 \mu\text{m}$. Radii measurements were performed using confocal microscopy with an objective of 50x and the radius was determined using a best fit circle tangent to both adjacent facets. The new pin that had a smaller average edge radius was better described as a true edge radius, closely matching that of the best fit circular curve. However, the used pins seemed to have a broken edge rather than a clear edge radius which did not match the best fit circular curve well. Instead, the 2 adjacent facets were separated by a small chamfer which likely has developed throughout the use of the pins. This fractured facet or chamfer between adjacent facets was observed to be approximately $40 \mu\text{m}$ wide. It is thought that the damage may occur when the electroplating (electroform die) is removed from the face of the pin-bundle.

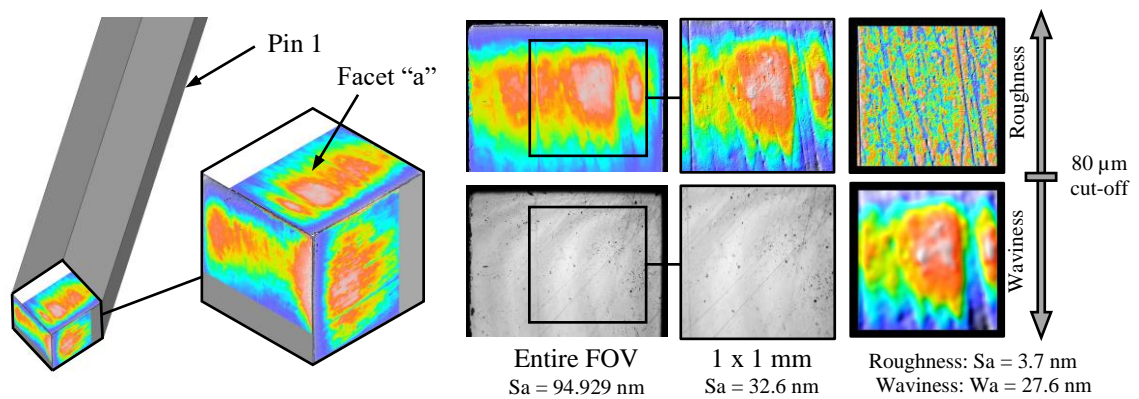


Figure 3.2 Measurement methodology of phase 1 element in traditional pin-bundling technique, hexagonal pin

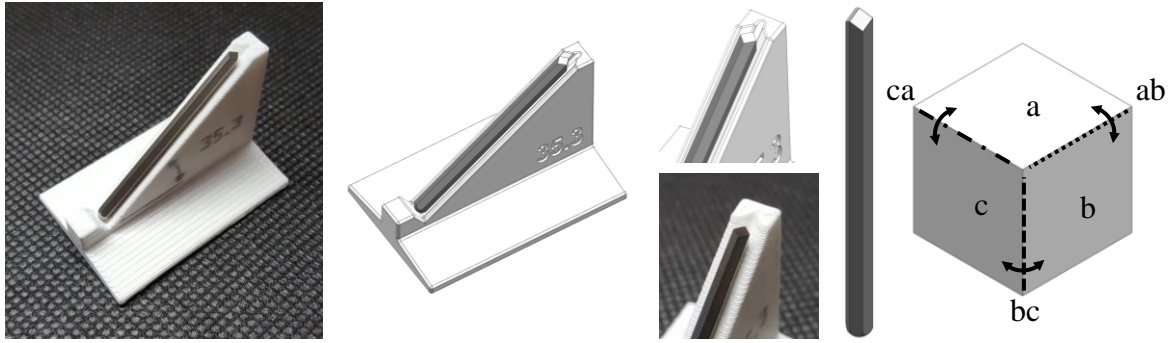


Figure 3.3 Geometric identification of phase 1 element in traditional pin-bundling technique, hexagonal pin

Sa (nm)		a	b	c	Avg.
Pin 1	Area 1x1 mm	32.6	29.3	26.0	29.3
	Roughness	3.7	4.9	2.6	3.7
	Waviness	27.6	22.5	21.2	23.8
Pin 2	Area 1x1 mm	17.9	20.7	24.5	21.1
	Roughness	1.6	1.6	3.7	2.3
	Waviness	13.8	11.3	21.2	15.4
Pin 3	Area 1x1 mm	8.8	9.9	6.6	8.4
	Roughness	1.8	2.2	2.1	2.0
	Waviness	7.0	8.2	5.2	6.8
Pin 4	Area 1x1 mm	5.7	7.6	11.6	8.3
	Roughness	2.6	3.5	2.4	2.8
	Waviness	4.9	6.1	9.6	6.9
Edge Radius (μm)		ab	bc	ca	Avg.
Pin 1	New	3.24	5.96	2.37	3.86
Pin 2	Used	26.07	28.07	27.68	27.27
Pin 3	Used	42.01	17.66	49.84	36.51
Pin 4	Used	49.26	25.37	5.43	26.68

Table 3.1 Geometric Assessment of phase 1 element in traditional pin-bundling technique, hexagonal pin. Surface roughness of retroreflective facets and edge radii between adjacent facets

3.2.3 Surface Assessment of Electroform Die

The surface assessment of Phase 2 has been performed on a single electroform die. The electroform die originally had a very complex geometry and therefore the specimen was

machined into hexagonal shape. This shape was selected specifically to aid in orientation throughout the assessment process. This modification was accomplished through careful orientation of the specimen and delicate machining practice. Once complete, the modified specimen consisted of 7 complete ICC hexagonal RRs. The orientation of the ICCs with respect to the outer perimeter of the specimen were in such a way that simple fixtures at critical angles would allow the sample to be position so to make the retroreflective facets parallel to the measurement platform. It was then possible to acquire surface topographic data from all retroreflective facets of the electroform specimen. A photographic image of the modified specimen is shown in Figure 3.5. Figure 3.4 represents the measurement methodology for a single facet of ICC 1, this process has been repeated for all electro facets. The average surface roughness of all 21 facets (7 ICCs x 3 facets/ICC) is 9.5 nm and the average waviness is 32.9 nm. The best observed S_a is 5.8 nm and the worst is 15.5 nm.

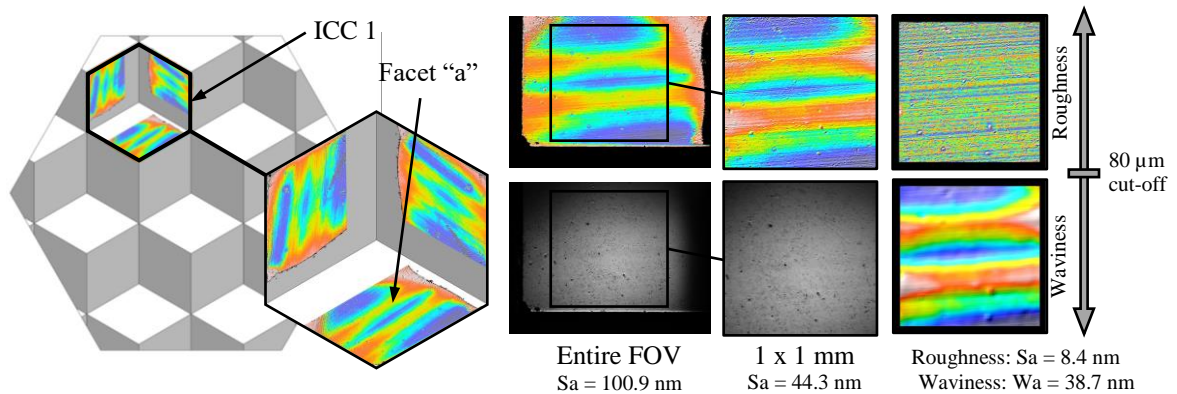


Figure 3.4 Measurement methodology of phase 2 element in traditional pin-bundling technique, electroform die

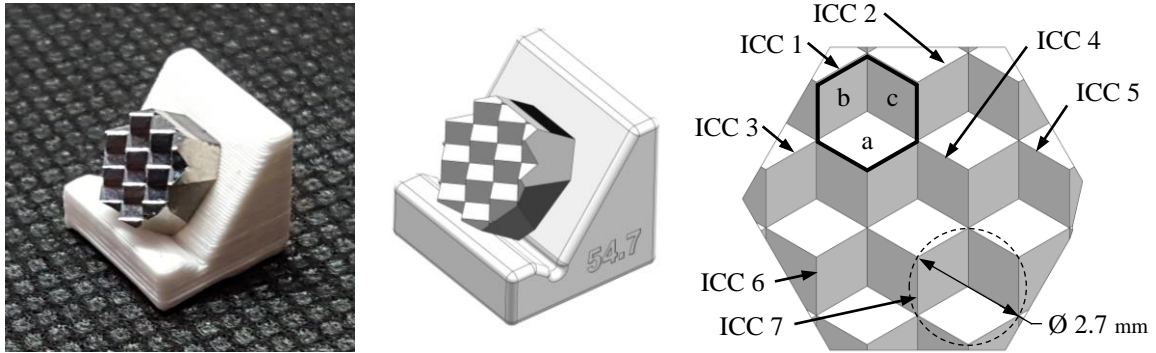


Figure 3.5 Geometric identification of phase 2 element in traditional pin-bundling technique, electroform die

Sa (nm)		ICC 1	ICC 2	ICC 3	ICC 4	ICC 5	ICC 6	ICC 7	Avg.
a	Area 1x1 mm	44.3	31.5	40.8	23.4	33.9	35.2	42.6	36.0
	Roughness	8.4	8.2	8.4	8.1	9.9	9.7	14.6	9.6
	Waviness	38.7	26.5	36.9	19.9	30.5	32.1	34.3	31.2
b	Area 1x1 mm	29.5	48.1	39.2	66.3	35.5	26.7	43.3	41.2
	Roughness	8.1	12.2	15.5	11.5	9.2	10.8	8.9	10.9
	Waviness	24.5	44.6	35.7	63.7	33.5	19.7	41.0	37.5
c	Area 1x1 mm	41.0	28.8	47.5	19.4	26.1	55.5	23.8	34.6
	Roughness	9.5	5.9	6.3	5.8	6.2	13.7	9.1	8.1
	Waviness	35.3	24.3	44.7	15.9	21.2	48.2	20.3	30.0

Table 3.2 Geometric Assessment of phase 2 element in traditional pin-bundling technique, electroform die. Surface roughness of retroreflective facets

3.2.4 Surface Assessment of Lens

Similar to the electroform specimen, the outer geometry of the lens was also modified into a hexagon. This was done for the exact same reasons and was done consistently to include 7 structures. The only difference is that this sample includes 7 convex corner-cubes (CC) to be consistent with the manufacturing process. To further explain, a single pin consists of 1 structure, which is a convex CC lapped onto the end of the pin. If you consider this single pin it will produce an ICC on the electroform and finally using injection moulding the lens will then revert to a convex CC theoretically identical to the structure of the pin.

Therefore, the process of geometrically identifying these specimens has been done in an equivalent manner. Figure 3.6 represents the measurement methodology for a single facet of CC 2, this process has been repeated for all lens facets. The average surface roughness of all 21 facets (7 CCs x 3 facets/CC) is 9.2 nm and the average waviness is 62.4 nm. The best observed S_a is 5.3 nm and the worst is 16.0 nm. This concludes the examination of the pin-bundling technique which is currently a universal manufacturing method within the automotive industry.

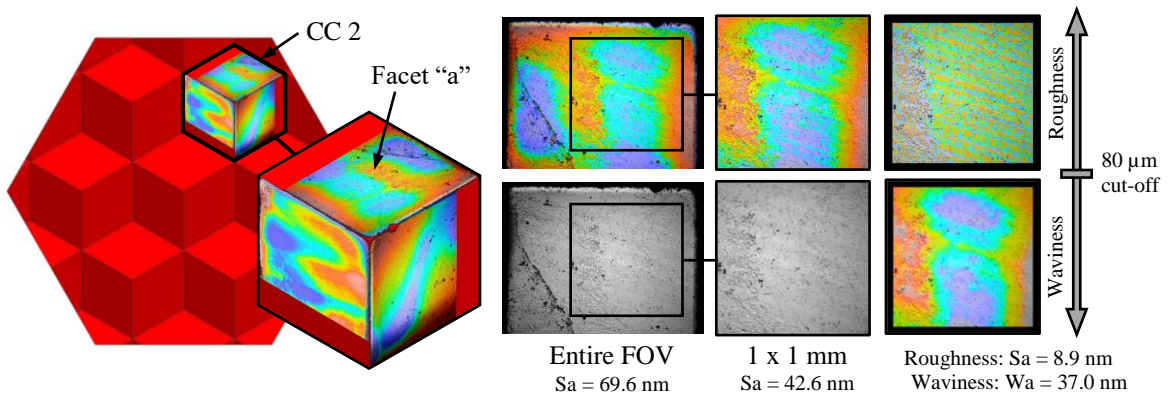


Figure 3.6 Measurement methodology of phase 3 element in traditional pin-bundling technique, retroreflective lens

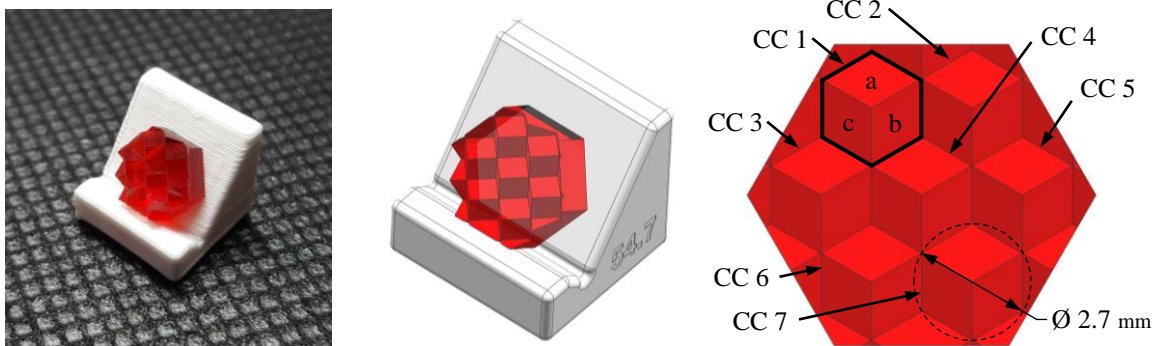


Figure 3.7 Geometric identification of phase 3 element in traditional pin-bundling technique, retroreflective lens

Sa (nm)		CC 1	CC 2	CC 3	CC 4	CC 5	CC 6	CC 7	Avg.
a	Area 1x1 mm	35.0	42.6	43.3	35.6	37.0	30.1	41.9	37.9
	Roughness	5.3	8.9	6.9	7.3	6.5	7.7	7.4	7.1
	Waviness	30.5	37.0	39.7	31.2	33.4	25.6	36.1	33.4
b	Area 1x1 mm	87.1	117.8	109.5	123.5	88.1	154.3	117.7	114.0
	Roughness	8.2	8.5	8.5	11.3	11.1	10.2	10.9	9.8
	Waviness	76.8	103.7	95.2	108.9	74.5	138.6	98.2	99.4
c	Area 1x1 mm	94.5	45.1	47.2	38.6	43.2	87.3	70.1	60.9
	Roughness	10.5	8.2	13.2	7.9	8.8	10.4	16.0	10.7
	Waviness	88.7	41.9	36.3	31.2	41.0	77.0	63.7	54.3

Table 3.3 Geometric Assessment of phase 3 element in traditional pin-bundling technique, retroreflective lens. Surface roughness of retroreflective facets

3.3 Assessment of USPIC Technology

Now that a preliminary benchmark has been developed, the USPIC technology can be examined. This novel manufacturing process has two physical elements, the tool and the workpiece, therefore both have been analyzed. The surface quality of the fabricated RTP has been assessed qualitative with respect to the manufacturing parameters DOC and feedrate. A quantitative assessment of the surface roughness has also been conducted similar to the methodology used in the previous sections. Further emphasis is placed on specific surface characteristics witnessed throughout the observation. Finally, a preliminary optical analysis has been performed upon a USPIC sample and a industry sample.

3.3.1 Qualitative Assessment of Facets

An experiment was conducted to observe the difference in surface quality with respect to cutting feedrate and DOC. The experiment was performed on a acrylic workpiece using a USPIC tool of approximately 1 mm in width. The fabricated facets were imaged using a Keyence light microscope and these images are presented in Figure 3.8. The experiment

consisted of 3 separate feedrates (10, 50, and 100 mm/min) and 20 separate DOCs (1 – 20 μm). Among these tests, only 15 images are shown which include all tested feedrates at 5 selected DOCs.

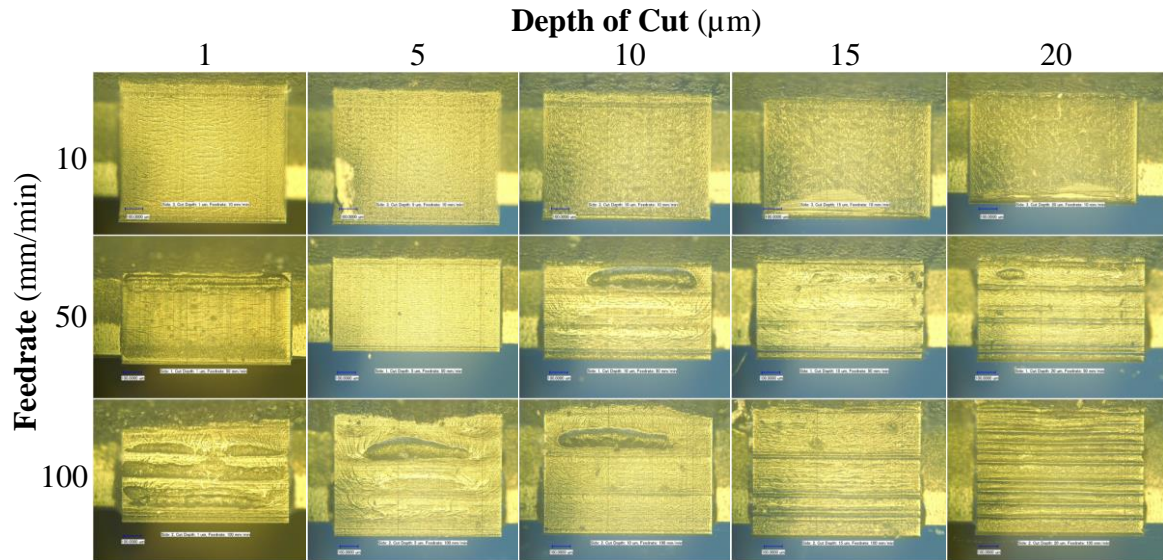


Figure 3.8 Optical microscopy of facets fabricated using USPIC technology

These images clearly show a trend related to these manufacturing parameters and the surface quality. The surface quality appears much lower on facets which have been fabricated at a high feedrate and large surface defects are present. The images taken from facets cut at 100 mm/min show the worst surface quality. At 50 mm/min surface defects are also seen at larger DOCs but the quantity and scale of these features are of a lower magnitude. The combination of 50 mm/min and 5 μm produced a greater surface quality than any created at 100 mm/min. Through the observation of the additional images not included in the figure above a region of higher quality is seen for the feedrate of 50 mm/min. The region of greater surface quality is from 4 to 7 μm for this specific feedrate. The surface quality that is achieved at 10 mm/min is generally much better than the other

feedrates tested and as DOC increases the quality reduces at a much slower rate. The quality of surface achieved with the combination of 10 mm/min feedrate and 20 μm DOC is greater than most at the other tested feedrates.

The obvious surface defects that are present in these images are horizontal in nature. The horizontal of the images is perpendicular to the direction of tool motion (i.e. across the feed direction). The tool motion relative to the figure above is from top to bottom. The more significant defects seen in the lower right image have a nearly periodic characteristic and are speculated as tool chatter. If the images are examined closer vertical lines can be seen throughout all the optical images. These imperfections are uniform throughout the images and the position and magnitude remain constant regardless of process parameters. These observations helped to identify the cause of the vertical defects. These scratches are associated to tool wear, specifically the accumulation of fractures in the cutting-edge.

3.3.2 Observation of Cutting Tool

The monocrystalline diamond tool used in USPIC is manufactured using the process of lapping. A newly lapped diamond tool typically has an approximate edge radius of 50 nm [36]. When the tool is received, standard practice is to image the tool's cutting edge prior to fabricating. Once the fabrication is complete the cutting-edge is examined again. This procedure identified small chip-fractures on the cutting-edge of the tool, the quantity of which increased with tool use. The missing fragment of the cutting-edge range in size up to a few micros across. The position of these chip-fractures correlated identically with the vertical scratches seen on the fabricated facets. The correlation between the location of the chip-fractures on the USPIC tool and the fabricated facet can be seen in Figure 3.9. This figure also shows an example of the fractures which occur on the tool's cutting-edge.

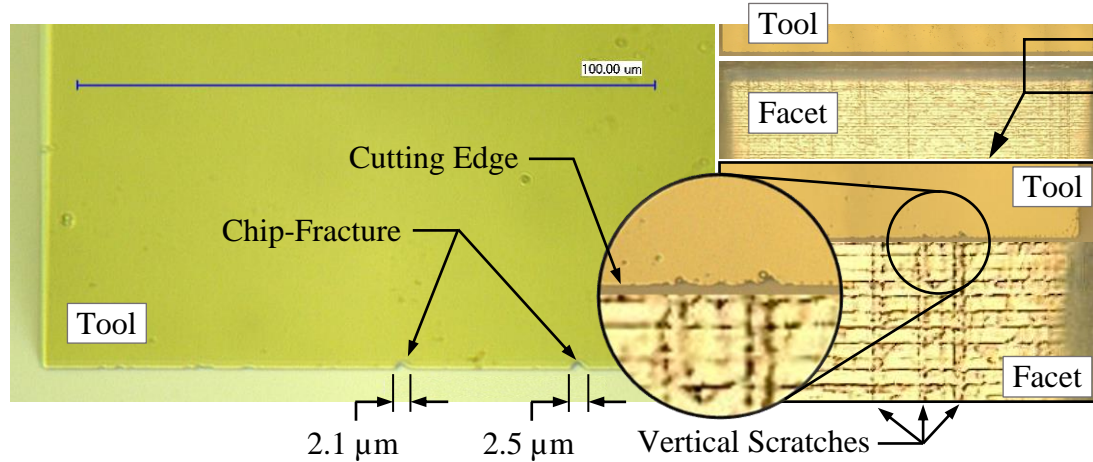


Figure 3.9 Observation of the USPIC tool and the correlation between cutting edge chip-fractures and linear scratches on fabricated facets

3.3.3 Optical Analysis

To further explore RR functionality of ICC-based and RTP-based structures, the optical performance of the two samples shown in Figure 3.10 was measured. The testing was conducted using a commercial luminance measurement system. The aperture size of the retroreflective structures within the samples are not equal in size and therefore a direct comparison leads to many speculations. For this reason, the preliminary optical analysis is presented to display the RTP structures functionality. The hexagonal aperture sample consists of approximately 500 structures over a surface area of $3,136 \text{ mm}^2$ ($\sim 56 \times 56 \text{ mm}$). The approximate hexagonal aperture size of the ICCs is 3 mm. The USPIC sample consists of a 25×25 offset array of RTPs with aperture $451 \times 451 \text{ }\mu\text{m}$. The surface area of the USPIC sample is approximately 127 mm^2 . Prior to the optical testing the hexagonal sample was partially covered with adhesive tape to make the surface areas similar in size.

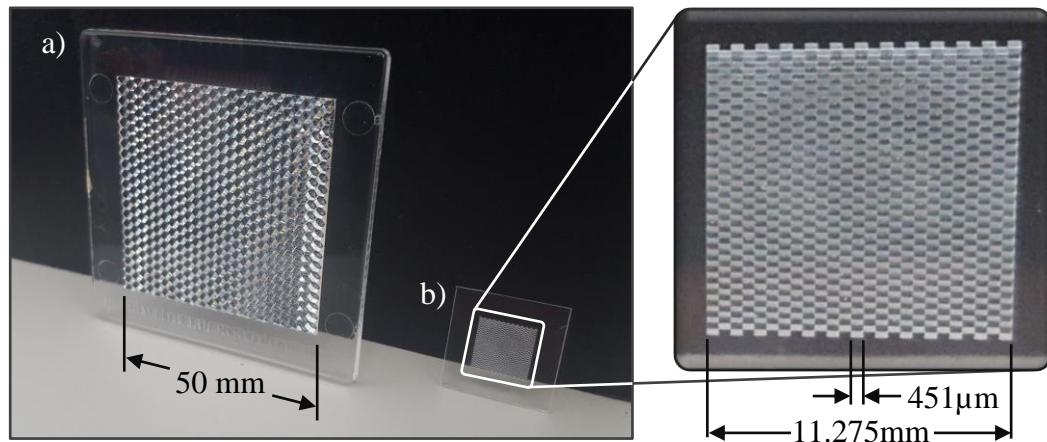


Figure 3.10 Samples assessed in optical performance testing: a) hexagonal ICC RRs via pin-bundling technique, and b) RTP RRs via USPIC technology

The commercial luminance measurement system was used in combination with an optical testing fixture. The fixture was designed and built to improve consistency of optical measurement. The fixture was designed to resemble the automotive industry performance testing apparatus although the scale of the apparatus is much smaller. The fixture used can be seen in Figure 3.11.

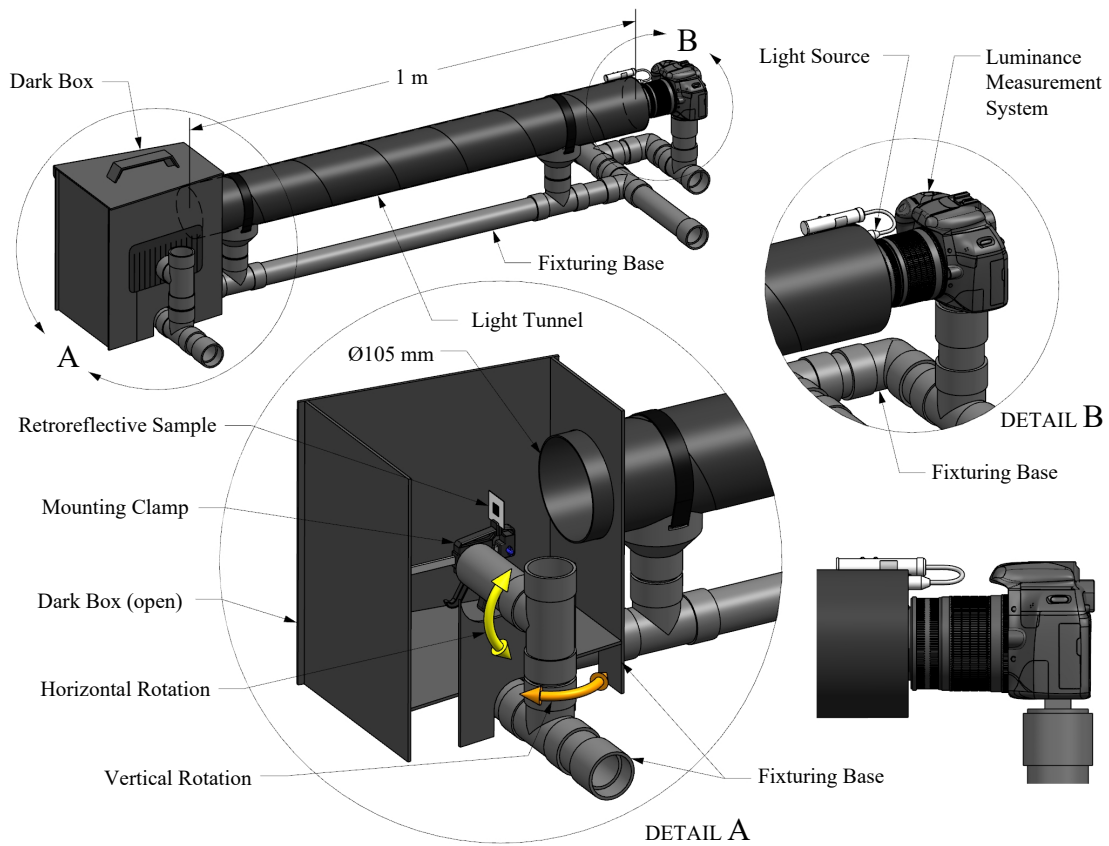


Figure 3.11 Fixture designed and fabricated for optical performance testing of retroreflective samples

The average luminance values measured for RTP-based and ICC-based structures were 5.6 cd/m^2 and $10. \text{ cd/m}^2$, respectively. Even though the RTP-based RR structure was characterized by a lower optical RR performance, the preliminary tests have indicated that the novel USPIC technology is capable generating optically-functional RR components. Without entering too many speculative details, it appears that the primary direction of improvement for the optical performance of the RTP-based RR structure is tightly correlated with the overall dimensional accuracy and surface quality of the fabricated reflective facets.

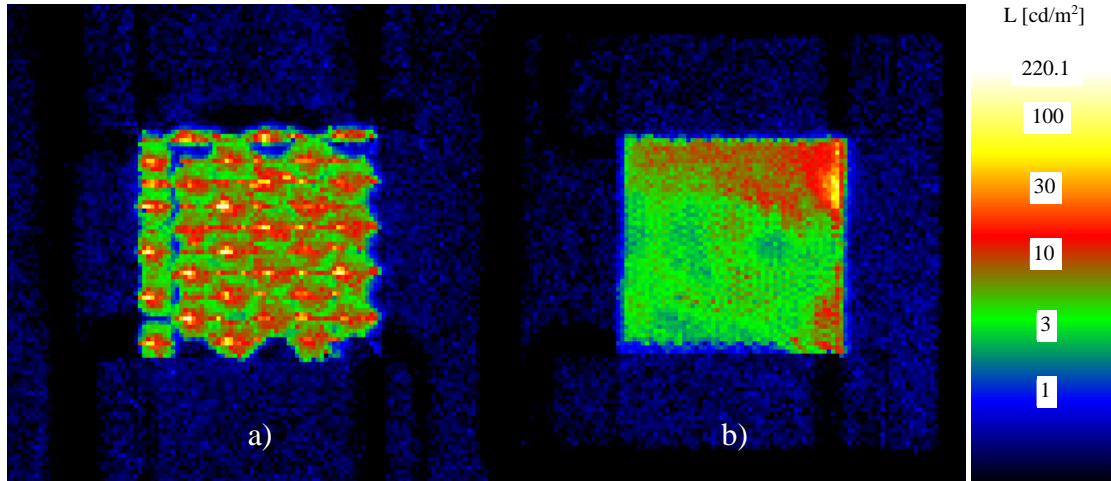


Figure 3.12 Optical performance testing: a) hexagonal ICC RRs via pin-bundling technique, and b) RTP RRs via USPIC technology

3.3.4 Quantitative Assessment of Facets

The surface topographical analysis for the USPIC technology has been performed in an identical way to the previous pin-bundling technique. The only exception is the defined sub-region is 0.5 x 0.5 mm due to the size of the RTP facets. Within table 3.4 five facets fabricated via USPIC have been assessed, their average S_a without the implementation of an 80 μm cut-off frequency is 48.9 nm. With the cut-off frequency implemented the average surface roughness is 19.7 nm and waviness is 29.9 nm. In contrast with the pin-bundling technique the roughness is approximately double (recall surface roughness: electroform die – 9.5 nm, automotive lens – 9.2 nm). The USPIC technology has a slightly better surface waviness, 3 nm lower than the electroform and 32.5 nm lower than the lens (recall surface waviness: electroform die – 32.9 nm, automotive lens – 62.4 nm). It may be possible that the injection moulding process introduces some waviness. Since the USPIC technology does not plan to eliminate this process there is still a potential for the surface waviness to increase when manufacturing the final lens from the USPIC fabricated die.

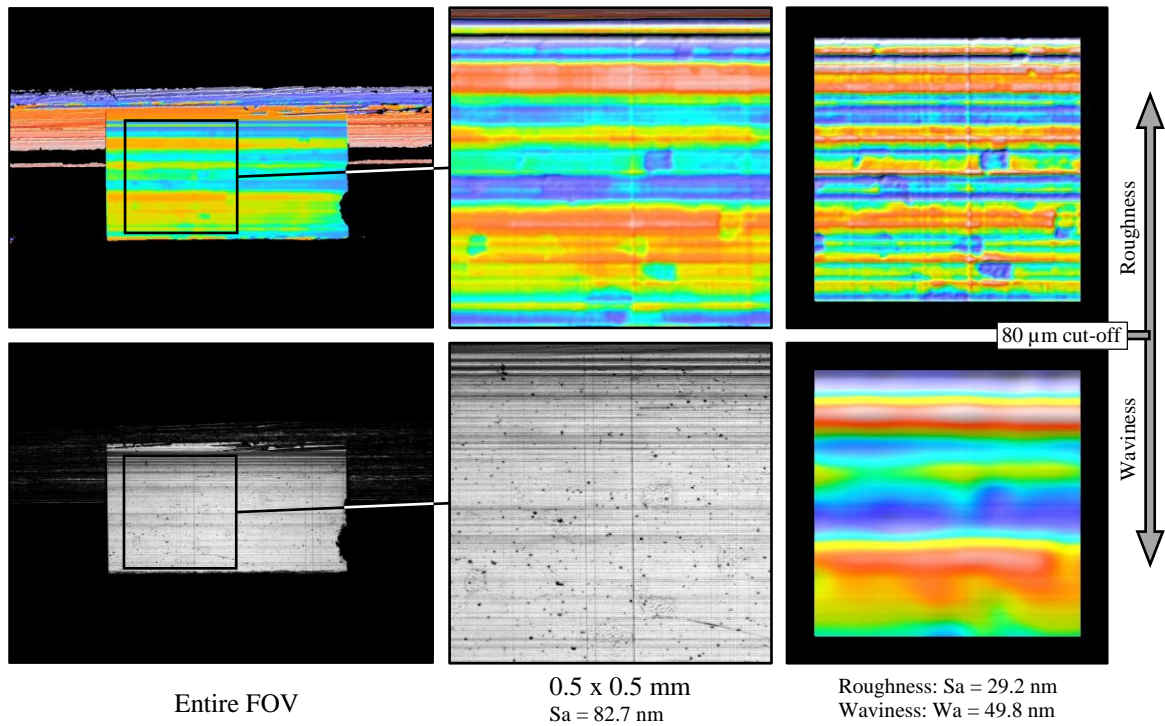


Figure 3.13 Measurement methodology for surface quality of RTP facets fabricated using USPIC technology

Sa (nm)	F1	F2	F3	F4	F5	Avg.
Area .5x.5 mm	82.7	38.1	38.6	40.5	44.8	48.9
Roughness	29.2	20.7	17.3	16.7	14.8	19.7
Waviness	49.8	24.8	22.2	26.4	26.2	29.9

Table 3.4 Geometric assessment of RTP facets fabricated using USPIC technology

The provided documentation establishes a current state of the art for the UPSIC technology and displays distinction from the current manufacturing method for RRs. The information regarding individual facet surface quality of the pin-bundling technique and novel USPIC process is a unique and unprecedented representation. The benefits to which are crucial towards further development of the USPIC technology.

3.3.5 Single Facet Analysis

During the observation of the fabricated facets it was apparent that there were 2 separate characteristics which contributed to surface imperfection. At this point in the study it was not clear what the magnitude of either of these imperfections were. Therefore, a quantitative analysis was performed on a single USPIC fabricated RTP facet. Figure 3.14 shows a facet of an RTP structure acquired using both a high-resolution optical microscope and an optical profilometer. The RTP facet chosen does not represent an ideal surface quality however this facet has good representation of surface deficiencies. The facet presented has an average S_a of 142 nm. It is observed that the facet has two predominate characteristics, with respect to the direction of tool motion these are parallel linear ridges (along the feed direction) and perpendicular oscillation (across feed direction). The characteristics across the feed are represented via 2D-profile lines P₁, P₂, and P₃ on the topographical image in Figure 3.14b. Alternatively, the characteristics along the feed are represented via 2D-profiles P₄, P₅, and P₆.

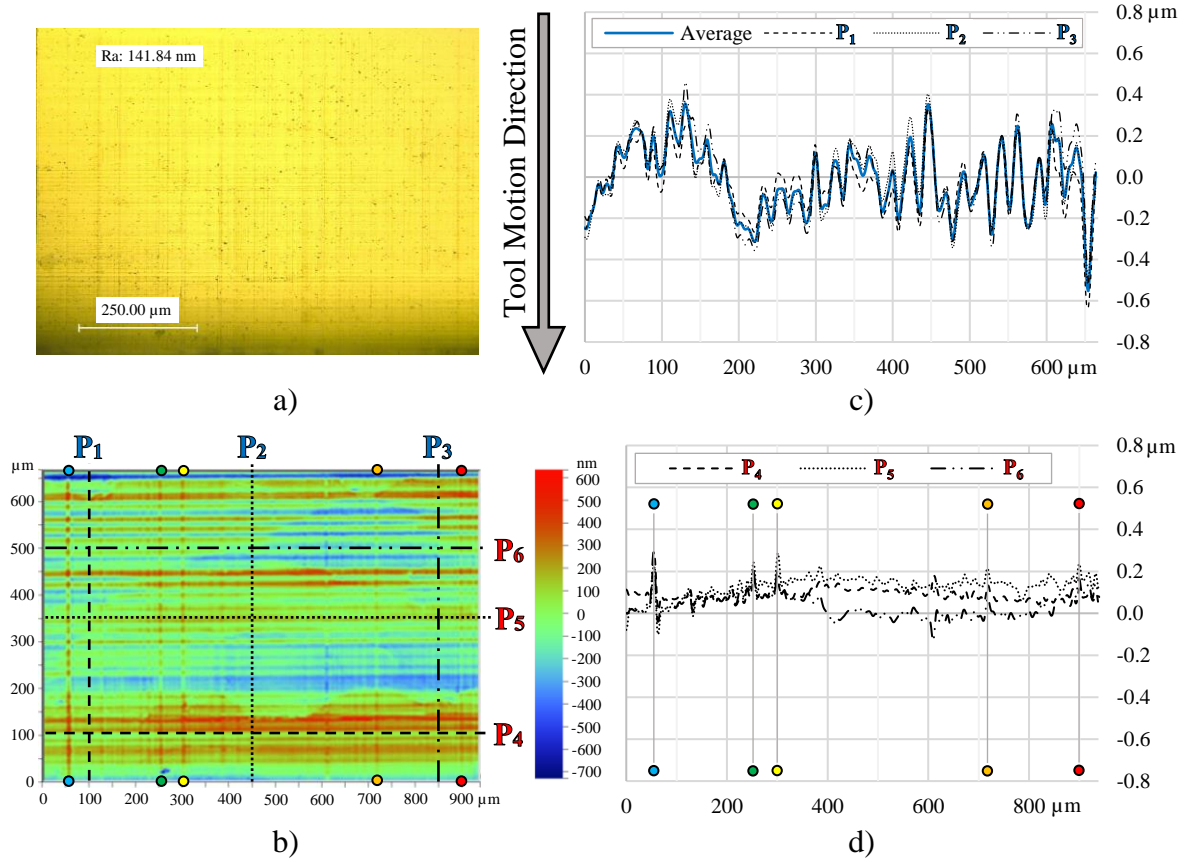


Figure 3.14 Surface quality and characteristics of an RTP facet fabricated by USPIC: a) optical image, b) surface topographical image, c) surface profiles along feed direction ($P_1 - P_3$), and d) surface profiles across feed direction ($P_4 - P_6$)

The inadequacies across the feed can be described as periodic with a spatial frequency of 42.4 mm^{-1} . The spatial frequency corresponds to approximately 7.07 Hz when derived from the associated plunging feedrate. Through observation of additional RTP facets it was identified that the periodic markings across the feed were present on all facets. In contrast, the markings along the feed were seen in larger quantities on facets which were fabricated later in the tool life. It was noted that initial structures which were fabricated using a new or newly lapped diamond tool did not have these linear ridges along the feed direction. Once a ridge was present on a single facet it would then be present on all subsequent facets. It was evident during routine tool inspection that the cutting edge was

accumulating small chip-fractures and they translate directly to the finished surface of the RTP facet.

The 2-D profiles presented in Figure 3.14c and 3.14d are formatted such that their Y-axis scale are equivalent. This allows for direct comparison between deficiencies along and across the feed direction. What is noticed is that the periodic characteristics across the feed have a much larger magnitude and therefore have a greater significance to the overall surface roughness. The linear scratches caused by the chip-fractures have a lower detrimental effect on the final surface quality. Within Figure 3.14b and 3.14d vertical scratches associated to cutting-edge fractures are identified via colour coded circles. Although the chip-fractures have a smaller impact on surface quality they are still undesirable and if the fabrication process length is to increase, the severity of these fractures is likely to increase as well.

The oscillations across the feed are not as clearly understood and their constant presence is suggestive of undesirable cutting mechanics. The periodicity of these surface characteristics is suspected to be system dynamics however, as a prerequisite it is important to understand cutting mechanics. This knowledge will help identify complications within the cutting kinematics and potentially allow for modification that will avoid tool damage and the introduction of undesirable system dynamics. The following chapter is a preliminary investigation of the microcutting with respect to 3-dimensional cutting forces.

CHAPTER 4

Cutting Mechanics of the USPIC Strategies

4 Cutting Mechanics of the USPIC Strategies

4.1 Experimental Setup

In the interest of identifying probable cause for tool edge chip-fractures and seeking understanding of the cutting mechanics an experimental setup was developed for measuring 3-dimensional cutting forces. This setup has been used for documenting the cutting mechanics of the two primary strategies of the USPIC technology. This experimental setup will also aid in future analysis of system dynamics. The ideal benefit of this contribution is to provide evidence and insight into the USPIC technology to improve the fabrication process.

4.1.1 Device Configuration

As it shown in Figure 4.1, a 3-axis Kistler 9256C2 dynamometer was mounted atop the C-axis of a five-axis micromachining center beneath the workpiece. Alignment of the dynamometer with the X-axis of the CNC machining center was corrected using a developed NC code. The capacitive signals from the dynamometer are transmitted to a Kistler dual mode amplifier containing three identical type 5010 amplifiers. The amplifiers convert the signals from pC to V based on calibrated coefficients. The signals were then gathered using a BNC-2110 terminal block and transmitted to a PCI data acquisition card (NI 6023e) both manufactured by National instruments. Additionally, the signals were displayed live via LeCroy Waverunner LT354 oscilloscope. The data acquisition (DAQ) card was installed in a desktop computer operating Windows 7. A program was written in LabVIEW to acquire data from each of the three channels at a rate of 10 kHz. This sampling rate was chosen to remove the natural frequency of the dynamometer axes which are approximately 4.0 – 4.8 kHz. During USPIC fabrication the workpiece and dynamometer

are rotated about A-axis 45 degrees. As a result, it was necessary to decompose the acquired force signals into the machine coordinate system (MCS). Once the raw data was recorded, separate LabVIEW programs were written to read and process the data. Among these programs the signals were decomposed into the proper machine coordinates as well as cropped and filtered.

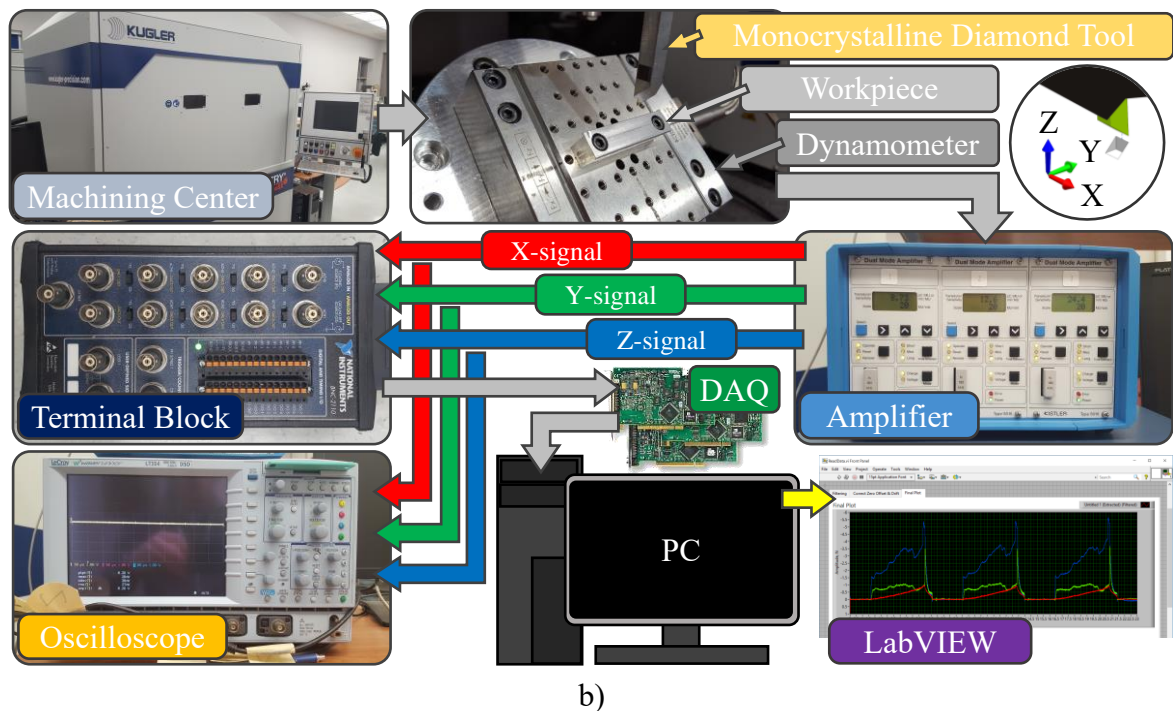
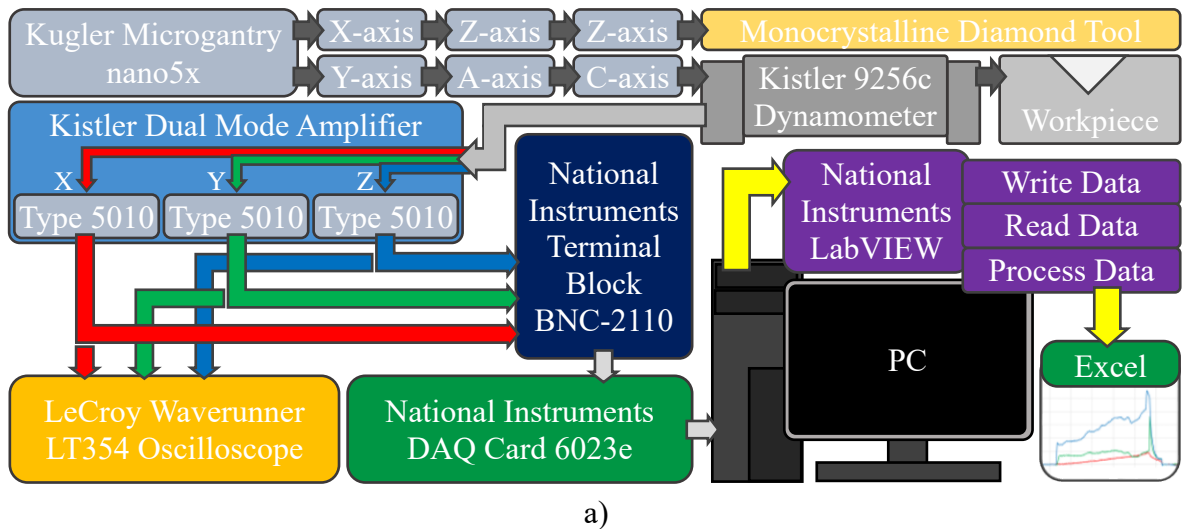


Figure 4.1 Experimental setup: a) block diagram flowchart, and b) photographic flowchart

4.1.2 Coding and Data Processing

Specific LabVIEW codes were written to analyze the data accordingly. Once the raw data was recorded the next step was to extract a critical section, such as a specific cut in the series (Figure 4.2a – b). The next program decomposes the forces such that the resultant forces aligned with the MCS (Figure 4.2b – c). This was performed because the MCS is better orientated with respect to the cutting kinematic than the coordinates of the dynamometer. After decomposition, the signals are filtered using a single low-pass filter with cut-off frequency of 50 Hz (Figure 4.2c – d). The graphical display of the forces is then inverted about the Y-axis (Figure 4.2d – e). Within the cutting strategies, the tool moves through positions which are not in contact with the workpiece and therefore during these times the cutting force is zero. However, a zero offset is seen in the force signals and this discrepancy is due to drift in measurement instruments. To eliminate the drift a linear regression line is defined by regions of the data that is specific to the tool not in contact with the workpiece (Figure 4.2f). The data is then shifted using this linear regression and the drift is corrected (Figure 4.2f – g). The final step of the LabVIEW programming saves a processed copy of the data for subsequent analysis.

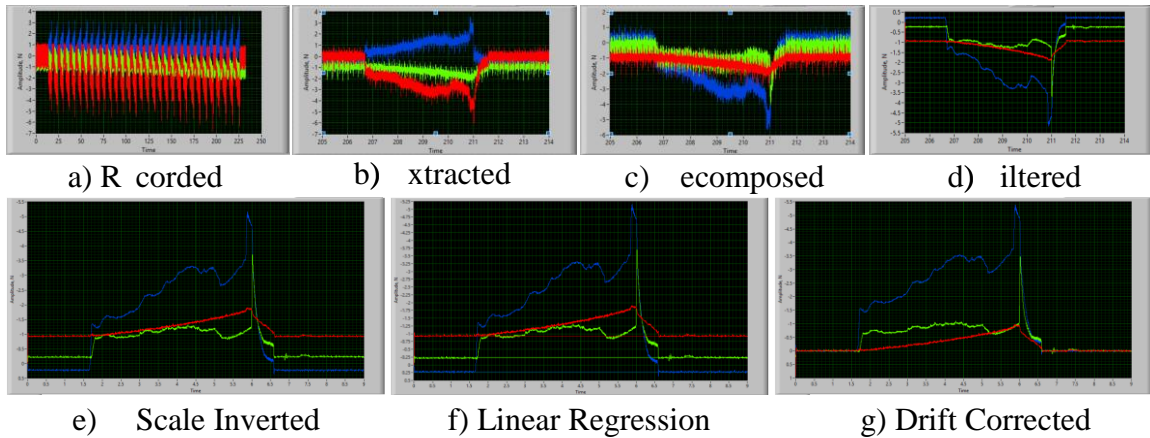


Figure 4.2 LabVIEW data processing procedure

4.1.3 Physical Configuration of Experiments

Specific experiments were designed to identify and understand characteristics of the cutting mechanics associated with USPIC. The tool geometry and fixturing was kept constant throughout this study. The tool material used was mono-crystalline diamond and the tool's critical geometric dimensions are a 50° included angle between rake and clearance face and a cutting-edge length (i.e. tool width) of approximately 1 mm. The tool was mounted within the tool holder such that its clearance face was at an angle of 3° with respect of the X-Z plane. The A-axis is set to $+45^\circ$, this tool-workpiece configuration represents a rake angle of positive 37° while plunging and negative 53° while ploughing. Another consistency throughout this study is that the data has been recorded near the end of the fabrication of the structure. This has been done because both strategies begin with extremely short and interrupted cuts and as the process continues the length of the plunging motion increases. This elongation of the process helps to clarify and associate the cutting motions with respect to the force signals. As the process nears the final cuts the plunge cutting length increases to $\frac{Base}{\sqrt{2}}$. In this study the aperture dimensions are chosen to be 1 x

1 mm (base x tool width). For this size of structure the final plunge cut length is equal to 0.7071 mm and with a feedrate of 10 mm/min this cut happens in 4.2 seconds without considering acceleration. Each cut prior to the final cut is a quantity of DOC shorter than the last and the first cut is always \leq the DOC (e.g. RTP structure of 1x1 mm aperture - 10 μm DOC – total cuts 71, last cut length 707.1 μm , 2nd last 697.1 μm , 3rd last 687.1 μm , and so forth, first cut 7.1 μm). The workpiece material used is Aluminum 6061 and has also been kept consistent throughout this study of cutting mechanics.

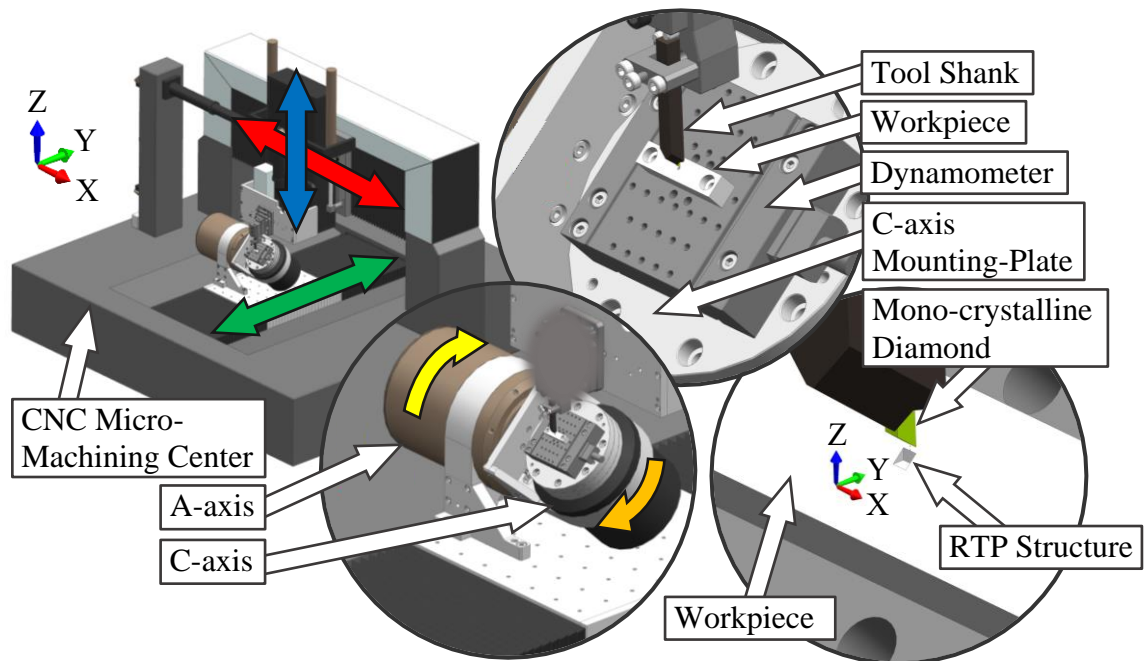


Figure 4.3 CAD representation of the CNC machining center, tool, dynamometer and workpiece

The first experiment is described as fabricating a single isolated structure using the unidirectional strategy. The term isolated is used to signify that the structure is cut into a flat surface with no previously cut structure(s) at any edge of its aperture (Figure 4.4a). Therefore, the cutting tool is fully engaged across its entire cutting edge and the tool side-

walls effectively determine the RTP width. This experiment has been conducted at 2 different DOCs, 5 and 10 μm . The cutting mechanics associated to this physical configuration can then be related to the manufacturing parameter DOC. The second experiment performed is identical to the first apart from the structure being isolated. This experiment was designed to simulate the USPIC unidirectional process in an orthogonal cutting condition.

Prior to cutting the structure and recording the force signals in the second experiment 2 structures were cut on both sides of the RTP (Figure 4.4b). The tool used in the first 2 experiments had an exact width of 982 μm and the positions of these 2 structures were such that the material between them was less than that of the tool width. Therefore, the cutting edge of the tool was not completely engaged but rather extended past the material of both side and thus this simulates orthogonal cutting. The midpoint of the 2 initial structures were positioned 1.8 mm apart in the X direction leaving 818 μm between them and an 82 μm overhang on both sides of the tool as calculated with respect to the tool width of 982 μm . Therefore, in addition to the configuration change (isolated to orthogonal) this experiment also decreases the chip load from a width of 0.982 to 0.818 mm; this can be represented as a 16.7% decrease. This experiment was performed at 5 μm DOC to be analyzed in contrast with the 5 μm isolated structure configuration.

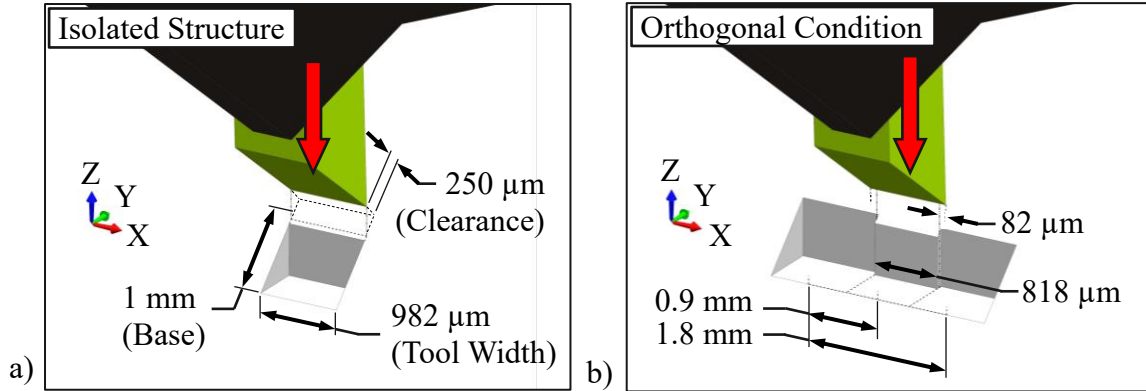


Figure 4.4 Experimental configuration: a) isolated cutting condition, and b) orthogonal cutting condition

Finally, the third experiment was conducted identical to the first however the bidirectional strategy was used rather than unidirectional. Due to changes in tool availability a different tool was used for the third experiment. The manufacturing specifications of the new tool were identical however slight difference between the tools is likely. Optical microscopy determined the width of the new tool to be 1032 μm . The configuration of the third experiment is an isolated structure cut without the use of ploughing motions. This experiment has been completed at a single DOC of 5 μm . In order to directly compare this strategy with the unidirectional strategy, an additional recording of the unidirectional strategy was taken using the new tool and setup. Although the setup is defined identical to the previous experiments the observations show some discrepancies in magnitude. It is difficult to identify the reason behind this and therefore a direct contrast will only be made with experiments performed within the identical setup.

4.2 Significant Kinematics

In recall of chapter 2, important positions and motions within each strategy will be highlighted. The analysis of cutting mechanics that follows is directly associated to the

significant positions and motions within the two strategies. The comprehensive description of each strategy can be referred to in chapter 2 if necessary. A greater focus will be placed upon the kinematics relating to tool-workpiece interaction.

The unidirectional strategy is presented in Figure 4.5. The motions within this strategy that are relevant to cutting forces are both plunging and ploughing, although forces are not generated until position B_i during the plunging. Therefore motions 2 and 3 and positions B_i , C_i , and D_i are significant to the cutting mechanics. The remaining motions in the strategy (motions 1, 4 and 5) represent the tool not being in contact with the workpiece and therefore are associated to no cutting forces. Position B_i represents the initial contact of the tool with the workpiece after this point the chip is formed through motion 2. Once the cutting edge of the tool reaches position C_i (the root of the cut) the cutting motion changes direction. The directional change in the tool path drastically effects the cutting mechanics, specifically it alters the rake and clearance angle by 90° . This quickly changes a positive rake angle during plunging to a highly negative rake while ploughing. It is known that a large negative rake angle is not preferable while machining.

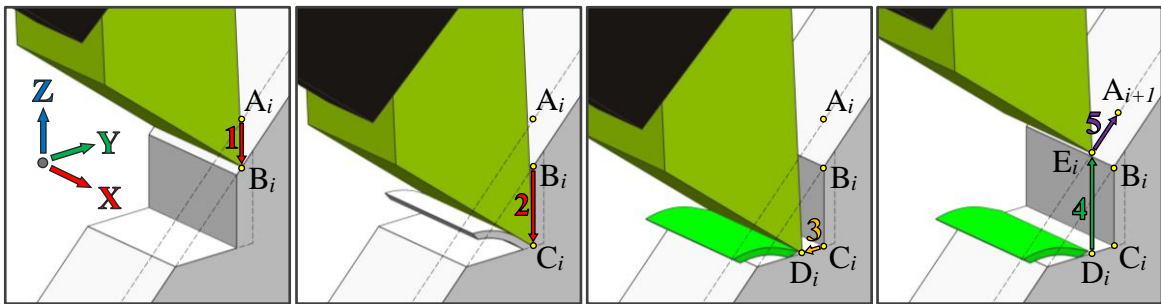


Figure 4.5 Significant kinematics associated to cutting mechanics of the unidirectional strategy

The bidirectional strategy avoids the use of ploughing and uses the capabilities of 5-axis machining to rotate the workpiece and finish both retroreflective facets with the preferred plunging motion. The cutting mechanics for this strategy are symmetrical about the bisector of the RTP. Figure 4.6 shows the critical positions and motions associated with cutting forces. Since the bidirectional strategy uses the C-axis to rotate the workpiece it is helpful to identify the participating facets of the RTP structure. Facet 1 is produced during plunging motion 2 and symmetrically facet 2 is produced during motion 2'. The remaining motions in the strategy represent the tool not being in contact with the workpiece and therefore are associated to no cutting forces. Motion 3 and 3' are used to retract the tool to the clearance height along the bisector of the RTP. The additional motions within this strategy are not presented in Figure 4.6 to condense the focus of this chapter.

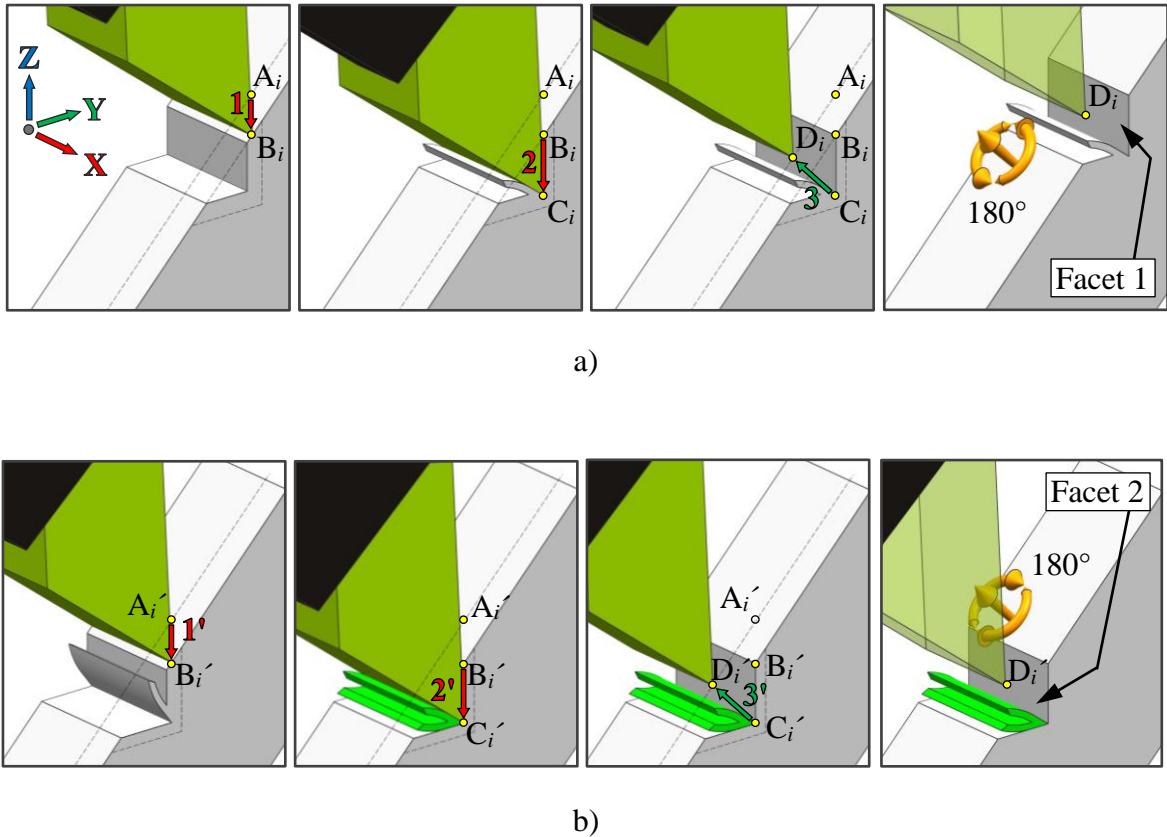


Figure 4.6 Significant kinematics associated to cutting mechanics of the bidirectional strategy: a) fabrication of facet 1, and b) fabrication of facet 2

4.3 Cutting Mechanics

During the first experiment the effect of chip thickness was observed during unidirectional cutting of an isolated RTP structure. The two DOCs which were tested are 5 and 10 μm . Multiple cycles (cuts) were recorded and then specific cuts were extracted and examined. The 3rd last-cut of the 5 μm process and the 2nd last-cut of the 10 μm process have been analyzed. These selections were made because these 2 cuts are identical in length.

i.e. $C_T = \text{Total number of cuts}$, $C_i = \text{Current cut}$

$$\frac{\text{Base}}{\sqrt{2}} - (C_T - C_{i(10\mu\text{m})})(\text{DOC}_{10\mu\text{m}}) = \frac{\text{Base}}{\sqrt{2}} - (C_T - C_{i(5\mu\text{m})})(\text{DOC}_{5\mu\text{m}})$$

$$0.707 - (71 - 70)(0.010) = 0.707 - (71 - 69)(0.005)$$

The consistency in length helps to compare the force profiles directly. The final cut for both processes is also equal in length however due to implications with the second experiment the final cut was not selected. In the second experiment the final cut is coincident with the adjacent facets of the two previously cut structures. Therefore, the final cut can not be ensured as truly orthogonal. For this reason, the selection of the cuts was made prior to the final cut. Experiment 2 compares the isolated and orthogonal configuration of the unidirectional strategy at a DOC of 5 μm .

The third experiment was conducted to analyze the cutting mechanics of the bidirectional strategy, both in contrast with the unidirectional strategy and among its symmetrical cutting motions. Since this experiment was completed at a later date and with a different tool the mechanics cannot be contrasted with the first two experiments. Therefore, identical manufacturing parameters were defined for both the unidirectional and bidirectional strategies and new recordings were taken. This ensures that the experiment configuration is comparable between the 2 sets of recordings. This experiment identifies similarities and differences between the two strategies and characterizes the differences between the symmetrical cuts within the bidirectional strategy. The cuts have been selected in the same manner as the previous experiment such that the plunge cutting length is equal.

4.3.1 Cutting mechanics of the Unidirectional Strategy

The cutting mechanics are described for a single cycle (i.e. cut) in the unidirectional strategy. Positions and motions presented in Figure 4.5 (recall: Figure 2.3) are identical to the labels used in subsequent cutting mechanic figures. In this section, the characteristics

of the force profiles will be highlighted with respect to the positions and motions of the strategy. The correlation between the kinematics and mechanics of the strategy will help to pinpoint any concerns which may arise in the analysis of the cutting mechanics. The magnitude of the force profiles will not be examined until the following section.

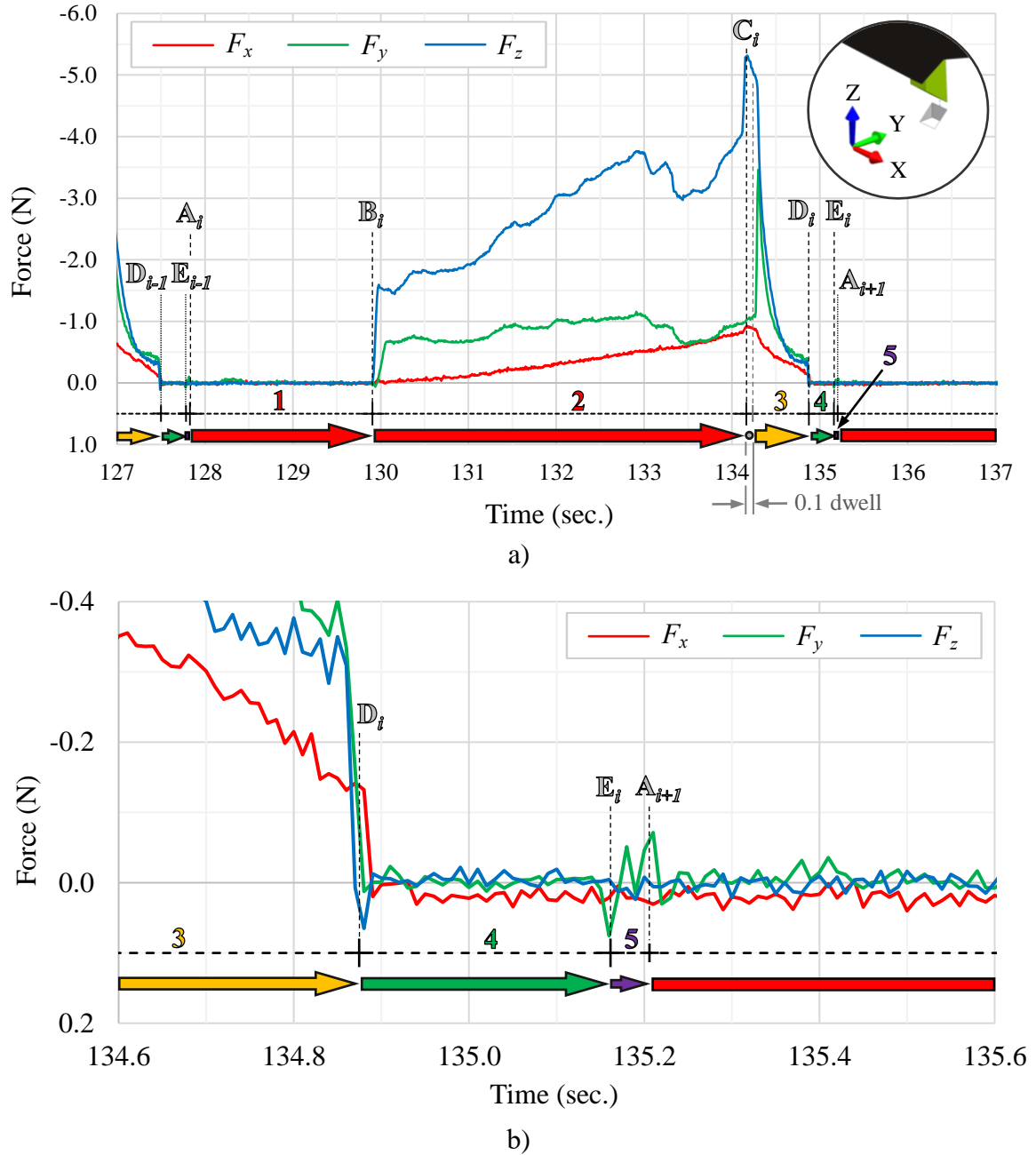


Figure 4.7 Detailed description of cutting force signatures during unidirectional USPIC strategy: a) complete cycle, and b) detail view of the final motions

Figure 4.7 displays the cutting mechanics for a generic cycle of the unidirectional strategy. The cycle begins at position A_i where the tool is at the clearance height and aligned with the facet to be cut. At this position, there are no forces present because the tool is not in

contact with the workpiece. The plunging motion commences and the tool moves from position A_i to B_i (motion 1). The significance of position B_i is that it represents the initial contact of the tool with the workpiece. The plunging motion includes both motion 1 and 2 and is only separated to emphasize position B_i . The motion itself does not change through passing this position.

Upon contact the Z-directional force (F_z) is introduced quickly, the force is negative with respect to the MCS due to the negative Z motion of plunging. The Y-directional force (F_y) is introduced shortly after, once the formation of the chip begins. F_y is also negative with respect to the MCS due to the rake angle of the tool. As the chip forms the lateral sides of the chip are still attached to the side-walls of the structure. The angle and edges of the rake face cause the chip to separate from the side walls and begin to curl. Once the tool reaches the full DOC and a constant-chip-load is reached, the rapid increase in F_z and F_y concludes. This can be seen shortly after position B_i in the cutting mechanics.

After the plateau, F_z continues to increase at a much lower rate while F_y stays relatively constant. The increase seen in the Z direction is roughly linear throughout the majority of motion 2. Immediately before reaching position C_i , the root of the cut, F_z increases rapidly one last time. Upon reaching position C_i the plunging motion ends and F_z reaches its maximum value. The rapid increase which occurs immediately before reaching the root of the cut is suspected to be chip build up between the rake face of the tool and the adjacent facet.

It is suspected that the slow linear increase in F_z is caused by friction between the sides of the diamond tool and the RTP structure. As the tool plunges it enters the RTP structure and

the sides of the tool are coincident with the sides of the RTP. The further the tool engages the structure the larger the contact area becomes. The increasing surface area is what is suspected to produce an increasing frictional force. Since the plunging motion is isolated to the Z-axis, any friction would only act against the direction of motion and therefore would not contribute to the F_y . Therefore, the observation that F_y does not show an increase throughout motion 2 agrees with this hypothesis. This hypothesis will be further investigated in subsequent sections.

The X-directional force (F_x) is presumably not significant to this method of fabrication because the motions and geometry do not suggest any force in this direction. However, the cutting mechanics have shown a linear increase in F_x during motion 2. It is suspected that the force is associated to misalignment of the tool with the relative Z-axial motion of the strategy. If the tool was improperly aligned such that it was rotated slightly about the Y one side of the tool would contact the side of the structure. This would cause an increase in F_x . Based on the force being negative, it can be assumed that the misalignment was of an -Y rotation.

After the tool reaches position C_i the program executes a 0.1 second dwell to ensure the tool reaches the appropriate point in the specified geometric path without filleting the apex of the RTP. During this time a small decrease in F_z is observed and this is suspected to be stress relaxation associated to the plastic deformation occurring in the workpiece. The remaining 2 forces do not show any significant change during this time. After the dwell is completed the ploughing motion commences.

At the beginning of the ploughing motion the tool is required to shear the chip from the adjacent facet. At position C_i , the chip is still attached by the full width of the structure and the DOC. The ploughing motion is effectively the chip-breaking and evacuation motion. The length of this motion is defined in the manufacturing parameters and is much greater than the DOC. Therefore, the chip is separated from the workpiece early in the motion and then it is pushed further along the adjacent facet. At the start of motion 3 in the cutting mechanics F_y spikes which represents the chip separating from the workpiece. After this, the force reduces for the remainder of the ploughing motion. F_z and F_x reduce upon the start of the ploughing motion.

At position D_i , the ploughing motion is complete and the tool retracts back to the clearance height. Motion 4 completes at a much higher feedrate and is a strictly Z-axis motion. All forces drop to zero immediately because the tool is quickly removed from contact with the workpiece. Figure 4.7b shows a detailed view of the final motions and is necessary because of their speed and minimal elapsed time. Upon the start of the retracting motion F_z becomes slightly positive for a short period of time and this is another indication of friction between the tool and the structure.

Once the tool reaches the clearance height at position E_i , the tool then moves parallel to the surface along the clearance plane to the next cycle starting point A_{i+1} . This motion is called translate (motion 5) and consists of a Y-Z combined motion. Due to the configuration of the CNC machining center the translate motion moves the dynamometer a small amount very quickly along the Y-axis. This sudden shift in the Y position of the dynamometer can be observed in the detailed view of the cutting mechanics. There are small spikes in F_y at positions E_i and A_{i+1} representing the acceleration and deceleration of the instrument and

workpiece. Since the tool is not in contact with the workpiece during this time this is unrelated to the cutting mechanics of this strategy, but it is helpful when identifying cycle positions.

4.3.2 Experiment 1: Isolated Config. Unidirectional Strategy vs DOC

Figure 4.8 shows cutting mechanics for the unidirectional strategy at 5 and 10 μm DOC with an isolated structure configuration. Common patterns within the force profiles can be seen amongst the 2 different DOCs. F_z shows a high rate of increase immediately upon the impact of the tool with the surface of the workpiece, point B_i : (1.00, 0.00) within Figure 4.8. Once the tool has engaged the full DOC the drastic rate of increase stops, this can be seen at data points: (1.07, -1.57)_{5 μm} and (1.10, -3.14)_{10 μm} . At this point F_z shows a perfect linear relationship to the DOC.

The change in force during the linear increasing phase of F_z is 2.19 and 2.79 N for 5 and 10 μm processes respectively. From data points: (1.07, -1.57)_{5 μm} and (1.10, -3.14)_{10 μm} to (5.18, -3.76)_{5 μm} and (5.13, -5.93)_{10 μm} . The increase in magnitude over this region is suspected to be friction and is nearly consistent between the processes. The final force spike occurs and the maximum values are reached at position C_i , data points: (5.23, -5.34)_{5 μm} and (5.23, -9.82)_{10 μm} . The relationship between the processes is near linear at this point and the discrepancy may be associated to inconsistent chip removal. After the dwell, the ploughing process (motion 3) begins and immediately F_z decreases. The rate of the decrease is similar between both DOCs.

F_y shows a high rate of increase until the constant-chip-load condition. This is illustrated at data points: (1.16, -0.66)_{5 μm} and (1.29, -1.38)_{10 μm} . A linear relationship

is once again seen with respect to the DOC. After these points F_y is nearly constant until the completion of the dwell (Figure 4.8: time 5.33 seconds). Once the ploughing motion commences F_y spikes and the maximum F_y recorded is $(5.36, -3.33)_{5 \mu\text{m}}$ and $(5.39, -5.81)_{10 \mu\text{m}}$. The linear trend with respect to the DOC continues and the small discrepancy is suspected to again be differences in chip removal.

Finally, the force in the X direction is similar in magnitude between the two processes. The force in this direction is associated to tool misalignment and the engagement of the tool into the RTP structure. Since these processes were performed using an identical setup they should have similar F_x profiles. F_x gradually increases throughout motion 2 to a maximum at data points: $(5.23, -0.95)_{5 \mu\text{m}}$ and $(5.23, -1.34)_{10 \mu\text{m}}$. The slight difference is suspected to be a small relationship between the DOC.

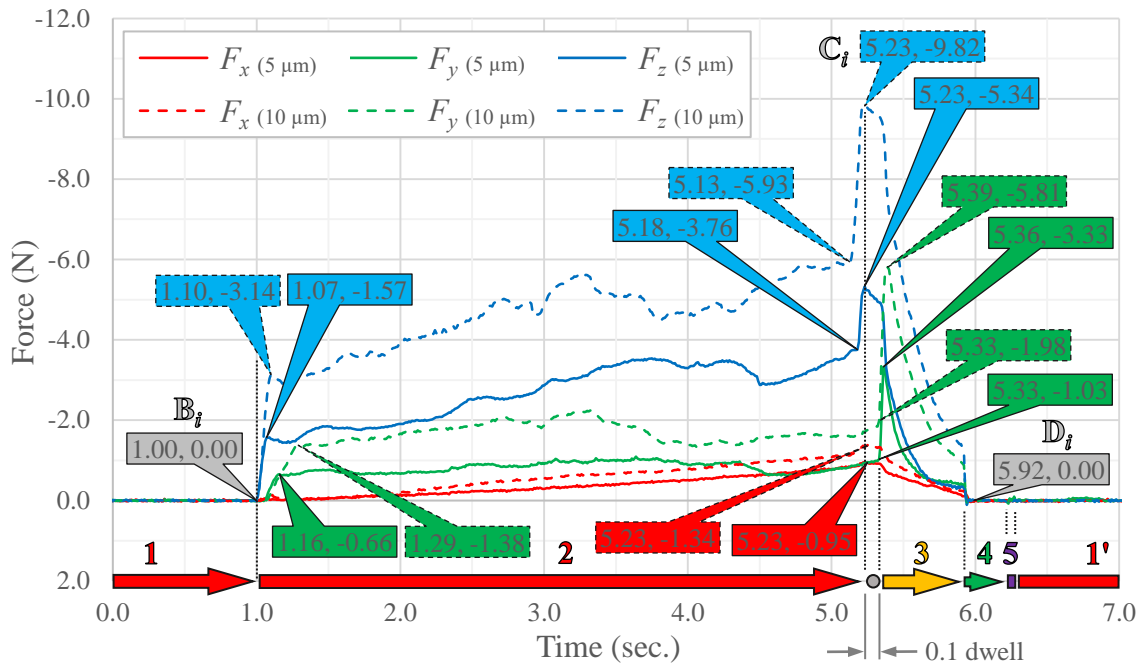


Figure 4.8 Cutting mechanics of the unidirectional strategy in isolated configuration at 5 and 10 μm DOC, experiment 1

4.3.3 Experiment 2: Unidirectional Strategy, Isolated vs Orthogonal

Figure 4.9 shows cutting mechanics for the unidirectional strategy at 5 μm DOC for both isolated and orthogonal cutting configuration. The critical difference between these configurations is that orthogonal cutting does not involve any interaction with the side walls of the tool. Therefore, the tool-workpiece interaction is strictly contained to the tool's cutting edge and rake face. An additional difference between the configurations is that the width of engagement is slightly less in the case of orthogonal cutting. This has been described previously in the experiment setup and is required to assure orthogonal cutting characteristics. The cutting width engagement is 982 and 818 μm for isolated and orthogonal configurations respectively, this is equal to 16.7% decrease in length.

Within Figure 4.9 the initial F_z spike just after the tool contacts the surface is -1.57 and -1.29 N for the isolated and orthogonal configurations respectively. This represents a 17.8% difference which is similar to the change in cutting width. At this early position in the plunging motion the tool is not engaged very far into the RTP structure, and therefore the frictional forces would be minimal at this point. The next Z-force peak is at the root of the cut (C_i) and has been recorded as -5.34 and -4.06 N respectively. This represents a 24.0% difference, which is larger than the change in cutting width and is evidence of a higher frictional force when the tool is full engaged in the structure.

In the orthogonal cutting configuration, the roughly linearly increase in F_z is not present. Therefore, the hypothesis of friction between the sides of the tool and the structure is plausible. As previously hypothesized the friction should not affect F_y

and this experiment shows that the isolated and orthogonal configurations have nearly identical F_y profiles from position B_i to C_i . This is additional verification of the plausibility of this hypothesis.

The cutting mechanics of the ploughing motion show a difference in the F_y between the configurations. The peak force in the isolated configurations is -3.33 N while the orthogonal configuration reaches only -1.73 N. This is because tool side-wall friction would impact F_y during ploughing because of the new direction of travel. The side-wall friction in the isolated configuration would oppose the -Y motion of ploughing and therefore increase the maximum force of F_y when the chip is separated from the workpiece. Additionally, the chip that is formed is still in contact with the sides of the structure for the isolated configuration and this would also increase the force needed to move the chip during the ploughing motion.

The last observation that can be made is of F_x , within the orthogonal configuration this force is eliminated. This is evidence that the force which is present in the isolated configuration is associated to the side-wall of the tool encountering the side of the structure. The presence of this unwanted force is reason for precise tool alignment and possibly a future modification to the geometric design of the tool.

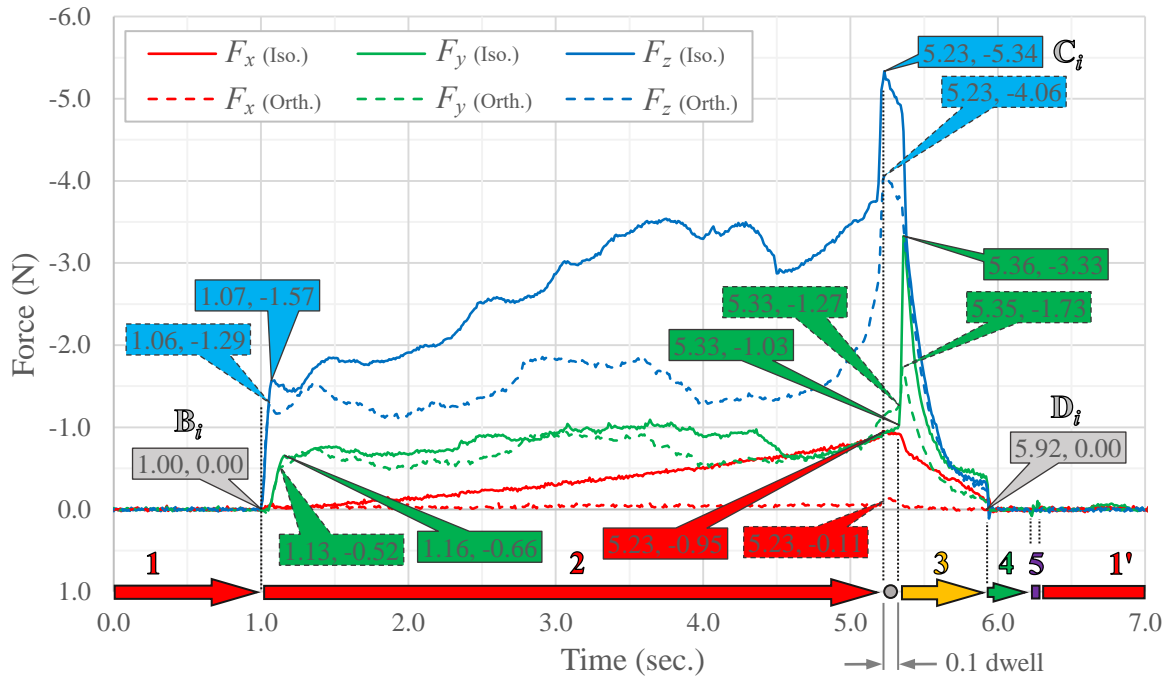


Figure 4.9 Comparative Cutting mechanics of the unidirectional strategy in isolated and orthogonal configurations

4.3.4 Cutting mechanics of the Bidirectional Strategy

The cutting mechanics are described for a single symmetrical cycle (i.e. cut) in the bidirectional strategy. Positions and motions present in Figure 4.6 (recall: Figure 2.4) are identical to the labels used in subsequent cutting mechanic figures. The data recording of this strategy could not be continuous because of the included C-axis rotations. The dynamometer is attached to the C-axis and therefore rotates with the workpiece. After the rotation, the dynamometer is in a new orientation and the resting force signals need to be reset to zero prior to recording force signals. For this reason, the data recording had to be started and stopped with each individual cut.

The description of the bidirectional strategy in chapter 2 (Figure 2.4) is comprehensive and includes all related motions however due to the movement of the dynamometer, some

of these motions could not be captured. The C-axis rotation and the translation required to align the tool with the next facet have not been recorded. Both motions are performed while the tool is at the clearance height and therefore no tool-workpiece interaction takes place. As a result, these motions are negligible with respect to the cutting mechanics. The motions which are associated to cutting forces are motions 2, 3, 2' and 3'. The cutting mechanics of these motions have been recorded.

The kinematics of the bidirectional strategy are symmetrical about the RTP's bisector, therefore to simplify the initial description of the cutting mechanics only one single cut will be analyzed. The cutting forces present in Figure 4.10 are associated to the cutting cycle for facet 1 of an RTP structure. The beginning of this strategy is identical to that of the unidirectional strategy. The tool starts at the position A_i and plunges along the Z axis to point B_i where it first meets the workpiece. Upon contact, F_z increases quickly, once a constant-chip-load is engaged the rapid increase stops and the force nearly plateaus. As the tool continues the plunging motion it enters the structure further and the contact area between the tool side-walls and the structure increases. A greater contact area results in higher frictional forces opposing the direction of motion. Thus, F_z increases consistently throughout motion 2. These characteristics are similar to the unidirectional strategy because the kinematics, up to this point, are identical.

As the tool approaches position C_i , the Z axial force spikes. This is consistent with the unidirectional strategy and is in part due to chip build up against the adjacent facet. However, the difference between the strategies is that the bidirectional strategy requires the tool to engage the adjacent facet the length of the DOC. This additional depth is suspected to increase the peak force of the Z-directional force. After the tool reaches the

root of the cut a 0.1 second dwell is implemented and a slight decrease in F_z is seen during this pause in machining. Once again it is suspected that this is due to stress relaxation associated to the plastic deformation occurring in the workpiece. Next, instead of performing a chip-breaking motion the tool retracts along the RTP's bisector. As suspected F_z rapidly drops to zero.

F_y initiates slightly after F_z once the chip begins to contact the rake face. The force increases rapidly until a constant-chip-load is reached and then the force plateaus. The force remains constant throughout the remainder of motion 2. When the retracting motion (motion 3) commences F_y spikes nearly instantaneously. In this example the unexpected spike occurs in 0.03 seconds. The kinematics of the retracting motion does not clearly show any reason for such force based on the tool geometry and direction of travel during this motion.

It is suspected that the force is associated to chip/workpiece material pressure on the rake face and the rapid feedrate used in the retracting motion. The retracting motion is a combined Y-Z axis motion of the CNC machining center, therefore poor axis-communication (synchronization) may also contribute to such an effect (e.g. the Y-axis motion initiates slightly before the Z-axis during the combined linear move). After the spike the force drops to zero as quickly as it increased. Similar to the unidirectional strategy, this strategy does not promote force in the X direction and therefore the characteristics of F_x are once again attributable to tool misalignment.

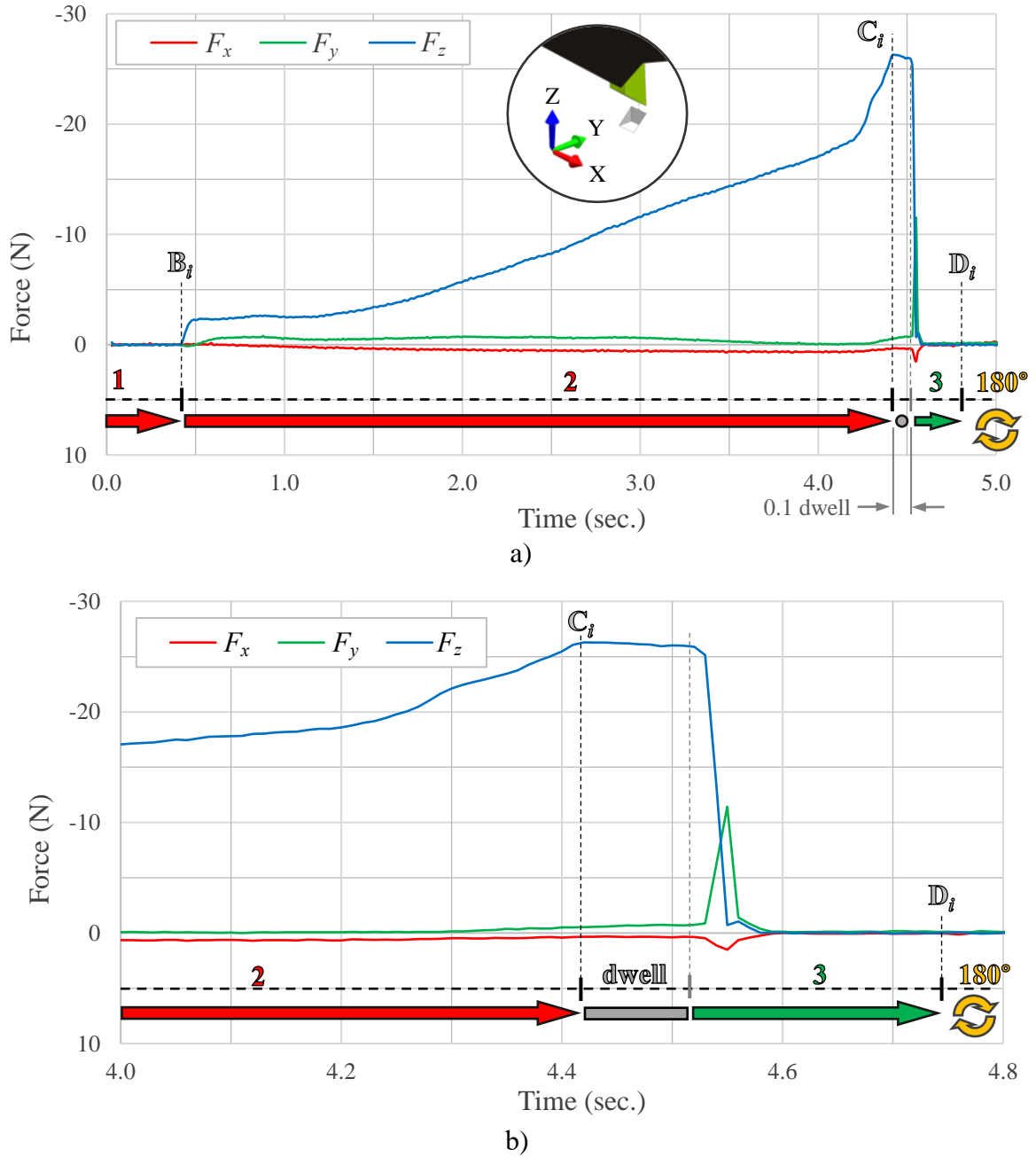


Figure 4.10 Detailed description of cutting force signatures during bidirectional USPIC strategy: a) single cut of facet 1, and b) detail view of retract motion

4.3.5 Experiment 3: Isolated Configuration, Bidirectional Strategy

As mentioned previously, this experiment was conducted at a later date and therefore the slight changes to the experimental setup were made. Therefore, the contrast between unidirectional and bidirectional strategy will be made on a new cutting force recording of the unidirectional strategy. Figure 4.11 displays both strategies for a DOC of 5 μm and an equal plunging length. Additionally, the X-directional force has been excluded because the forces are once again associated to tool misalignment and are not significant to the analysis.

Upon review of the data, the first significant observation is that the force profiles for both strategies follow a very similar trend initially. This was to be expected due to the similar kinematics of the strategies. The most significant difference between the strategies occurs after the plunging motion, at this point in the unidirectional strategy the plough motion commences however in the bidirectional strategy the tool is immediately retracted at 45° angle along the RTP's bisector. The change in the strategy results in a very logical change in cutting mechanics. Once the plunge is completed a 0.1 second dwell is added to the NC code identical to the unidirectional strategy. After this delay the tool retracts and the forces drop to zero as the tool is no longer in contact with the workpiece.

F_z within the bidirectional strategy shows a higher peak force than the unidirectional strategy because the tool must plunge past the adjacent facet by the length of the DOC. The peak force occurs at the root of the cut and the forces are -18 and -26 N for the unidirectional and bidirectional strategies respectively. The bidirectional F_z is also slightly higher during the linear increasing region of the force profile. This region is dependent on tool side-wall friction, and therefore the difference may be a result of different coolant stream orientations or different amounts of lubricant present during the microcutting.

The Y-directional forces recorded in this experiment are near constant during the plunging motion for both strategies. The maximum of F_y which occurs in the unidirectional strategy is just after the start of the ploughing motion, however for the bidirectional strategy the Y force spikes nearly instantaneously at the beginning of the retracting motion. This spike is difficult to see in the figure below, however the peak of this spike is identified by a data callout (4.55, -11.43). Within a very short amount of time the tool is no longer in contact with the workpiece and the force drops to zero.

It was first assumed that this force should not be nearly as larger as the force required to shear the chip in the ploughing motion of the unidirectional strategy. However, in the data analysis the maximum F_y are nearly equal. The reason for this is because the feedrate of this motion is 200 mm/min, which is 20 times larger than the plunging and ploughing motions at 10 mm/min. The retracting motion of this particular cycle is approximately 700 μm in length and therefore it is completed in about 0.225 seconds. In contrast, the ploughing motion presented in this experiment is 250 μm in length and at a feedrate of 10 mm/min this completes in 1.5 seconds. The drastic difference in feedrate may be the reason that the maximum forces in the Y direction are nearly equal. Force spikes such as this cause undesirable vibration and stress on the cutting tool, these types of forces should be avoided if at all possible.

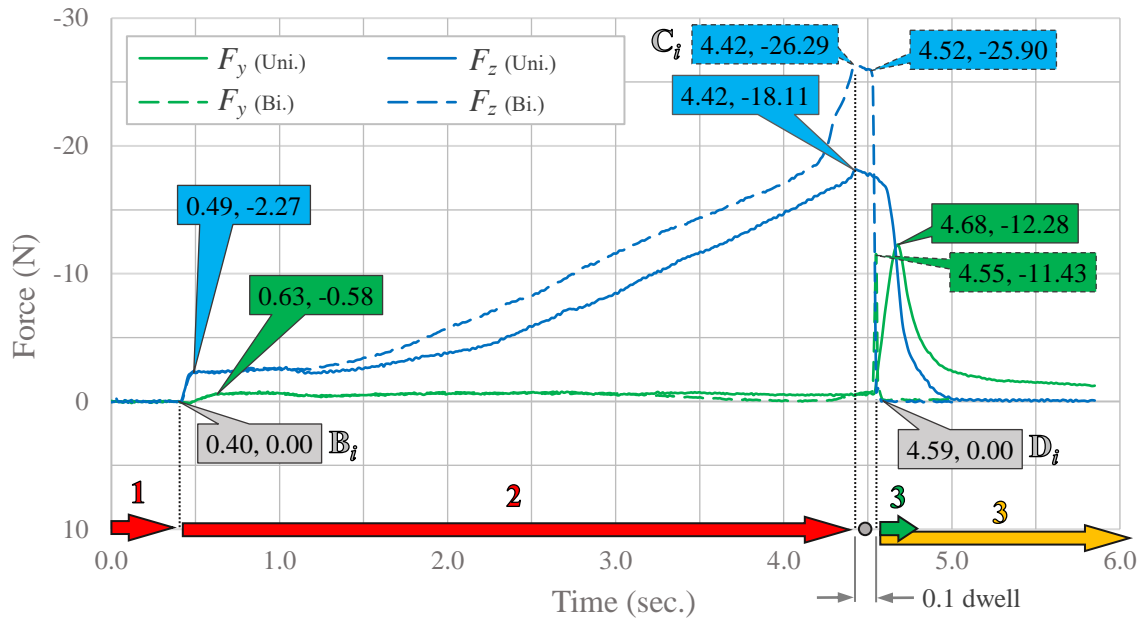


Figure 4.11 Comparative Cutting mechanics of the unidirectional strategy and bidirectional strategy in isolated configuration

The bidirectional strategy is symmetrical about the RTP's bisector; however the cutting mechanics are not. The plunging motion of facet 1 is required to proceed past the adjacent facet by the DOC while the plunging motion of facet 2 must only continue up until this newly cut facet to release the chip. It was suspected that this would cause the forces during plunging of facet 1 to exceed the symmetric motion for facet 2. During this experiment the plunging motions for both facet 1 and facet 2 were recorded.

The next bidirectional analysis will be comparing the symmetrical motions used for facet 1 and 2 of the RTP structure. Figure 4.12 details the Y and Z directional forces for both symmetric motions of the bidirectional strategy, the X-directional force has again been excluded. The Z-directional force of the unidirectional strategy from the previous analysis is also present in the figure for comparison purposes.

The first observation is that the forces associated to the bidirectional cutting motion for facet 2 are significantly lower than for facet 1 at the root of the cut. This was suspected due to the formation of the chip in this strategy. To recall, the first plunging motion for facet 1 continues past the adjacent facet by a distance equal to the DOC. At the completion of this plunging motion the chip is not released from the workpiece. The second plunging motion for facet 2 is require to separate the chip from the workpiece.

The maximum F_z that occurs during the plunging of facet 2 is much closer to that of the unidirectional strategy (maximum F_z : unidirectional -18.11 N, bidirectional facet 1 -26.29 N, and bidirectional facet 2 -15.74 N). At the beginning of all three cuts it is seen that the forces are nearly equal and this is due to their identical cutting kinematics at the beginning of the process. The differences in the Z-force profiles which arise at approximately 1.2 seconds in the figure are dependent on tool side-wall friction. It is not yet understood why the plunging motion of facet 2 has such a dramatic difference. This particular profile seems to show little tool side-wall friction and this may be because of the 180° rotation and the fact that the structure is flipped. The contacting points will have changed and the flow of lubrication will have also.

All bidirectional force profiles drop to zero rapidly upon the start of the retracting motion. F_y does display a nearly instantaneous force prior to dropping to zero for both symmetrical motions of facet 1 and 2. The difference between the F_y profiles is only the magnitude of these sudden force spikes (maximum F_y : bidirectional facet 1 -11.43 N, and bidirectional facet 2 -6.21 N).

When comparing the maximum forces of F_z and F_y between the symmetrical cutting motions it is discovered that forces associated with facet 2 reach a much lower maximum value, 59.9% in F_z and 54.3% in F_y . Lower forces during cutting motions associated to facet 2 have been observed in all recorded bidirectional cuts however the magnitude of this phenomenon and the overall force magnitudes are reduced in an orthogonal cutting configuration of the bidirectional strategy. This represents once again a strong relationship between the tool side-wall friction and cutting forces.

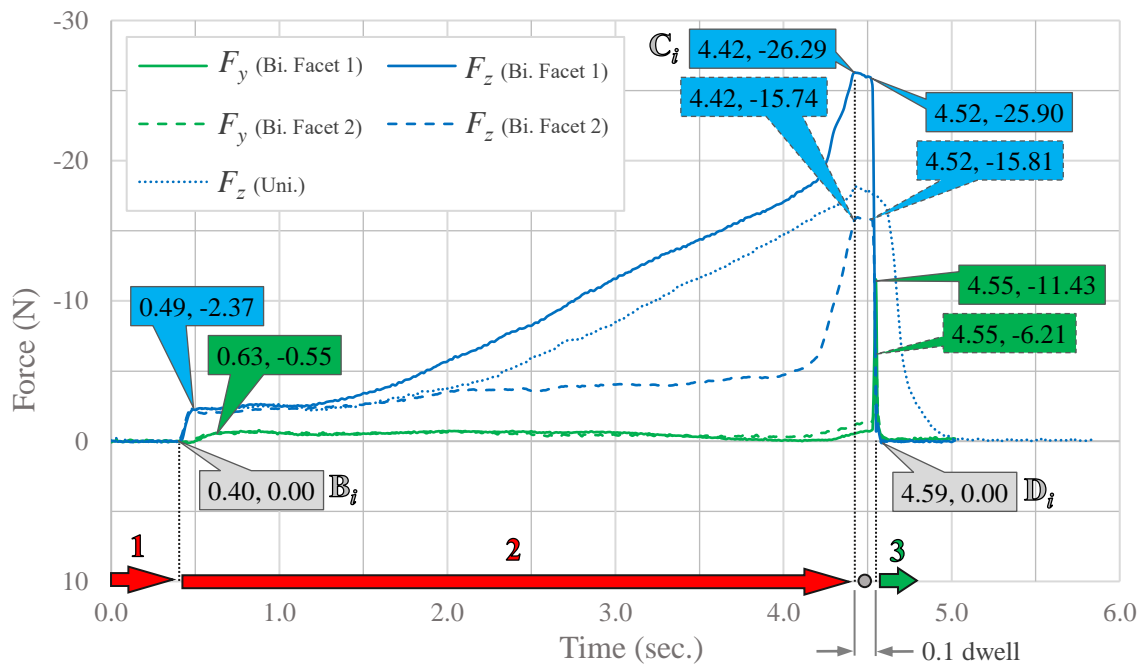


Figure 4.12 Comparative Cutting mechanics of the symmetric cutting motions of the bidirectional strategy in isolated configuration

4.4 Significance of Cutting Mechanics

The analysis of cutting mechanics associated to USPIC strategies provides many advantages to the development of this technology. This preliminary investigation of has identified relationships between manufacturing parameters and process kinematics. This

documentation also provides experimental data which can be used to validate future computer aided engineering (CAE) efforts. The understanding of the process cutting mechanics will allow enhancements to be made to each of the strategies and increase the overall quality of this technology. Incite into this diamond microcutting process will provide advantages to further improve other microfabrication techniques. Advancements made within precision diamond micromachining will drive the future of manufacturing micro-optical components [12, 37-39].

With respect to cutting kinematics, motions can be altered to avoid excess forces and sudden force impulses. The observation of tool side-wall friction suggests a modification to the tool geometry. In the unidirectional strategy, the Y-force profile spikes as the chip is sheared from the adjacent facet, after this spike the force drops but does not go to zero until the retracting motion. This represents the tool cutting edge dragging on the adjacent facet. The length of the chip breaking motion is oversized to assist with chip evacuation, however the analysis shows the exact length needed to shear the chip. After the chip is sheared the tool could potential retract slightly from the surface before continuing the full length of the chip breaking motion. This would help to reduce the amount of cutting-edge dragging and potentially the tool wear. The Y-force spike seen in the bidirectional strategy was not expected and this analysis identifies the exact kinematic motion to which it is associated. This helps to understand the specific part of the NC code which is causing the undesired force.

During this study, preliminary research was done developing a CAE model of the USPIC technology. Due to more pressing topics and the general progression of the research this path was not pursued much further then a few initial simulations. CAE is a useful and cost

effective tool in engineering and therefore an accurate model of this technology can help to understand many additional parameters. The significance of the cutting mechanics previously detailed is that it provides experimental data to cross reference with CAE simulations.

The cutting mechanics allow for enhancements to be made to the USPIC technology and therefore will improve upon the fabricated retroreflective structure. The goal being to achieve optical quality facets while increasing the tool life. Tool cutting-edge fractures need to be reduced or prevented and therefore excessive cutting forces and sudden impacts need to be addressed. When the scratches along the feed from the tool and the oscillation across the feed are reduced the surface quality of the RTP facets will increase. The oscillation across the feed direction is a larger factor in the surface roughness and this is suspected to be dynamics of the system. It is essential to identify where this vibration is coming from and therefore future analysis of the process dynamics must be done. The cutting mechanics and correlated kinematics will provide the basis for future work to explore cutting dynamics.

CHAPTER 5

Conclusion and Final Remarks

5 Conclusion and Final Remarks

5.1 Summary and Conclusion

The work presented in this thesis is an enhancement and assessment of the novel USPIC technology. This technology is an alternative manufacturing method for fabricated retroreflective structures, specifically RTPs. This technology offers many design benefits thanks to the capabilities of micromachining. These benefits are offered with a lower manufacturing time and therefore the feasibility of this technology exceeds that of the automotive industry standard. This industry relies upon retroreflective components and currently the lighting sector is thriving thanks to the arrival of micro-optical structures and micromachining technologies. This technology is idealized as a novel tool for automakers to stay at the forefront of the industry.

Improvements have been made to the manufacturing strategies and process planning. The material removal strategies have been thoroughly detailed for in-depth analysis of kinematics. Process planning has been improved such that it is both more efficient and logical. Sub-routines allow for improved process planning and kinematics are relative to the tool geometry rather than axial misalignments. RTP structures are fabricated in logical sequence and finishing routines are performed simultaneously rather than consecutively. Post processing capabilities have been added to enhance design capability and possible structure arrangements. CAM software has been used to verify the accuracy of NC code generation and identify machine limitations and potential collisions. Validation of fabrication strategies has been confirmed and process versatility displayed. Finally, the fabrication time associated to USPIC has been documented for specific manufacturing parameters.

An in-depth assessment of geometrical accuracy and surface roughness has been performed on both the USPIC technology and the pin-bundling technique. White light interferometry and confocal microscopy have been used to analysis surface roughness and geometric accuracy of retroreflective facets. A thorough analysis of the traditional pin-bundling technique has also been performed as the information was not previously documented. This information provides an important target for the USPIC technology and helps to benchmark the progression of this research. The current achievements of this research have been recorded and a more detailed observation of RTP facets show inciteful surface characteristics. Scratches along the feed direction are seen on the fabricated facets which are associated to tool wear, more specifically cutting-edge chip fractures of up to 3 μm across. Oscillation across the feed direction is also present and represent an approximate 7 Hz. frequency within the system. Optical testing has been performed on samples which have been fabricated via USPIC. The testing performed shows optical functionality of the RTP geometry and validates the novel manufacturing method.

USPIC mechanics have been recorded and analyzed for future improvements and technological developments. The cutting mechanics have been detailed with respect to the kinematics of each strategy. This allows for a thorough understand of cutting forces associated to specific positions or motions with the strategies. Critical analysis of the force profiles has been made and hypotheses confirm thorough strategic experimental configurations. To improve upon the quality of this technology and its fabricated structures improvements must be made to the geometrical accuracy and surface quality. Therefore, it is essential to reduce tool wear and eliminate excess and sudden cutting forces. The documented cutting mechanics provide useful incite into each strategy and will aid in future

modification to the fabrication process. The experimental data will also be highly useful in the development of any CAE models of the USPIC process.

To conclude this study has provided advancements to the USPIC technology by modifying, assessing, and analyzing different aspects. Manufacturing strategies and process planning have been improved, validated and efficiency document. A structural quality benchmark has been established through an in-depth assessment of multiple elements in both the USPIC technology and pin-bundling technique. Finally, cutting mechanics of the two primary strategies of USPIC have been analyzed. Process characteristics and critical positions/motions have been identified.

5.2 Future Work

As the research progresses, many additional branches have begun to form. At its infancy, this technology consisted of two streams of research, manufacturing and optical functionality. The contributions of this thesis are relevant to both these primary research areas however it introduces a few more specific streams. These being: manufacturing techniques (kinematics), process optimization, quality control, performance with respect to structure geometry and accuracy, and finally cutting mechanics.

The future of this research will continue to develop these areas of interest and it is suspected that system dynamics will be an increasingly important topic. Currently, additional effort is being put forth to analyze tool vibration and improve upon the experimental setup to analyze tool deflection during USPIC. CAE models are being developed and will eventually be used as a more convenient method for observing changes to process parameters. Enhancements are being made to the design capability of RTP structures. This

technology is spreading into more focus areas and its further development and progression are certain.

5.3 Recommendations

Based on the observations and analysis made in this thesis recommendations can be made for future efforts. The oscillation surface characteristics seen in the RTP facets are associated to a 7 Hz. frequency. The source of this frequency needs to be identified and eliminated if possible. The surface quality of the fabricated facets will show a large improvement upon addressing this issue. As mentioned above, tool vibration and system dynamics are a priority for future work in this research.

A significant observation made in this study is the occurrence and effect of tool side-wall friction. Within all experiments, it was seen that this friction had a negative impact on the cutting forces. Therefore, in effort to eliminate this friction it is recommended that the tool geometry be altered. The side-walls of the USPIC tool should include a small clearance angle such that a small misalignment does not result in undesired tool-workpiece contact. The clearance angle would also improve upon the coolant/lubricant flow throughout the tool-workpiece interaction.

The undesired frictional forces that were seen in the observations of the cutting mechanics were inconsistent. It is suspected that the lubricant flow played a role in the fluctuation however the spray mist pressure was not monitored throughout these experiments. Any future work should attempt to document the pressure and quantity of coolant used during fabrication. The orientation of the coolant may also be of interest to reduce unnecessary forces and improve the cutting mechanics.

The unidirectional strategy is used for a large majority of the fabrication, this is typical for a roughing procedure. Therefore, this process will most likely have a greater impact on tool wear. It is suspected that the ploughing motion causes tool damage and the force profiles show that the tool continues the motion even after the chip is sheared. The continued motion is used to aid in chip evacuation however it is not necessary for the tool to remain coincident to the adjacent facet. The tool can be retracted slightly prior to the continuation of the ploughing motion.

The cutting mechanics of the bidirectional strategy displays an unexpected and undesired Y-force spike. A modification should be implemented to this strategy such that the retract motion commences at a slower speed and potentially in a more vertical direction. At the root of the cut there is still pressure from the chip against the rake face of the tool. Therefore, a small vertical retracts prior to exiting the structure may eliminate the undesired force.

This technology has many advantages thanks to micromachining. It is therefore recommended that this technology continue to explore new innovative design ideas associated to geometrical dimensions, location, and orientation of retroreflective structures. Versatile structure arrangements can have a significant use in lighting aesthetics. The geometrical dimensions, specifically the included angle of the RTP, have been consistently set to theoretical value (90°) and the USPIC technology can adjust this dimension. Therefore, a recommendation to optically observe the change to this parameter is recommended. Implementation of this novel manufacturing method on inclined, curved and freeform surfaces will improve this technologies capability to be used within the automotive industry.

The final recommendation is to transfer the knowledge of fabricating RTP structures to having the capability to fabricate different aperture RR. Each retroreflective structure has a unique efficiency profile and therefore may be applicable in different applications. The cutting strategies associated to RTPs may be applicable to fabricating triangular and hexagonal RRs as well. Additionally, the experience fabricating RTPs and understanding microcutting mechanics should benefit in the development of new strategies for different geometric RRs.

References

- [1] Nilsen RB, Lu XJ. Retroreflection technology. *Optics and Photonics for Counterterrorism and Crime Fighting*. 2004;5616:47-60.
- [2] MnDOT. MnDOT Pavement Marking Field Guide. Department of Transportation Minnesota. 2015.
- [3] Luoma J, Schumann J, Traube EC. Effects of retroreflector positioning on nighttime recognition of pedestrians. *Accident Analysis & Prevention*. 1996;28:377-83.
- [4] Bernacki BE, Anheier N, Krishnaswami K, Cannon B, Binkley K. Design and fabrication of efficient miniature retroreflectors for the mid-infrared. *Infrared Technology and Applications XXXIV, Proc SPIE*. 2008;6940.
- [5] Park J, Won J, Kim D, Jo MS, Park JY. Piezoelectrically operated MEMS corner cube retroreflector for optical communications. *Journal of Micromechanics and Microengineering*. 2012;22.
- [6] Burge JH, Su P, Zhao C, Zobrist T. Use of a commercial laser tracker for optical alignment. *Proc SPIE*. 2007. p. 66760E.
- [7] Zhou L, Kahn JM, Pister KS. Corner-cube retroreflectors based on structure-assisted assembly for free-space optical communication. *Journal of Microelectromechanical Systems*. 2003;12:233-42.
- [8] Mount GH, Rumburg B, Havig J, Lamb B, Westberg H, Yonge D, et al. Measurement of atmospheric ammonia at a dairy using differential optical absorption spectroscopy in the mid-ultraviolet. *Atmospheric Environment*. 2002;36:1799-810.
- [9] Liow JL. Mechanical micromachining: a sustainable micro-device manufacturing approach? *Journal of Cleaner Production*. 2009;17:662-7.
- [10] Stobenau S, Sinzinger S. Ultraprecision machining techniques for the fabrication of freeform surfaces in highly integrated optical microsystems. *Proc SPIE*. 2009. p. 742608.
- [11] Chen ZZC, Dong ZM, Vickers GW. Automated surface subdivision and tool path generation for 3 1/2 1/2-axis CNC machining of sculptured parts. *Computers in Industry*. 2003;50:319-31.
- [12] Davies MA, Evans CJ, Vohra RR, Bergner BC, Patterson SR. Application of precision diamond machining to the manufacture of microphotronics components. *Proceedings of SPIE*. 2003. p. 94-108.

- [13] Hussein S, Hamilton B, Tutunea-Fatan OR, Bordatchev E. Novel Retroreflective Micro-Optical Structure for Automotive Lighting Applications. *SAE Int J Passeng Cars - Mech Syst.* 2016;9:497-506.
- [14] Hussein S, Hamilton B, Bordatchev E, Tutunea-Fatan OR. Parameter-Driven Geometric Modeling of Retroreflective Features. 25th Canadian Congress of Applied Mechanics (CANCAM 2015). London, Ontario, Canada. 2015. p. 96-9.
- [15] Heasley JH. Pin for forming reflector. Google Patents. 1978.
- [16] Brinksmeier E, Gläbe R, Schönemann L. Review on diamond-machining processes for the generation of functional surface structures. *CIRP Journal of Manufacturing Science and Technology.* 2012;5:1-7.
- [17] Brinksmeier E, Gläbe R, Flucke C. Manufacturing of molds for replication of micro cube corner retroreflectors. *Production Engineering.* 2008;2:33-8.
- [18] Brinksmeier E, Gläbe R, Schönemann L. Diamond Micro Chiseling of large-scale retroreflective arrays. *Precision Engineering.* 2012;36:650-7.
- [19] Hamilton BW, Hussein S, Tutunea-Fatan OR, Bordatchev EV. Fabrication of Right Triangular Prism Retroreflectors Through Ultraprecise Single Point Inverted Cutting. ASME 2016 11th International Manufacturing Science and Engineering Conference. Blacksburg, Virginia, USA. 2016. p. V002T04A46.
- [20] Hamilton B, Milliken N, Hussein S, Tutunea-Fatan OR, Bordatchev E. Enhanced Bidirectional Fabrication of Right Triangular Prismatic Retroreflectors. 31st ASPE Annual Meeting. Portland, OR, USA. 2016. p. 36-41.
- [21] Hamilton B, Hussein S, Bordatchev E, Tutunea-Fatan OR. Strategies in Single Point Inverted Cutting for Fabrication of Structured Surfaces. 25th Canadian Congress of Applied Mechanics (CANCAM 2015). London, Ontario, Canada. 2015. p. 108-11.
- [22] Hamilton BW, Hussein S, Milliken N, Tutunea-Fatan OR, Bordatchev EV. Fabrication of right triangular prism retroreflectors through 3^{1/2}/2-axis ultraprecise single point inverted cutting. *Computer-Aided Design and Applications.* 2017:1-11.
- [23] Global market review of automotive lighting - forecasts to 2028. Bromsgrove. 2013.
- [24] Weule H, Hüntrup V, Tritschler H. Micro-Cutting of Steel to Meet New Requirements in Miniaturization. *CIRP Annals - Manufacturing Technology.* 2001;50:61-4.

- [25] Morgan CJ, Vallance RR, Marsh ER. Micro machining glass with polycrystalline diamond tools shaped by micro electro discharge machining. *Journal of Micromechanics and Microengineering*. 2004;14:1687.
- [26] Dornfeld D, Min S, Takeuchi Y. Recent Advances in Mechanical Micromachining. *CIRP Annals - Manufacturing Technology*. 2006;55:745-68.
- [27] Fang F, Liu X, Lee L. Micro-machining of optical glasses—A review of diamond-cutting glasses. *Sadhana*. 2003;28:945-55.
- [28] Ehmann K. The mechanics of machining at the microscale: assessment of the current state of the science. *Transactions of the ASME: Journal of Manufacturing Science and Engineering*. 2004;126:666-78.
- [29] Nadolny K, Kapłonek W. Analysis of the effects of the single abrasive-grain microcutting scratch on INCOLOY® Alloy 800HT® by using advanced CLSM-SEM techniques. *Proceedings of the Institution of Mechanical Engineers, Part J: Journal of Engineering Tribology*. 2015;229:733-45.
- [30] Stephenson DA, Agapiou JS. *Metal cutting theory and practice*. Boca Raton, FL: CRC Taylor & Francis. 2006.
- [31] Chen ZC, Dong Z, Vickers GW. Automated surface subdivision and tool path generation for 3 1 2 1 2 -axis CNC machining of sculptured parts. *Computers in Industry*. 2003;50:319-31.
- [32] SPI A-1 - Surface Finish Standard, The Society of the Plastics Industry (SPI).
- [33] Malloy RA. *Plastic part design for injection molding*: Hanser Publishers New York. 1994.
- [34] Rebeggiani S, Rosén BG. Quantitative evaluation of the surface finish of high gloss polished tool steels. *Surface Topography: Metrology and Properties*. 2014;2:014002.
- [35] SAE J594 FEB2010 - Surface Vehicle Standard, Reflex Reflectors. Society of Automotive Engineers (SAE) International. 2010
- [36] Gubbels GPH. *Diamond turning of glassy polymers*. 2006.
- [37] Cheung C, To S. A microplasticity analysis of micro-cutting force variation in ultra-precision diamond turning. 2002.
- [38] Yuan W, Chan CY, Li LH, Lee WB. Investigation of the surface profile along the cutting trajectory and its correlation with cutting forces in single point diamond turning. *INTERNATIONAL JOURNAL OF ADVANCED MANUFACTURING TECHNOLOGY*. 2017;89:1327-38.

- [39] Sawangsri W, Cheng K. An innovative approach to cutting force modelling in diamond turning and its correlation analysis with tool wear. *Proceedings of the Institution of Mechanical Engineers, Part B: Journal of Engineering Manufacture*. 2016;230:405-15.

Curriculum Vitae

Name: Nicolas Milliken

Post-secondary Education and Degrees: The University of Western Ontario
London, Ontario, Canada
2010-2014 B.E.Sc.

The University of Western Ontario
London, Ontario, Canada
2015-2017 M.E.Sc.

Honours and Awards: Province of Ontario Graduate Scholarship
2015-2016

Related Work Experience Teaching Assistant
The University of Western Ontario
2015-2017

Publications:

Hamilton B, **Milliken N**, Hussein S, Tutunea-Fatan OR, Bordatchev E. Enhanced Bidirectional Fabrication of Right Triangular Prismatic Retroreflectors. 31st ASPE Annual Meeting. Portland, OR, USA. 2016. p. 36-41.

Hamilton BW, Hussein S, **Milliken N**, Tutunea-Fatan OR, Bordatchev EV. Fabrication of right triangular prism retroreflectors through 3½/2-axis ultraprecise single point inverted cutting. Computer-Aided Design and Applications. 2017:1-11.

Milliken N, Hamilton B, Tutunea-Fatan OR, Bordatchev EV. Enhanced Bidirectional Ultraprecise Single Point Inverted Cutting of Right Triangular Prismatic Retroreflectors. Precision Engineering – Journal of the International Societies for Precision Engineering and Nanotechnology. Submitted.